2014-01-01

# Furthering Our Understanding And Assessing The Effectiveness Of Scaling Patterns And Controls Of Land-Atmosphere Carbon Exchange In A Shrubland Of The Chihuahuan Desert With Novel Cyberinfrastructure

Aline Jaimes
*University of Texas at El Paso*, ajaimes07@gmail.com

# FURTHERING OUR UNDERSTANDING AND ASSESSING THE EFFECTIVENESS OF SCALING PATTERNS AND CONTROLS OF LAND-ATMOSPHERE CARBON, WATER AND ENERGY EXCHANGE IN A CHIHUAHUAN DESERT SHRUBLAND WITH NOVEL CYBERINFRASTRUCTURE

ALINE JAIMES HERNANDEZ

Environmental Science and Engineering

APPROVED:

Craig Tweedie, Ph.D., Chair

Tom Gill, Ph.D.

Vanessa Lougheed, Ph.D.

Marcy Litvak, Ph.D.

Vladik Kreinovich, Ph.D.

Bess Sirmon-Taylor, Ph.D.
Interim Dean of the Graduate School

# Dedication

To my dear family, friends and colleagues who encouraged me to complete this project.

# FURTHERING OUR UNDERSTANDING AND SCALING PATTERNS AND CONTROLS OF LAND-ATMOSPHERE CARBON, WATER AND ENERGY EXCHANGE IN A CHIHUAHUAN DESERT SHRUBLAND WITH NOVEL CYBERINFRASTRUCTURE

By

ALINE JAIMES HERNANDEZ, M.S.

DISSERTATION

Presented to the Faculty of the Graduate School of
The University of Texas at El Paso
in Partial Fulfillment
of the Requirements
for the Degree of

DOCTOR OF PHILOSOPHY

Environmental Science and Engineering Program
THE UNIVERSITY OF TEXAS AT EL PASO
May 2014

# Acknowledgements

The completion of this project would have not been possible without the support of many people (students, technicians, and other collaborators) who actively participated on this research project. Specific collaborations are acknowledged in each chapter.

I would like to express my gratitude to my advisor Dr. Craig Tweedie for you mentorship and sharing your drive toward innovation in environmental sciences and technology. Thank you for welcoming me in your lab and offering me a home at SEL, where I have been very fortunate to share ideas, experiences, and laughs with a group of highly motivated students.

I also extend my gratitude to committee members. Tom Gill has been a great mentor sharing ideas, insights not only to strengthen the analysis presented on this document, but also for sharing his drive and excitement for science and academic life. Marcy Litvak gave us the opportunity to learn from her research group the art of setting up a Flux tower, and also for believe in us since the beginning of this project. Vladik Kreinovich provided great feedback especially in the Cyberinfrastructure chapter, where much collaboration was inspired by his vision towards the application of mathematical theories to environmental sciences. Vanessa Lougheed provided valuable feedback to the project and aided to the completion of it through the assistance in data collection from her former masters and undergraduate students.

I have been truly grateful to have shared earlier years of the program with my fellow lab mates for whom I have the outmost respect and I will always be proud to be part of this cohort of

students, postdocs and staff, including: Sandra Villarreal, Ryan Cody, Sergio Vargas, Santonu Goswami, Dave Lin, Paul Hotchkins, Becky Marin, Jerald Brady, Adrian Aguirre, Walker Johnson, Juan Carlos Franco, Mark Lara, Gesuri Ramirez, Geovanny Ramirez, Christine Laney, Libia Gonzales, Jose Herrera, Naomi Luna, and Christian Andersen. Both, my dissertation and academic training were greatly benefited from the collaboration with the staff, professors, and students from the UTEP - Cyber share Center of Excellence. Many of these collaborations were successfully published and more importantly, they open up opportunities for me in the field by participating in working groups and conferences. Special thanks to Dr. Ann Gates, Diana Pennington, Leonardo Salayandia, and Javier Garcia.

Our collaborators from the Jornada Experimental Range were critical to the implementation of this project especially during the site selection, deployment, and maintenance of instruments at the field site. Then, I would like to express my sincere gratitude to Kris Havtad and Deb Peters for their guidance at the beginning of the project and their feedback during the Jornada symposiums. Dave Thatcher and the group of field technicians, their great support in the field was very valuable. I also would like to acknowledge Jeff Anderson for providing long-term data sets from the climatology project.

I am grateful with the funding agencies for the financial support received to pursue the doctoral program provided by the US National Science Foundation through the CREST Cyber-ShARE Center of Excellence at UTEP; also to the National Council of Science and Technology (CONACyT-Mexico) who awarded the scholarship to pursue doctoral program; and finally to the department of Environmental Science and Engineering Program that awarded teaching

assistantship to fulfill the completion of the doctoral program, special thanks to Dr. Benjamin Flores and Laura Orozco for their guidance and words of encouragement to complete this process.

I am deeply grateful to have a group of friends and colleagues who always were ready to help and answer questions, including Joe Verfaillie, Cove Sturtevant, HongYan Luo, and Stephen Chan. I would like to acknowledge the FLUXNET Young Scientist Network for providing a friendly forum to address questions and provide advice from friendly colleagues. Also to the great application engineers team from Campbell scientific: Ed Swiatek, Sasha Evans, and Jesse Hess, who provided much appreciated feedback and advice to get me jump started on programming the eddy covariance system.

I want to acknowledge the GLEON-Fellowship program cohort 1 for providing great mentorship and understanding the contribution of my research in a broader scale. Kathie Weathers and Paul Hanson were excellent mentors. I am greatly thankful for all the experiences provided and to my fellows who inspired many interesting discussions. It was an honor to be part of this fellowship.

A mi familia Ivonne Hernandez, Ivonne Jaimes, Sofia Renee Portales, gracias por su inspiracion y paciencia y apoyo para completer esta trayectoria. Agradezco su apoyo y por compartir la alegria de poder completer este objetivo. Finally, to my other family in this foreign land, Carlos Ramirez has been the voice of reason to achieve this milestone. My little four legged family member that kept me sane over the last years.

To **Olympia Caudillo**, I have no words, Thank you very much for your support.

Thank you all!

## Abstract

Over the last century, arid and semiarid regions have undergone intense desertification and in many regions, vegetation has shifted from grassland to shrubland dominated ecosystems. This land cover change has important implications for how desert ecosystems function – especially with regards to land-atmosphere exchange of carbon, water, and energy. Although the extent of desertified landscapes is expected to expand over the next 30 to 40 years, there is a relatively poor understanding of how this state transition will impact ecosystem function and feedbacks to other components of the earth system. Key to addressing this challenge is an improved understanding of ecosystem dynamics and land-atmosphere interactions at the landscape scale, and a capacity to extrapolate ecosystem dynamics to regional scales using remote sensing. This study addresses both the scientific and technical aspects of the above challenges to further our understanding of biophysical controls of ecosystem fluxes of carbon of shrublands representative of the Northern Chihuahua Desert, and also assess the effectiveness of scaling ecosystem fluxes using spectral and greenness indices derived from two spectral platforms using established, repurposed, and novel Cyber infrastructure. The study was completed through interdisciplinary collaborations within the University of Texas at El Paso's (UTEP) Cyber-ShARE Center that includes faculty and students affiliated with the environmental, computational, geological, social, and computer sciences. Several publications and conference proceedings have arisen from these collaborations. This project also intends to facilitate long term and synthesis studies through data submission to the  network, and to provide a data stream for the data information system developed by fellow staff and graduate students of the Systems Ecology Laboratory at UTEP.

The study site was located in the southeastern portion of the USDA ARS Jornada Experimental Range (JER), located about 25 km northeast of Las Cruces, New Mexico, USA. The following questions were addressed:

- What biophysical factors control land-atmosphere exchange of carbon in a northern Northern Chihuahuan desert shrubland; how do these manifest to affect annual sink/source dynamics; what are the thresholds and tipping points controlling ecosystem fluxes?
- How do extreme events impact land-atmosphere exchange of carbon; and how important are extreme events in altering cumulative seasonal and annual fluxes?
- Can land-atmosphere fluxes of carbon be adequately modeled using a range of ground-based remotely sensing methods; which spectral indices most closely correlate with ecosystem fluxes of carbon, why and when; and do spectral indices capture Inter-annual variability of ecosystem fluxes in a desert shrubland?

Using a case study approach, a range of new cyberinfrastructure tools developed during this dissertation are also presented. These include :(1) an end-to end concept map that improves documentation of data provenance, identifies needs for interoperability, and shares knowledge for the intricacies of the eddy covariance method used at the site; (2) a quantitative method that optimizes site selection of an eddy covariance tower; (3) an interoperable work-flow driven software that enhances processing and visualization of eddy covariance data and derives data products typically expected by the community; (4) a tool for gap filling micrometeorological data; and (5) an evaluation of the accuracy of eddy covariance system used at the JER study site.

Results indicate that shrublands of the JER constitute a small annual sink of carbon with very low evaporation rate, and throughout the study period. Biophysical factors controlling land-atmosphere exchange of carbon (carbon uptake and respiration) are intrinsically linked to soil temperature and water content at 10 cm depth, air temperature, photosynthetic active radiation, and greenness index - an index of canopy foliar development derived from phenocams. Identification of Extreme events was done by the use of methodology that has been proposed by IPCC (2007), which identified drought, warm and cold anomalies during the study period that were relative to a 30-year climate record for the region. Even though extreme events are erratic in occurrence and duration (from days to 2-months), their incidence have important implications on regulating ecosystem fluxes because they modify biophysical controls of ecosystem fluxes. Drought and warm events decreased carbon uptake in comparison with cold and SPEI-wet events. Whereas, Cold and wet conditions favored carbon uptake over respiration; whereas; warm and dry conditions inhibit the accumulation of significant carbon. The use of the 2GRBi greenness index derived from phenocams was correlated well with carbon uptake. However, there is a limitation to account for delay on the peak of green-up depicted by 2GRBi under dry conditions. Derived spectral indices are more sensitive to photosynthetic activity and may potentially function as bioindicators of plant stress. The end-to-end framework to complement various components of the standard work flow for eddy covariance systems used by the community through the exploration and developments of cases studies approach was successful as it allow the integration of different processes and methods designed and built by the flux community and also exported methods from other disciplines. The above constitutes the first steps towards a more integrative approach from which other research groups from small labs can benefit.

# Table of Contents

# List of Tables

# List of Figures

# Chapter 1: Introduction

Arid and semiarid ecosystems represent about 40% of the world's land cover (Okin et al., 2009). These regions are home of about 35% of the world's population (Geist, 2005). Over the last century arid and semiarid regions have been affected by desertification, exemplified by vegetation shifting from grassland to a shrubland dominated ecosystem (Geist, 2005; Peters et al., 2004). The consequences of desertification are loss of fertile soil for agriculture (Farmer 1990), promote loss of particles to the atmosphere, land susceptible to soil and water erosion, famine, migration of communities seeking more fertile lands for agriculture, among many others (Geist 2005). Also associated with desertification is the increase of albedo and latent heat due to the gaps that are formed between shrubs that function as dark surfaces releasing long wave radiation especially at night, therefore increasing near surface temperature (Yufei *et al.* 2010). Although recent hypotheses suggest that the extent of desertified landscapes will expand over the next 30 to 40 years (Seager et al., 2007), there is a relatively poor understanding of how the transition to this new system state will impact ecosystem function and feedbacks to other components of the earth system such as the atmosphere. Key to addressing this challenge is an improved understanding of ecosystem dynamics and land-atmosphere interactions at local scales and also improved capacity to extrapolate these dynamics to regional scales using remote sensing.

In this study, the term 'land-atmosphere interactions' will be used to refer to the exchange of carbon between the land (vegetation and soil) – atmosphere interface. The term flux refers to the amount of a property (in this case carbon) that moves across land-atmosphere interface and is measured as the rate of exchange per unit area of land surface per unit time (Burba & Anderson, 2010). Eddy Covariance has become recognized as being among the most adequate methods to measure the vertical turbulence that drives the mass exchange of carbon within the atmospheric boundary layer (Baldocchi, Hincks and Meyers, 2008; Burba and Anderson, 2010).

Only 5% of the world's Eddy Covariance towers are located in a biome that amasses 45% of global land surface area (FLUXNET n.d.), from which approximately eleven experimental arrays correspond to eddy covariance towers deployed in grasslands or shrublands that dominate arid and semiarid landscapes in the US southwest over the past two decades (FLUXNET n.d.). The majority of these sites are or have been associated with the  network, which gathers and shares long-term carbon, water, and energy flux measurements by a cohort of sites that span a spectrum of climate and ecosystems across the Americas (LBNL, 2014). These study sites have been designed to address some of the most urgent challenges affecting land-atmosphere exchange of carbon. These include, but are not limited to examining the interconnected nature of energy, water and carbon dynamics in water-limited ecosystems and determining how woody plant encroachment affects water and carbon cycling by understanding the differences between semiarid grasslands and shrublands (Kurc & Small n.d.; Loarie *et al.* 2011; Schwalm *et al.* 2012; Litvak *et al.* 2013; Thomey *et al.* 2014).

Despite arid regions historically under sampled in global network, critical studies have aid elucidating the complexity of carbon cycling (Scott *et al.* 2004; Litvak *et al.* 2013), evapotranspiration (Mendez-Barroso & Vivoni 2010; Cavanaugh *et al.* 2011; Sanchez-Mejia 2013), and energy balance (Castellvi *et al.* 2008; Krishnan *et al.* 2012) in arid and semiarid regions. Sarcocaulescent shrublands of the Sonoran Desert were found to be a small sink of carbon (-39 to -52$gCm^{-2}yr^{-1}$) during 2002-2003 (Hastings *et al.* 2005), as were Californian grasslands (-88 gCm-$2yr^{-1}$) (Xu & Baldocchi, 2004). Californian savannas and New Mexico grasslands have been identified as carbon sources (155 $gCm^{-2}yr^{-1}$ and ~30 $gCm^{-2}yr^{-1}$) (Siyan et al. 2007; Anderson-Texeira et al. 2011). Desert grasslands of the Jornada Experimental Range were also found to be sources of carbon (~143 $gCm^{-2}yr^{-1}$) between 1996 to 2001 (Gutschick & Snyder, 2006).

Inter-site differences and factors controlling fluxes are not yet well understood, however, it has been suggested that differences in land cover, as well as changes in timing and magnitude of precipitation events are important drivers of ecosystem fluxes (van der Molen et al. 2011, Kurc and Small 2004). The impact of extreme events on ecosystem fluxes are not entirely clear and are difficult to examine due to lack of periodic events, and in some cases close approximation of measurements to 'noisy' data, yet in extreme environments such short term events could be important controls of longer term flux dynamics. Vegetation responses to environmental variability can, however, be assessed spectrally (Cheng *et al.* 2009; Middlenton 2010), or phenological (Richardson *et al.* 2009), and the combination of these with flux measurements from eddy covariance towers offers a potential venue to isolating potential controls on fluxes at finer spatiotemporal resolutions.

The combination of spectral products (e.g., hyperspectral reflectance (Goswami, Gamon, & Tweedie, 2011), phenocams (A. Richardson et al., 2007)) and flux measurements from eddy covariance systems could also provide a capacity to search for more effective ways to scale net ecosystem exchange estimations to larger spatial scales (Gamon et al., 2011). However, the issue of defining the appropriate scale at which spectral measurements accurately represent the footprint of the eddy covariance flux measurements is not yet well understood; hence, there are no standard or well-accepted methods or protocols for combining these sampling approaches at eddy covariance sites, thereby limiting the scalability of flux measurements to landscape and regional scales using remote sensing approaches (Balzarolo et al., 2011). Another limitation to regional scaling and deeper understanding factors controlling fluxes in desert regions appears to be the capacity for scientists to be able to reuse and share data and knowledge in synthesis studies, which is benefited from standardized instrumentation, processing routines and data documentation protocols. Although a new handbook for the eddy covariance method has recently been released (Ubinet *et al.* 2012). In other scientific networks, innovations in Cyberinfrastructure have greatly improved capacities for data management, data discovery, interpretation, and reuse (Lincoln 2008).

The motivation for this study is to enhance understanding of factors controlling land-atmosphere carbon exchange in a desert shrubland that represents a future ecosystem state for much of the Northern Chihuahuan desert using standards and protocols developed by the eddy covariance and optical remote sensing communities and new Cyberinfrastructure tools adapted from other scientific fields. This effort has been performed through interdisciplinary

collaborations with other UTEP faculty and graduate students to explore more and optimal ways to collect, archive, visualize, share, and reuse data from these sensor arrays.

### 1.1 OBJECTIVES AND SCIENTIFIC QUESTIONS

The overarching goal of the proposed study is to furthering our understanding land-atmosphere carbon exchange for a regionally representative Northern Chihuahuan desert shrubland dominated by creosote bush (*Larrea tridentata*) and honey mesquite (*Prosopis glandulosa*) using both established, repurposed, and novel Cyberinfrastructure. This dissertation focuses on addressing key objectives and underlying research questions:

**Research Objective 1**. - Assess the temporal variability and controls of land atmosphere of carbon on a desert shrubland in the northern Northern Chihuahuan desert, using eddy covariance datasets spanning 2010-2012 and identify what environmental factors are associated with these, and how they impact fluxes over multiple time periods.

- What biophysical factors control land-atmosphere exchange of carbon in a northern Northern Chihuahuan desert shrubland?
- How do these manifest to affect annual sink/source dynamics?
    - What are the thresholds and tipping points controlling ecosystem fluxes?

**Research Objective 2.** - Assess the effect of extreme climatic events on ecosystem fluxes of carbon in shrubland ecosystem, and assess how important these events are relative to annual sink-source dynamics.

- How extreme events impact land-atmosphere exchange of carbon; and
- How important ecosystem impacts from the identified extreme are relative to cumulative seasonal and annual fluxes.

Results are discussed with a mindset for interpreting how an increased frequency of extreme events that are expected with climate change may impact ecosystem function of comparable desertified landscapes in the future.

**Research Objective 3.-** Evaluate the effectiveness of range of spectral indices derived from hyperspectral robotic tramline system and phenocams to model ecosystem fluxes of carbon in shrublands.

- Can land-atmosphere fluxes of carbon be modeled using optical remote sensing methods?
- What spectral indices respond better (linear) to ecosystem fluxes of carbon, why and when?
- Are spectral indices sensitive to Inter-annual variability of ecosystem fluxes?

**Research Objective 4.-** Design an end-to-end Cyberinfrastructure to improve i) site selection, ii) semantic description of the data acquisition and processing methods, and iii) gap filling techniques for eddy covariance datasets.

- How can an end-to-end Cyberinfrastructure can be structured for the eddy covariance method?
-

## 1.2 OVERVIEW OF THE STUDY SITE AND METHODS

### 1.2.1 Study site

The study site is situated on the USDA ARS Jornada Experimental Range (JER), located about 25 km northeast of Las Cruces, New Mexico, USA. The mission of the JER is to investigate the causes and consequences of desertification and how environmental drivers, transport vectors, and historic legacies interact with vegetation structure to influence ecosystem dynamics across different spatiotemporal scales (Peters & Laney 2009). The JER is representative of the northern Northern Chihuahuan desert, this region has documented desertification since 1858, when grasses comprised more than 80% of the vegetation cover; by 1998 grass cover was reduced to 7% whereas shrub cover increased to 59% (Figure 2) (Havstad *et al.* 2006b; Beltran-Przekurat *et al.* 2008).

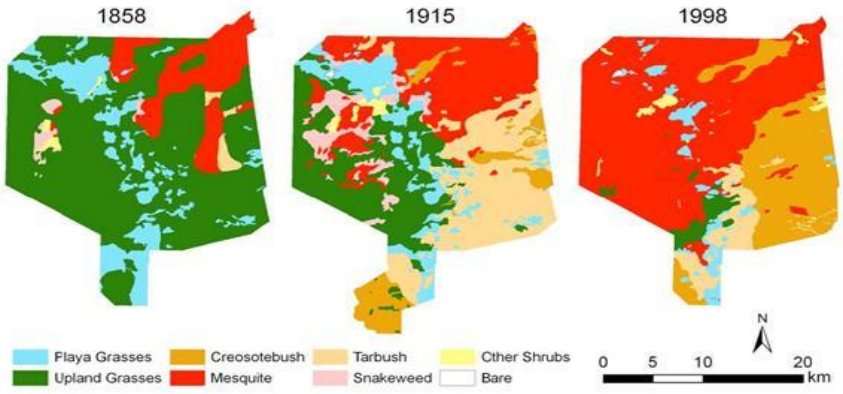


**Figure 1** Vegetation maps listed by dominant species from 1858 to 1998. Taken from Havstad et al. (2006)

The study site is located in the southeastern portion of the JER (32.5655 N, -106.6598 W; Figure 3). The area is dominated by a mixed creosote bush (*Larrea tridentata*) – honey mesquite (*Prosopis glandulosa*) shrubland. Creosote bush is an evergreen, drought-resistant C3 perennial

shrub (Peters *et al.* 2006). Honey mesquite is a deciduous, thorny, long lived C3 shrub that is characterized by very deep and laterally extensive root systems (Peters et al., 2006). Other species found at the site include tarbush (*Flourencia cernua*), the grass bush muhly (*Muhlenbergia porter*), fluff grass (*Dasyochloa pulchella*), and black grama (*Bouteloa eripoda*), as well as a variety of forbs. The shrub average canopy height is approximately 2.0 m. Soils are classified as Ustic Calciargids (Northern Chihuahuan desert Rangeland Research Center 1980 Doña Ana Soil Survey).

### 1.2.2 Instrumentation

In this section a brief description of the study site, instrumentation and other protocols is presented. The infrastructure includes an extended open path eddy covariance system, a hyperspectral reflectance tramline with automatic cart, a sensor network, a network of four phenocams, and plot phenology measurements.

#### *Extended open path eddy covariance system*

A 10-m tall tower hosting an open path eddy covariance system designed to measure land-atmosphere flux exchange was deployed in November 2009 (Figure 2). This system provides digital output of the fluctuations of carbon dioxide density, latent heat, sensible heat, momentum, temperature, humidity, horizontal wind speed and wind direction, net radiation, soil heat, soil temperature, and soil water content (Campbell Scientific, 2009). The system was designed following standard protocols of national and international networks (, 2012) to match similar research sites situated in grasslands and open shrublands throughout the US southwest to facilitate future synthesis studies. Manufacturer protocols were followed for installation, maintenance, and calibration (Campbell Scientific, 2002, 2003, 2005; Zonen, 2004). Every

season the $CO_2$ signal of the IRGA is calibrated against gas mixtures with concentration of $CO_2$ at 500ppm; the span for the water vapor is calibrated with a dew point generator (model Li 610, Li-COR Inc). Zero spans for both $CO_2$ and water vapor channels are calibrated with 99.99% nitrogen gas. With adherence to the protocol, 30 min fluxes are calculated from fast response instrumentation and independent measurements from slower response sensors are used to measure and calculate background meteorological variables.

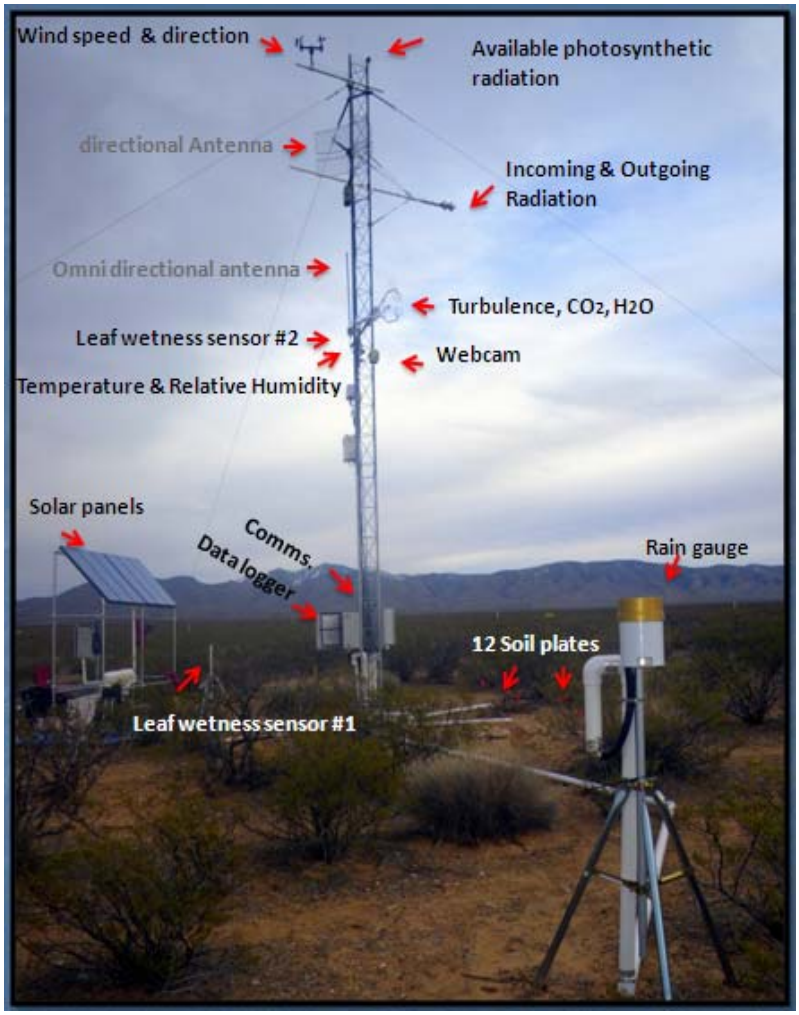


**Figure 2** Extended Open Path Eddy Covariance System. UTEP ecological station located on the Jornada basin Experimental Range

The EC tower has a total of 22 instruments: of a three dimensional sonic anemometer (CSAT3-SONIC CSI), an infrared gas analyzer (IRGA, LI-7500 Li-COR Inc) located at 5m height, a four-component net radiometer situated 20m to the east of the main eddy covariance tower at a height of 3m (CNR1- Kipp and Zonen), a photo-synthetically active radiation sensor (PAR-LITE - Kipp and Zonen) located at 10m height, a temperature and humidity sensor (HMP45C-L - CSI) at 5m height, a barometer (CS106 –CSI) located inside an enclosure about

1.30m height, a 2D anemometer (03002-L -CSI)at 10m height, a tipping bucket rain gauge (TE525-L), eight probes to measure soil temperature and volumetric water content (ECTM – decagon), and four soil heat flux plates (HFP01 Hukseflux CSI). Soil instruments are distributed into two subsystems of soil profiles installed to capture underground temperature, volumetric water content, and heat from underneath a mesquite and bare soil. These profiles are located at 2cm, 10cm, 15cm and 20 cm depth. All data is collected and stored in a Campbell Scientific CR3000 data logger. The system is powered by a 300W 10-panel solar array. The solar panels are mounted on an aluminum structure located 35m north and downstream of prevailing winds at the EC tower. The panels face south to maximize battery recharge. The system uses four 12VDC sealed deep cycle batteries, and the load is regulated through a morning start ProStar 15 Amp 12/24 charge controller. Data files are stored on a 2GB card and are retrieved remotely using an internet connection. This connection is established by a Virtual Private Network that passes via a point to point Wi-Fi connection that links an antenna situated at 9m on the eddy covariance tower to the headquarters of the JER from where it then routes to UTEP servers through hardwired Ethernet. The system also provides a 500m Wi-Fi bubble from an Omni-directional antenna situated at 5m on the eddy tower and connects multiple wireless devices associated with the local sensor network at the study site

In order to accurately estimate land-atmosphere fluxes of carbon dioxide, water vapor, and energy, raw eddy covariance data needs to be corrected and processed (Burba & Anderson, 2010) according to site-specific design and sampling conditions. Some of these are shown in Figure 3 and include (1) the northward, eastward, and vertical separation to estimate high frequency flux losses due to the distance between the instruments that measure the vertical wind component (SONIC) and the gas concentration (IRGA) (Burba & Anderson, 2010; Campbell

Scientific, 2005); (2) the north offset - the angle between the main axes of the anemometer, which faces the prevailing wind direction (240 204 degrees at the study site); (3) the displacement height or zero plane displacement (d) that accounts for the distance above the ground at which a non –vegetated surface should be placed to provide a logarithmic wind field equal to observed one (d=0.67 x canopy height); and (4) roughness length, which is the height at which wind speed is zero (indicated by Z0) and thereby provides an estimate of the average roughness elements of the surface ( calculated as Z_o=0.15 x canopy height).

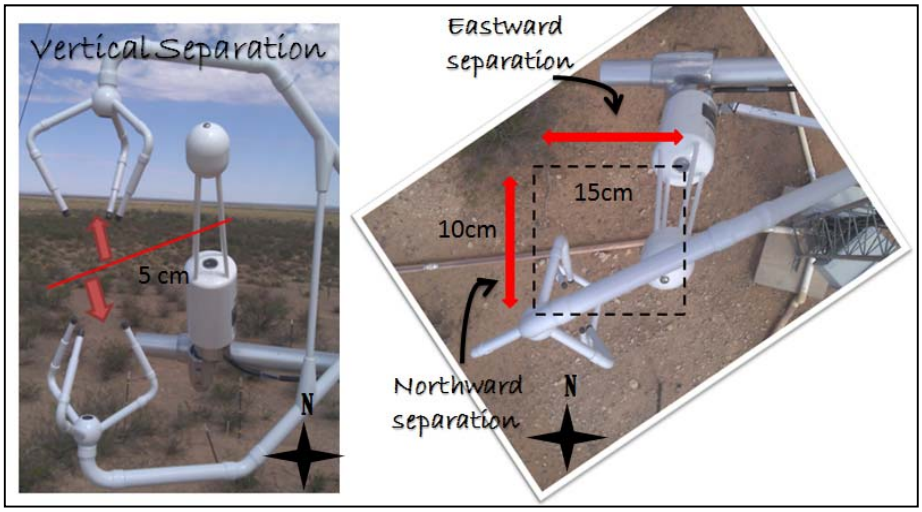


**Figure 3** Image of the spatial configuration of the CSAT and LI-7500. Left image, vertical sensor separation is positive since the IRGA's sample volume is located above the center of the SONIC's sample volume; otherwise the vertical separation would be negative.

Corrections and calculations can be computed in a range of data processing software. In this project the open source EddyPro 4.1.0 RC2 software is being used to calculate fluxes from 10Hz TS data. The corrections and calculations performed by EddyPro 4.1.0 RC2 software include: coordinate rotation, correction for sensor separation, de-spiking and raw data statistical screening, crosswind correction, anemometer tilt correction, turbulent fluctuations, conversion of raw data to mixing ratios, detection and compensation for time lags, and calculation of ambient

and cell statistics (i.e. averages, standard deviation, skewness, and kurtosis), ambient and cell parameters, average gas concentrations and densities, micrometeorological variables, four different levels of fluxes (corrected and uncorrected), spectral corrections, flagging flux quality, and flux estimates (LICOR, 2011). Accuracy assessment of the current EddyPro 4.1.0 RC2 flux processing routine has been accomplished by hosting a site evaluation performed by Stephen Chan, postdoctoral research associate from the QA/QC laboratory (LBNL, 2014)

***Hyperspectral reflectance***

To meet the challenge of scaling flux measurements to satellite remote sensing that will aid regional assessments of ecosystem dynamics, field reflectance measurements were made weekly with a tramline system similar to that described by Gamon et al. (2006) and Goswami et al. (2011). This customized system consists of a 110m east-west oriented tram rail system that provides the reflectance platform. A dual-detector field portable spectrometer with a nominal range of operation between 400 and 1000 nm (Unispec DC, PP Systems, Amesbury, MA, USA) is placed on a semiautonomous robotic cart, which is started manually and travels along the tramline. A mechanical switch mounted on the base of the cart passes over crossbars situated every meter along the tramline triggering the spectrometer to make a measurement. The spectrometer simultaneously measures irradiance (incoming radiation from the sky) and radiance (outgoing radiation from the vegetation/ground). The two detectors are cross calibrated using a white panel with 99% reflectance at the beginning and end of each tram run. Three or four runs are usually performed consecutively once per week, and within two hours of solar noon. Additionally, during one run, a webcam is mounted on the cart arm, facing downward. One image is taken at every meter along the tramline. These data sets also provide the capacity of

studying seasonal variability of phenology by obtaining spatially explicit time series of surface reflectance and phenology every meter along the tramline. These data sets have been collected and processed by two graduate students at SEL since spring 2010.

***Phenology***

A key component to enhance understanding and monitoring of ecosystem health and stress imposed by environmental factors such as drought, freezes, etc., is to characterize the timing and intensity of changes in plants growth and reproductive cycles (phenology). To address this issue, the research site has implemented several phenology sampling protocols that consist of plot level measurements and phenocams. Plot level measurements follow protocols of the US National Phenology Network. This study was established at the study site in March 2010 by a graduate student of the System Ecology lab (Gonzalez, 2011). Three phenology transects were situated northwest, south, and east of the tower to monitor phenophase development of dominant perennial shrubs and grasses. The south and northwest transects (300m each) have six monitoring sites spaced 50m apart. At each site, three individuals of five key species are monitored (with some exceptions where some species are not present). The east transect spans the length of the tramline and tagged individuals of each species occur within the tramline sampling footprint wherever possible to enable cross-comparison of phenophase and reflectance measurements. The phenocam network includes four commercially available web cameras (webcam model Vx7000, with 1600 x 1200 pixel resolution (2 MP), 58° of horizontal view angle, with a manually fixed focus for the specific experimental area), have been mounted at the top of the eddy covariance tower (~9m). The phenocams are connected to a Belkin USB Plus 4-Port Hub (5V/2.6 A), mounted on a customized weatherproof camera enclosure, with a 36ft

Tripp Lite U042-036 USB2.0 A/B repeater cable extension. Three digital phenocams cover a 170 degree (from South to Northwest) view of the flux tower footprint and the fourth camera spans a 58 degree to the East of the flux tower that includes the tramline footprint. One image is taken from each camera every hour from 7:00 to 19:00 hrs. Images are stored with in a minimal compression factor JPEG format and offer a visual record of phenological development through spectral indices derived from Red-Green-Blue (RGB) channel extractions. This analysis was embedded in a customized graphical user interface within MATLAB® 7.8.0 software that allows for the selection of regions of interest (ROI's) (Gonzalez, 2011). Images are analyzed following a method similar to the reported by the Harvard forest group (Richardson, A et al., 2009).

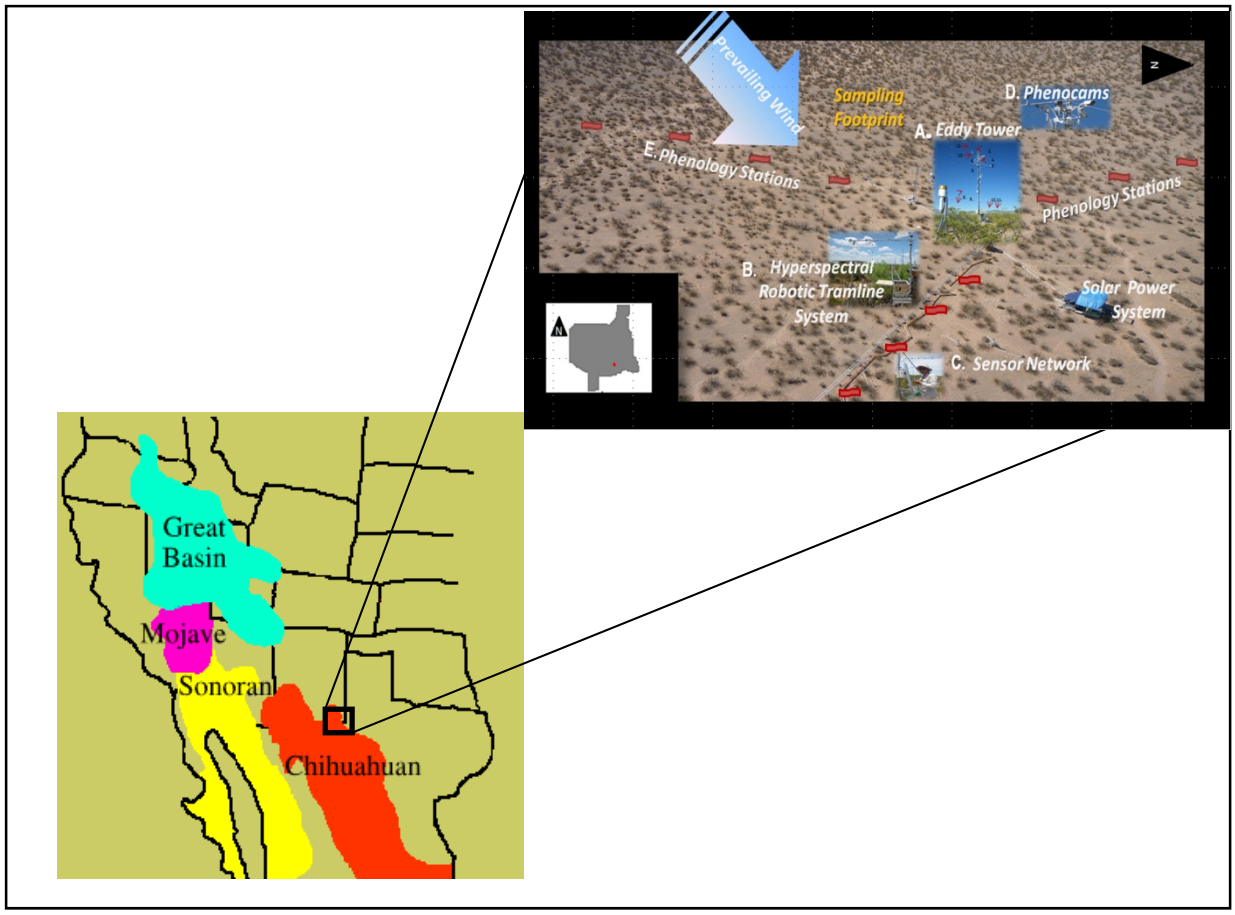


**Figure 4** Location of the area of study and the instrumented site. Schematic of the site taken from a kite aerial photography system by Craig Tweedie on April 2011. Inset: Bottom left red circle represents station's location within the JER area, which is outlined in gray. A) Extended open path eddy covariance tower. B) Robotic tramline system that measures hyperspectral reflectance. C) Micrometeorological and phenostations sensor network. D) Phenology cameras, E. Phenology stations. Blue arrow indicates predominant wind direction. Yellow font indicates the dominant flux tower footprint. Instrumentation is mostly powered from a remote solar and battery system, which also powers point to point and local area Wi-Fi communications at the site.

## 1.3 STRUCTURE OF DISSERTATION

This dissertation contains four data-intensive chapters formatted for publication in peer reviewed journals (Chapters 2-5). Chapter 2 studies the biophysical controls of land-atmosphere exchange of carbon exchange in a shrubland representative of the northern Northern Chihuahuan desert, this analysis was performed using data from 2010 to 2012, and a model evaluation was done using 2013 as independent dataset. Chapter 3 examines the effects of stochastic climatic events in land-atmosphere exchange of carbon in desert shrublands of the Northern Chihuahuan desert during 2010-2013. Chapter 4 assess the effectiveness of scaling carbon dioxide and water vapor fluxes through integrating spectral and flux measurements in a shrubland ecosystem during 2010-2013. Chapter 5 describes case study based prototype tools that aided data management and quality control of the eddy covariance data collected during the study. Chapter 6 presents the general discussions and conclusions of the dissertation. Each of these data chapters address research objectives outlined above.

# Chapter 2: Biophysical controls of land-atmosphere exchange of carbon, water and energy in shrublands of the northern Chihuahuan Desert

## 2.1 ABSTRACT

This study aimed at improving the understanding of biophysical controls of ecosystem fluxes (carbon) of desert shrublands of the Northern Chihuahuan desert. Specific objectives were to: (1) Characterize microclimate; (2) Quantify daily, monthly and seasonal variations in net ecosystem exchange of carbon; (3) Investigate the biophysical factors driving net ecosystem exchange by using robust statistical modeling (4) Evaluate the relative importance of biophysical controls and the specific relationships between the most important biophysical controls of ecosystem fluxes. The study used three years (2010-2012) of eddy covariance and webcam-derived greenness index data from the UTEP-Ecological station located in the Jornada Experimental Range (JER). The JER is located 20Km northeast of Las Cruces, NM and represents the Northeastern portion of the Chihuahuan Desert. This study used a combination of random forest tree analysis and deterministic model to explore biophysical drivers of net ecosystem exchange, and their relative importance to control ecosystem fluxes. Results indicated the random forest tree analysis has not been used in micrometeorology studies; however, results from it underpinned the top predictors of NEE, GPP and R in desert shrublands are similar to other arid and semiarid regions, in which temperature and water availability in different partitions of the ecosystem and the atmosphere. Although the results suggest that ecosystem fluxes have similar biophysical controls, their top ranked importance, based on the increase of percentage mean squared error, is different. This has implications for further modeling, in which less than five predictor variables can be used to model the response of fluxes.

## 2.2 INTRODUCTION

The rate of carbon accumulation in arid and semi-arid landscapes is considered modest in comparison with other world biomes. However, approximately 40% of global land area is covered by dryland ecosystems (Yi *et al.* 2012) and the integrated rate of carbon accumulation over this area is almost twice the total carbon stored in more productive ecosystems such as temperate forests (Hilton *et al.* 2013). Thus, arid and semiarid areas are critical on the global carbon balance. Climate models predict dryland systems are expected to expand to cover more than half of the land surface area on Earth as a result of desertification and climate change (Feng & Fu 2013). Such change, typically indicated by the transition of grasslands to shrublands (D'Odorico *et al.* 2010), has been ongoing in the US desert southwest for the last century (Geist 2005; Okin *et al.* 2009), where the impact of such state transitions on land-atmosphere exchange of carbon exchange (Ge & Zou 2013) and land management (Archer *et al.* 1995; Shevliakova *et al.* 2009) remain a concern.

Land cover transitions from grassland to shrublands have the capacity to modify near surface microclimate and energy balance through land–atmosphere interactions (Xu 2004; Beltran-Przekurat et al. 2008). For instance, shrublands typically have a larger fraction of bare soil than grasslands and are poorly insulated by vegetation; hence a greater percentage of day time solar radiation is absorbed in shrublands than in grasslands (Yufei *et al.* 2010). This stored energy is then released at night causing surface air temperatures to be higher at nighttime in shrublands compared to nearby grasslands (Beltran-Przekurat *et al.* 2008). Other changes associated with grassland to shrub land cover change include a decrease in vegetation cover, leaf area index, soil water holding capacity, albedo, and carbon dioxide sequestration capacity, and

increases in local air temperature, respiration, sensible heat and evapotranspiration (Anderson-Texeira et al. 2011).

The complexity of understanding historical, present, and future ecological states caused by transitions between grasslands and shrublands, and the subsequent implications for energy, water and carbon exchange is critical as the treats that interact in different spatiotemporal scales are result of cumulative local scales that have the ability to propagate and influence broad-scale ecosystem dynamics (Peters *et al.* 2007). Ecosystem dynamics is usually driven by complex interactions which include local hydrology (Cavanaugh *et al.* 2011), microclimate variability (Joos *et al.* 2001), plant phenology (Penuelas *et al.* 2009; Kurc & Benton 2010). These interactions occur during different spatiotemporal scales from days to years, and from minutes to hours; and those interactions can also be affected by environmental disturbances such as drought, fires, among many others (Nicholson *et al.* 1998; Vargas *et al.* 2010; Munson *et al.* 2013) (Figure 5). Few studies have examined interactions between multiple controls concomitantly in arid and semiarid regions. From those studies we know that water and heat stress are important inhibitors of carbon uptake (Anderson-Texeira *et al.* 2011). photosynthesis is also inhibited under high deficits of vapor pressure and consequently soil water deficit (Yuan *et al.* 2007); also, low and small precipitation events that only wet the soil surface promote higher surface evaporation rates (Scott *et al.* 2006); thresholds of photosynthetic active radiation above 1150umol $m^{-2}$ $s^{-1}$ also limit carbon uptake in Mongolian steppes (Shao *et al.* 2013a).

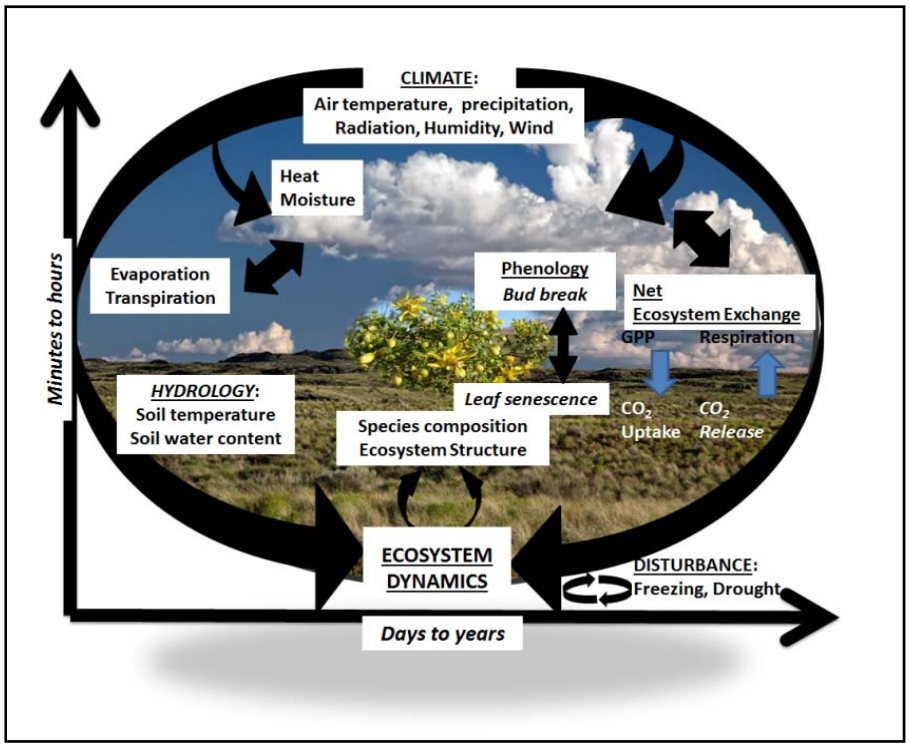


**Figure 5** Conceptual diagram illustrating the complexity of land-atmosphere interactions in shrublands of the northern Northern Chihuahuan desert

Examining the interactions of biophysical drivers of carbon, involve the use of integrative approach to capture the complexity of biophysical controls of carbon uptake, ecosystem respiration, water and heat. This has not been extensively examined between multiple controls concomitantly in arid and semiarid areas. Uncertainty of local threats influencing land – atmosphere interactions is high as the northeastern portion of the Northern Chihuahuan desert remains poorly studied. Initial attempts to quantify carbon fluxes were conducted using Bowen ratio in grasslands between 1996 and 2001 in the Jornada basin (Gutschick & Snyder 2006);

however, instrument failure and large gaps in data highlighted the importance of using another method with better temporal coverage in the area.

This study aims at improve the understanding of biophysical controls of ecosystem fluxes (carbon) during a three year period (2010-2012). Specific objectives are (1) Characterize microclimate; (2) Quantify daily, monthly and seasonal variations in net ecosystem exchange of carbon; (3) Investigate the biophysical factors driving net ecosystem exchange by using robust statistical modeling (4) Evaluate the relative importance of biophysical controls and the specific relationships between the most important biophysical controls of ecosystem fluxes. (5) Identify environmental thresholds and tipping points controlling ecosystem fluxes

## 2.3 MATERIAL AND METHODS

### *2.3.1 Study site*

The study was conducted in the southeastern section of the Unites States Department of Agriculture's Jornada Experimental Range (JER, 32.5655 N, -106.6598 W; Figure 2). The landscape in this region of the JER has transitioned from grassland to shrubland over the past century (Havstad *et al.* 2006a), likely as a result of increasing $CO_2$, and air temperatures (Geist 2005; Wang *et al.* 2012). The study area is approximately 7 km east of the San Andres Mountains, with gently slopes West to East (*ca.* 2º slope*)* and is dissected by occasional arroyos that rarely exceed 10m in width and 1m in depth. Soils are Ustic Calciargids (Northern Chihuahuan desert Rangeland Research Center 1980 Doña Ana Soil Survey). The long-term average rainfall at the JER Headquarters was 245.1 mm from 1915 to 1995, with a standard deviation of 85.0 mm(Wainwright 2006a). More than half of this precipitation occurs during

summer monsoon events (Gao et al. 2003, Bestelmeyer et al. 2004). The mean annual air temperature at the JER headquarters was 14.70°C with a standard deviation of 0.58°C between 1915 and 1993 (Wainwright 2006). Vegetation at shrubland study site is dominated by a mix of creosote bush (*Larrea tridentata*) and honey mesquite (*Prosopis glandulosa*). Creosote bush is an evergreen, drought-resistant C4 perennial shrub (Peters et al. 2006). Honey mesquite is a deciduous, thorny, long lived C4 shrub that is characterized by very deep and laterally extensive root systems (Peters et al. 2006). Other species found at the site include tarbush (*Flourencia cernua*), the grass bush muhly (*Muhlenbergia porter),* fluff grass (*Dasyochloa pulchella*), as well as a variety of mostly annual forbs. Mean shrub canopy height is approximately 2.0 m and in similar shrublands elsewhere on the JER.

This site was chosen in 2008 to be representative but meet constraints of EC technologies. Site was built out during 2009 to be fully operational by mid-2010 and includes EC tower, robotic tram system that measures hyper spectral reflectance, phenocams, phenostations, phenology observations, soil respiration plots, solar power. Study area includes footprint of EC tower that is maintained devoid of human interference and bordered by phenology transects, tramline area, and experimental study area. This research was sponsored by NSF-CREST training grant and has included students from environmental science, computer and computational sciences working across traditional disciplines to advance our knowledge of properties and processes related to desert shrubland ecosystem structure and function.

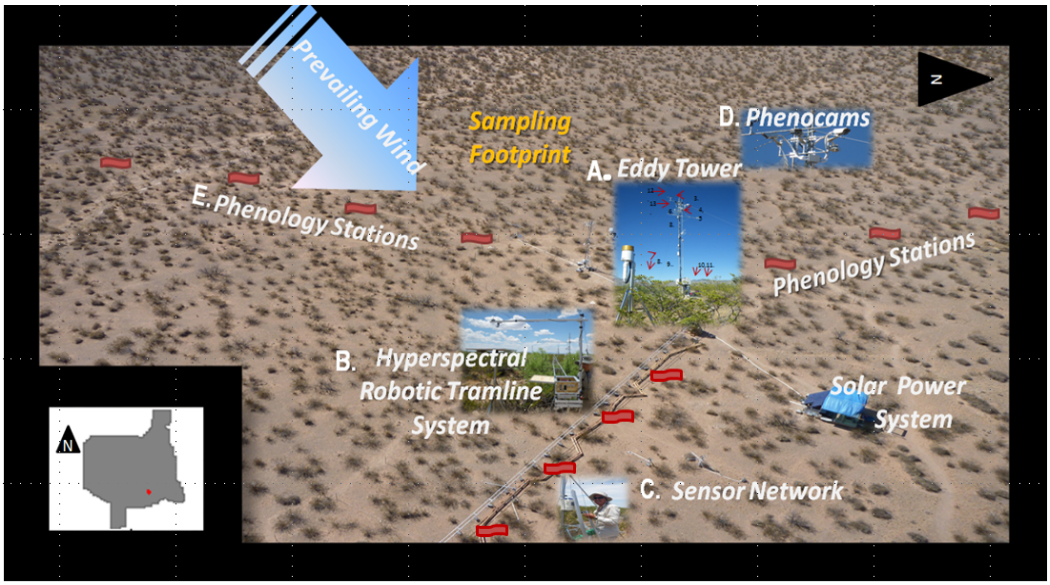


**Figure 6** Schematic of the study site on the JER taken from a kite aerial photography system by Craig Tweedie, April 2011. Inset: Bottom left red circle represents station's location within the JER area, which is outlined in gray. A) Extended open path eddy covariance tower. B) Robotic tramline system that measures hyper spectral reflectance. C) Micrometeorological and phenostations sensor network. D) Phenology cameras, E. Phenology stations. Blue arrow indicates predominant wind direction. Yellow font indicates the dominant flux tower footprint. Instrumentation is mostly powered from a remote solar and battery system, which also powers point to point and local area Wi-Fi communications at the site.

### 2.3.2 Biophysical Measurements and Data Analysis

***Microclimatic measurements and open path eddy covariance system***

The open path eddy covariance system consists of 22 instruments distributed on a 10m height tower. Instrumentation consists of a three dimensional sonic anemometer (CSAT3-SONIC CSI), an infrared gas analyzer (IRGA, LI-7500 Li-COR Inc) located at 5m height, a four-component net radiometer situated 20m to the east of the main eddy covariance tower at a height of 3m (CNR1- Kipp and Zonen), a photo-synthetically active radiation sensor (PAR-LITE - Kipp and Zonen) located at 10m height, a temperature and humidity sensor (HMP45C-L - CSI) at 5m height, a barometer (CS106 –CSI) located inside an enclosure about 1.30m height, a 2D anemometer (03002-L -CSI)at 10m height, a tipping bucket rain gauge (TE525-L), eight probes to measure soil temperature and volumetric water content (ECTM – decagon), and four soil heat flux plates (HFP01 Hukseflux CSI). Soil instruments are distributed into two subsystems of soil profiles installed to capture underground temperature, volumetric water content, and heat from underneath a mesquite and bare soil. These profiles are located at 2cm, 10cm, 15cm and 20 cm depth. All data is collected and stored in a Campbell Scientific CR3000 data logger. The system is powered by a 300W 10-panel solar array. The solar panels are mounted on an aluminum structure located 35m north and downstream of prevailing winds at the EC tower. The panels face south to maximize battery recharge. The system uses four 12VDC sealed deep cycle batteries, and the load is regulated through a morning start ProStar 15 Amp 12/24 charge controller. Data files are stored on a 2GB card and are retrieved remotely using an internet connection. This connection is established by a Virtual Private Network that passes via a point to point Wi-Fi connection that links an antenna situated at 9m on the eddy covariance tower to the headquarters of the JER from where it then routes to UTEP servers through hardwired Ethernet.

The system also provides a 500m Wi-Fi bubble from an Omni-directional antenna situated at 5m on the eddy tower and connects multiple wireless devices associated with the local sensor network at the study site.

Adherence to manufacturer protocols for installation, maintenance, and calibration have been persistent to assure proper system performance (Campbellsci 2004, 2005, 2009; Zonen 2004). The IRGA has been calibrated against a gas mixture of 500 ppm $CO_2$ and water vapor was calibrated with a dew point generator (Li 610, Li-COR Inc). The IRGA was zeroed for $CO_2$ and water vapor using 99.99% nitrogen gas. With adherence to the protocol, 30 min fluxes were calculated from fast response instrumentation and independent measurements from slower response sensors were used to measure and calculate background meteorological variables. Data collection and data processing was assessed and validated by an scientist who visited the site in late August 2012 and utilized a portable eddy covariance system and the custom MATLAB processing routine.

***Flux calculations, QA/QC and data gap filling***

Flux calculations were computed with EddyPro $^{TM}$ 4.1 software. Following, a moving average window of 5 days was used to reject spikes following the method described by Lee et al. (2004). To eliminate the influence of the stable lower boundary conditions, all flux data recorded with a friction velocity threshold (u*) less than $0.1ms^{-1}$ were discarded. Day and night time separations of net ecosystem exchange were based on threshold values of 10umol for photosynthetic photon flux density. Gap filling and flux partitioning performed using the method described by Lasslop et al. (2010). This method was used to estimate gross primary production (GPP) using equation 1 as described by (Reichstein *et al.* 2012). Gap filled fluxes were used to

estimate annual budgets of component ecosystem fluxes, however, data with gaps were used in further statistical analysis. Half hourly meteorological data were gap filled using image Inpainting method (Ramirez *et al.* 2012).

$$GPP = R - NEE$$ *Equation 1* (Reichstein *et al.* 2012)

The results obtained with the use of eddy covariance system represent the average functioning of land-atmosphere interactions within the footprint area. Footprint size is a combination of measurement height, atmospheric conditions such as wind speed and stability and surface characteristics (Kjun et al. 2004) and was calculated using a combination of the footprint models from (Kormann et al. 2001) and (Kjun *et al.* 1997) made functional by EddyPro 4.1.0 (LICOR 2011). The 90% daytime footprint contribution distance reached a yearly average of 370m.

***Greenness index and phenology monitoring***

Landscape greenness, a measure of vegetation productivity and photosynthetic capacity (Kurc and Benton 2010), was derived as the 2GRBi index (Richardson *et al.* 2007) calculated from digital photography acquired by three phenocams situated at 9m on the eddy covariance tower. Phenocams each span approximately 170º from South to Northwest view of the flux tower footprint (webcam model Vx7000, with 1600 x 1200 pixel resolution (2 MP), 58° of horizontal view angle, with a manually fixed focus for the specific experimental area). This analysis only considered daily images taken at noon. Then an analytical estimation of 2GRBi index was calculated from Red-Green-Blue (RGB) channel intensities extracted by a custom software

written in MATLAB® 7.8.0 and reported by Gonzalez (2011). The growing season was defined as the day by which overnight change in temperature is less than 10°C.

Phenophase development was monitored since March 2010 on three transects (Figure 7). Foliar growth and reproductive phenological cycles of the five perennial shrubs and grasses at the area of study were monitored weekly by fellow graduate students (Gonzalez 2011). The choice of plants for phenological observation followed protocols developed by the US National Phenology Network USA-NPN (for additional information, see http://www.usanpn.org). Phenophases included categories for leaf development (breaking leaf buds, leaves), flower development (open or unopened flowers), and the status of fruit (ripe or unripe fruits). A detail description of this measurements is provided on Gonzalez (2011).

### 2.3.3 Statistical modeling: Analysis of the biophysical controls of ecosystem fluxes

The success of this study is the need to ascertain the relative importance of how multiple biophysical factors interact to control ecosystem fluxes of carbon. To further investigate these relationships, and to evaluate the relative importance of biophysical controls and the specific relationships between the most important biophysical controls and associated thresholds of ecosystem fluxes, I used random forest method whose performance is similar to some machine learning methods (i.e. boosting, neuronal networks, etc.); however, it is simpler to implement (Hastie et al. 2011). In this study random forest models were constructed using an implementation written for the R statistical system by Breiman and Cutler (2013).

Random forest (RF) is an improved version of recursive partitioning methods (regression tree) which have become increasingly popular in ecological studies as predictive models that allow the user to overcome multicollinearity between predictors (Karels *et al.* 2004). In a standard regression tree analysis, response data are recursively split into groups based on the values of predictor variables. Tree models can represent complex, non-linear relationships between variables, because the same predictor variable can appear at multiple branch points (Cutler *et al.* 2007). However, tree algorithms tend to over-fit the data, and cross-validation is required to determine their predictive power. When predictors are strongly inter-correlated, tree models select arbitrarily among them, which can lead to a loss of information and biological plausibility in the final tree (Karels *et al.* 2004). Random forest techniques allow the user to overcome these limitations by reducing the variance in the output assembly of trees by building an ensemble classifier using a combination of many decision trees (i.e. a "forest" of individual trees), where the largest possible trees are grown and bootstrapped sampled versions of the training data are averaged. The result of the random forest analysis is an unbiased and low variance classification (Hastie *et al.* 2011). The mean squared error (MSE) was calculated for each tree by comparing its predictions for the out-of-bag data set with observed values in order to generate an estimate of the percent of variance in the response variable that could be explained by the tree. These values are averaged over the entire 'forest' of regression trees to produce a cross-validated estimate of model fit (Liaw & Wiener 2002a; Archer & Kimes 2008). In addition to its benefits when compared to standard regression tree models, the random forest algorithm is a robust alternative to more common multivariate techniques like multiple linear regression and other types of generalized linear models. These methods, although familiar and relatively simple to interpret, are highly sensitive to multicollinearity, and require the explicit specification of

interactions between variables at a cost of increased model complexity. In contrast, random forest models are relatively insensitive to the distributions of predictor variables. The characteristics of random forest models make them particularly well-suited to complex analyses with large numbers of potentially important predictor variables (Cutler *et al.* 2007).

### *Variable of importance*

Random forest analysis also aids the evaluation of the relative importance of predictor variables for output decision tree (Breiman and Cutler 2013). Model-averaged variable importance estimates can be generated using out-of-bag data (Archer and Kimes 2008), and can be interpreted heuristically in much the same used when results are averaged across multiple generalized linear models (Burnham and Anderson 2002). To calculate variable importance, out-of-bag values for a given variable and trees are randomly permuted, and the tree mean squared error (MSE) is then estimated using both the original and the permuted out-of-bag data set. The resulting percent increase in MSE reflects the predictive power of that variable compared to random chance. Model-averaged variable importance values reflect the mean influence of a variable on model fit, regardless of which other variables are included. Because they are generated stochastically, model-averaged variable importance values can vary slightly between model runs. As a result, the rank order of variables with similar importance may vary on a run-by-run basis, which can complicate the interpretation of model output. However, if the top-ranked variables in a random forest result have substantially higher importance values than all others, their position should remain unchanged from run to run. Random forest analysis also allows for the examination of relationships between individual and combined predictor variables using partial dependence plots, which is a tool to visualize the effects of single or multiple

variables on the regression models. In essence, partial dependence functions represent the effect(s) of the examined predictor variable after accounting for the average effects of all other predictors.

### *Model structure*

Random forest model were constructed by using as input daily mean values of all predictor variables that are hypothesized as operating drivers of ecosystem fluxes at local scale (Table 2). In this model, ecosystem fluxes of carbon, water, and energy are hereafter referred as responses and the output variables of importance are recognized as predictors. In this study, 500 regression trees were generated using random forest methods based on bootstrap samples (random sampling with replacement). The model-averaged percent variance explained, which can be interpreted similarly to the $r^2$ value of a multiple regression model, us used to evaluate the relative support for each of alternative hypotheses.

**Table 1** Biophysical predictors used to estimate drivers of fluxes

| ***Variable*** | ***Description*** | ***Units*** |
|---|---|---|
| AT | Air temperature | °C |
| ST1 | Soil temperature (2cm depth) | °C |
| ST2 | Soil temperature (10cm depth) | °C |
| VPD | Vapor pressure deficit | KPa |
| 2GRBi | Greenness index | Unitless |
| volumetric water content1 | Volumetric water content (2cm depth) | $m^3/m^3$ |
| volumetric water content2 | Volumetric water content (10cm depth) | $m^3/m^3$ |
| WS | Wind speed | m/s |
| WD | Wind direction | Degrees |
| SH1 | Soil heat flux (5cm depth) | $W/m^2$ |
| SH2 | Soil heat flux (15cm depth) | $W/m^2$ |
| PAR | Photosynthetic active radiation | $umol/m^2$ |
| Rg | Net radiation | $W/m^2$ |

### *Model validation*

Further exploration of the response variables and top ranked predictors was performed through response curves and partial dependence plots. This exploration was done to assess the potential thresholds on the predictors of ecosystem fluxes. Furthermore, results from the random forest were validated by using deterministic model via multilinear regression model. The quadratic model was then selected as an intermediate choice for modelling data that has no linear correspondences. The model formulation was built for a five dimensional parameter space (Equation 5). The quadratic modeling reduces to finding the coefficients a0, a1 and a3 tp a5 of the quadratic function represented on equation 8. The correspondence between predicted and observed values was determined by the use of the coefficient of determination ($r^2$) to assess the predictive ability the random forest model. The implementation of this model was done in

Matlab. Initially the model was trained using 2010-2012 data. However, 2013 data was used independently to test the predictive ability of the top five predictors of the random forest model. Finally, a sensitivity test was conducted to verify the number of predictors that explained most of the variance of ecosystem fluxes. This test consisted on modifying the dimensions of the quadratic model and subsequently finding the coefficient of determination ($r^2$) to assess the predictive ability of using only one to five of the top predictors identified by the random forest tree.

$$F(x) = a_0 + a_1x_1 + a_2x_2 + a_3x_3 + a_4x_4 + a_5x_5$$
$$+ a_{11}x^2_1 + a_{12}x_1x_2 + a_{13}x_1x_3 + a_{14}x_1x_4 + a_{15}x_1x_5$$
$$+ a_{22}x^2_2 + a_{23}x_2x_{23} + a_{24}x_2x_4 + a_{25}x_2x_5$$
$$+ a_{33}x^2_3 + a_{34}x_3x_4 + a_{35}x_3x_5$$
$$+ a_{44}x^2_4 + a_{45}x_4x_5$$
$$+ a_{55}x^2_5$$

$$\boldsymbol{f(NEE) = (x1', x2', x3', x4', x5')}$$

*Equation 2 Quadratic modeling reduces to finding the coefficients a0, a1 and a3 to a5*

## 2.4. RESULTS

### 2.4.1. Biophysical environment 2010-12

Mean annual rainfall for 2010 to 2012 was 148.8mm. A regional absence of precipitation between DOY 294 in 2010 to DOY 182 in 2011 was recorded as the longest period between rain events since 1953 (NOAA, 2011). The minimum and maximum annual precipitation registered at the study site was 98.4 mm in 2011 and 191.5 falling in 2010 respectively. Peak rainfall in each year of study occurred between July and August with sporadic fall/winter rains between October-January (Figure 7).

The mean annual temperature during 2010-2012 was 16.6 °C. The minimum temperature recorded at the site was -24.4°C on DOY 32 of 2011. The maximum recorded was 37.9 °C on DOY 175 of 2011. Peak mean monthly temperatures occurred in June and August when the monthly average oscillated around 35°C (Figure 7).

The mean annual wind speed during 2010-2012 was 3.32 m/s. Mean wind speeds were highest from April, May, and June. The mean monthly maximum wind speed was 4.66 m/s in May 2011. The lower mean monthly wind speed occurred in August 2011 (2.5 m/s). Summer months have lower average wind speeds, but with important gust related to afternoon atmospheric convection. The dominant wind direction is WSW (Figure 7)

On the annual basis the vapor pressure deficit averaged 1.33KPa. The year with the highest vapor pressure deficit was 2011 with 1.57KPa. The following year, vapor pressure deficit decreased considerably to 1.09 KPa (Figure 8).

The characteristics of the soil profile located under the bare soil (BS) were significantly different to those from the soil profile system located under mesquite (UM). Soil heat fluxes were very similar in the deep profiles (15cm) in both BS and UM. However, surface soil heat fluxes were in average 5W/$m^2$ higher in BS than UM. This difference is more conspicuous during June, the month with the highest monthly mean soil heat (4.90 W/$m^2$ in 2012, 4.36 W/$m^2$ in 2011, and 3.99 W/$m^2$ in 2012). The mean annual soil heat flux was 0.40 W/$m^2$ at BS 5cm in 2010, 2.24 W/$m^2$ at BS 5cm in 2011, and 1.82 W/$m^2$ at BS 5cm in 2012. Whereas, the mean annual soil heat flux on at 15cm -073 W/$m^2$ in 2010, 0.0084 W/$m^2$ in 2011, -0.195 W/$m^2$ in 2012. The profile system located under mesquite recorded at 5cm -0.145 W/$m^2$ in 2010, 0.388 W/$m^2$ in 2011, -0.198 W/$m^2$ in 2012; whereas, the mean annual soil heat flux on at 15cm -015 W/$m^2$ in 2010, 0.39 W/$m^2$ in 2011, -0.20 W/$m^2$ in 2012 (Figure 9).

Peak mean monthly soil volumetric water content occurred in July 2010 when the mean water content was 0.19 $m^3/m^3$, and lowest mean monthly soil volumetric water content was recorded was 0.02 $m^3/m^3$ in March of 2011. In the bare profile system, the mean annual volumetric water content was 0.13 $m^3/m^3$ at 5cm, 0.09 $m^3/m^3$ at 10cm, 0.07 $m^3/m^3$ at 15cm, and 0.05 at 20cm depth in 2010. In 2011, the mean annual volumetric water content was 0.09 $m^3/m^3$ at 5cm, 0.08 at 10cm, 0.07 at 15, and 0.05 at 20cm. In 2012, the mean annual volumetric water content was 0.06 $m^3/m^3$ at 5cm, 0.06 $m^3/m^3$ at 10cm, 0.055 $m^3/m^3$ at 15cm, and 0.055 $m^3/m^3$ at 20cm depth. In the profile system located under mesquite, the mean annual volumetric water content was 0.13 $m^3/m^3$ at 5cm, 0.11 $m^3/m^3$ at 10cm, 0.08 $m^3/m^3$ at 15cm, and 0.04 $m^3/m^3$ at 20cm depth in 2010. In 2011, the mean annual volumetric water content was 0.06 $m^3/m^3$ at 5cm, 0.06 $m^3/m^3$ at 10cm, 0.05 $m^3/m^3$ at 15cm, and 0.05 $m^3/m^3$ at 20cm depth. In 2012, the mean

annual volumetric water content was 0.08 $m^3/m^3$ at 5cm, 0.08 $m^3/m^3$ at 10cm, 0.05 $m^3/m^3$ at 15, and 0.05 $m^3/m^3$ at 20cm (Figure9).

The mean annual soil temperature ranged from 20.39°C to 19.30°C in BS and from 20.83°C to 18.78°C in UM system. In profile system located under mesquite, the mean annual temperature was 20.83°C at 5cm, .20.41°C at 10cm, 19.03°C at 15, and 18,78°C at 20cm in 2010. In 2011, The mean annual temperature at 5cm depth was 20.51 °C at 5cm,.20.28°C at 10cm, 19.30°C at 15, and 19.14°C at 20cm. In 2012, the mean annual temperature was 20.06°C at 5cm,.19.86°C at 10cm, 19.04°C at 15, and 18.99 at 20cm depth. The minimum soil temperature recorded was °C on July 2011 and the maximum 33.2 °C on 2011. Peak mean monthly soil temperature occurred on July 2011 when the average was 33.2°C, and lowest mean monthly soil temperature was recorded in January 2011 (Figure 9). Overall, there was a most significant difference on soil profiles was shown in volumetric water content. Soil water content on bare soil reaches deep soil layers faster than under mesquite. Soil temperature was pretty similar on both systems. Average temperature of soil profiles closely follow air temperature patterns, however temperatures cool down as they reached 15cm depth (Figure9).

The estimated growing season length was 166.6 days. The initial day varied each year starting on DOY 110 in 2010 and 2012, and DOY 190 in 2011. The initial growing season seems to be trigger by creosote and mesquite leave phenophase (Figure 10). The peak of the growing season occurred between DOY 150 – 250. There was an 80 day delay in the star of the growing season in 2011, which is largely attributed to the dry conditions described for that year (Figure 7).

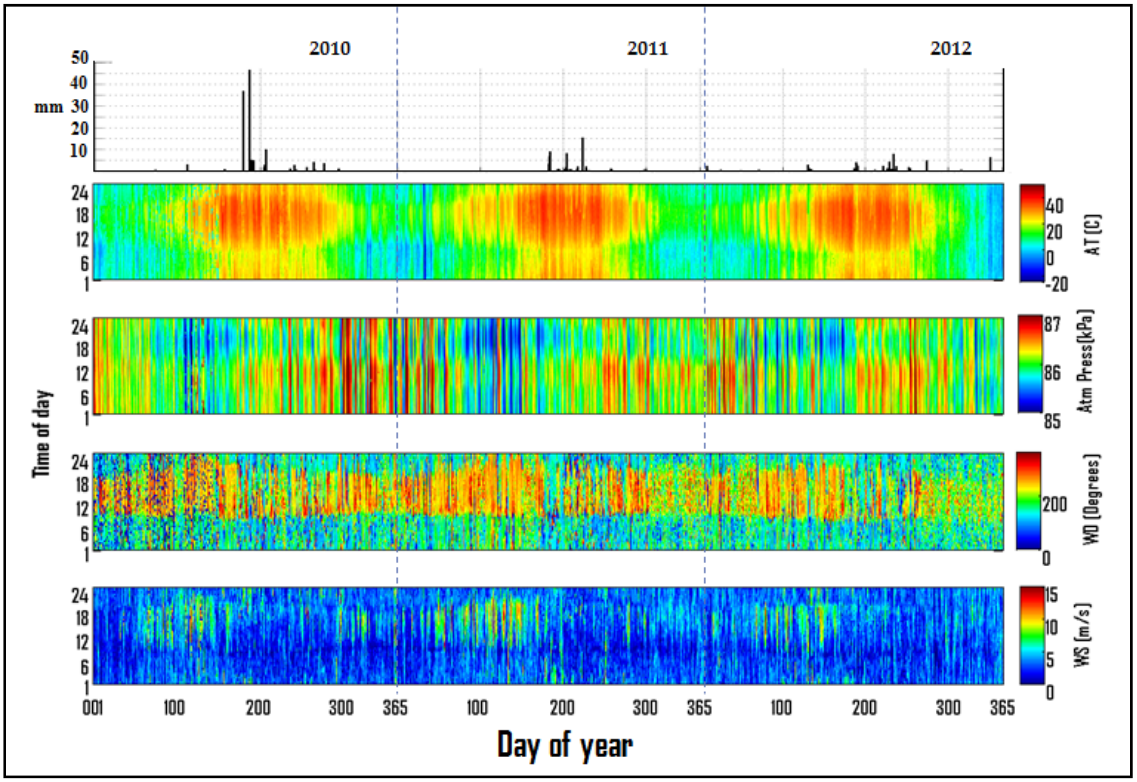


**Figure 7** Seasonal climatology of the area from 2010 to 2012. A) Daily precipitation in mm. 30-min data of: B) Air temperature in C, D) Atmospheric pressure, E) Wind direction, F) Wind Speed.

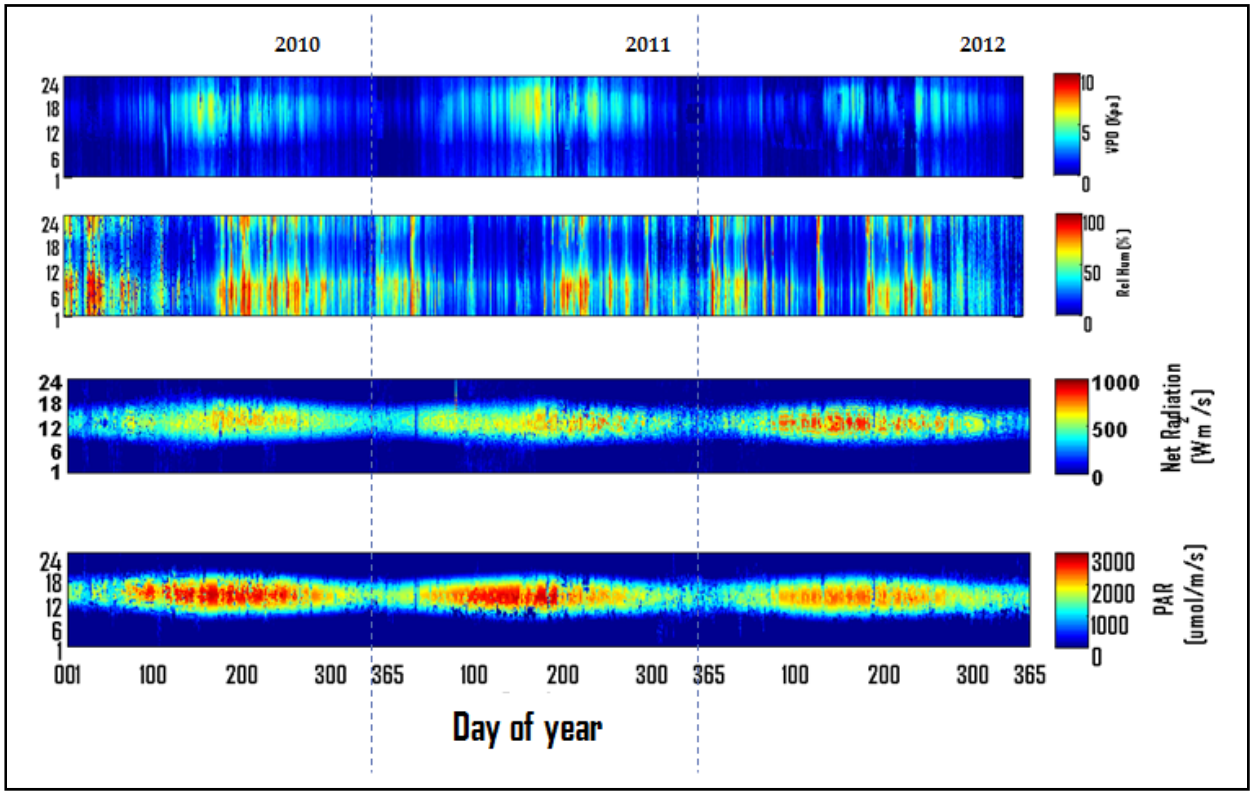


**Figure 8** . Seasonal climatology of the area from 2010 to 2012. 30-min data of: A) Vapor pressure deficit, B) Relative humidity, C) Net radiation, D) Photosynthetic active radiation.

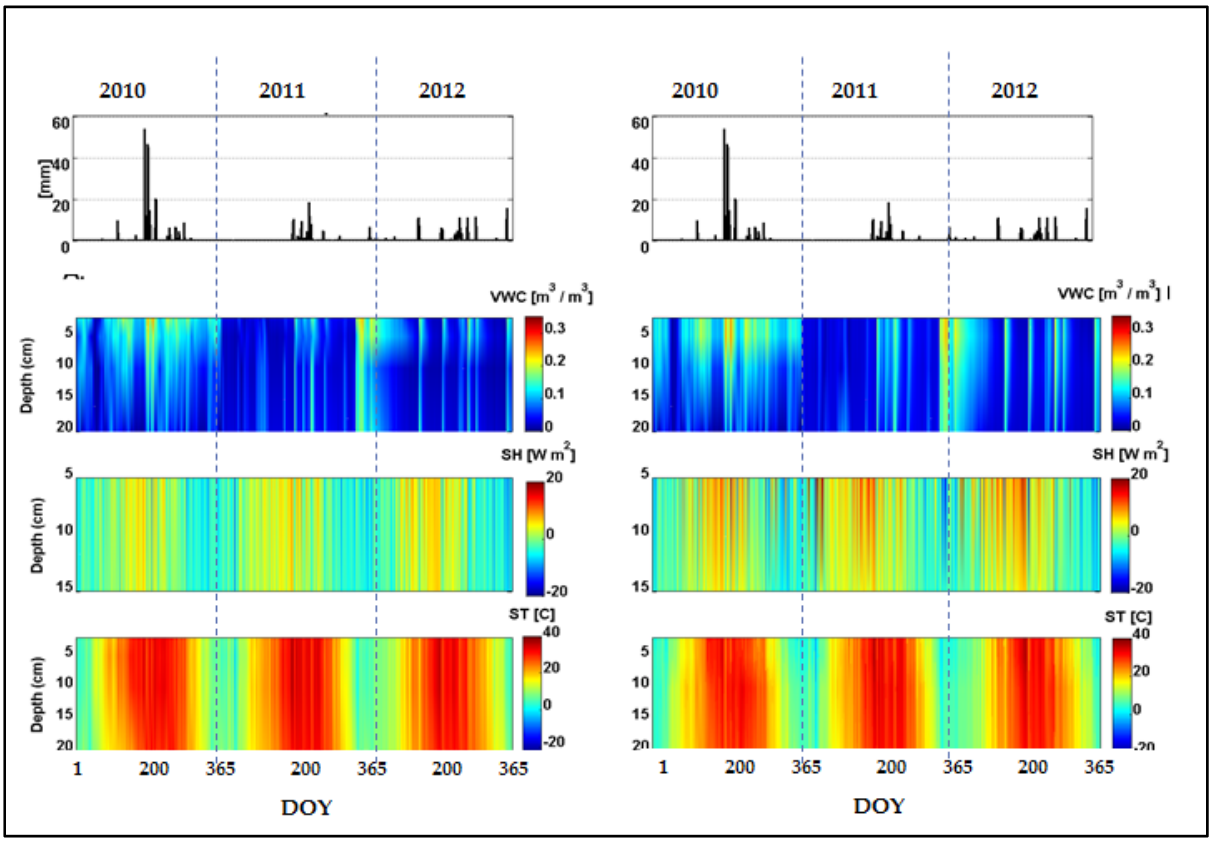


**Figure 9** Soil profiles a. under a mesquite and b. under bare soil.

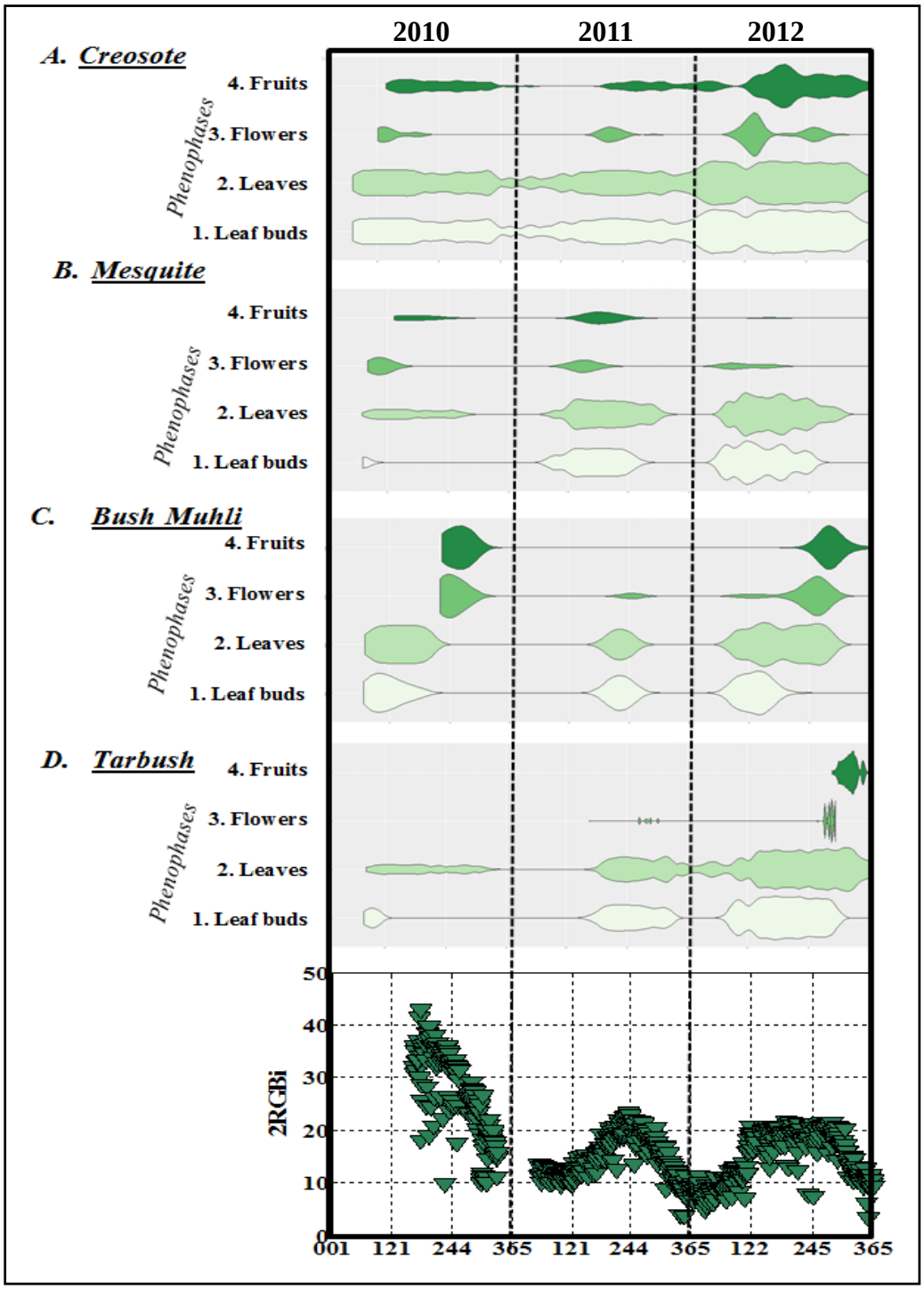


**Figure 10** Violin plot indicating the occurrence of Phenophases of the four main vegetation types encountered along the footprint of the eddy covariance tower. 2GRBi index is shown to compare the relationship with the occurrence of green-up and peak 2GRBi. Note: Phenology data were collected by Libia Gonzalez, Christine Laney, and Naomi Luna. Violin Plot was taken from phenology shiny app by Laney (2013).

### 2.3.2. Ecosystem fluxes

#### *2.3.2.1 Carbon*

Diurnal variations

The system acted as an incipient source of carbon at night between 19:00 pm and 6:00 am. Carbon uptake starts right after 6:00 am; the maximum uptake is reached around 1:00pm, with slight variations per year. For instance, in 2010 the maximum uptake was reached at 10:00 am and sustained until 4:00pm, whereas in 2011 the maximum carbon uptake was constrained to a 1hour period between 16:00pm to 15:00pm, and in 2012 the carbon uptake was very similar to the diurnal pattern found in 2011, however, it reached higher magnitude. Respiration rates tend to close or flat to zero during the peak of carbon uptake. Overall, respiration tends to zero, however, in 2011 respiration slightly shifted towards a more positive diurnal trend (Figure 11).

*Seasonal* variations

The peak of carbon uptake occurred around DOY 120 in the three years of the period of study. In 2010, there were two maximum peaks of carbon uptake, the 1$^{st}$ occurred around DOY 108, and it lasted 35 days; and the 2$^{nd}$ occurred in DOY 207 and it was sustained for 27 days. In 2011 there was only one maximum peak of carbon uptake in DOY 96 and some other scattered dates in DOY 129-132. The most conspicuous event in 2011, was that the system became a small source of carbon to the atmosphere from DOY181 to DOY 192 reaching values of 1.8gCm$^{-2}$. In 2012, there was also one maximum peak of carbon uptake between DOY 105 and DOY160. The peaks of maximum ecosystem respiration occurred in 2010 between DOY 19 to DOY 30 during

this period ecosystem respiration reached values above $3gm^2$. The second peak of respiration in 2010 occurred in between DOY 191 to DOY 206, the magnitude was slightly above 33gm^2. The magnitude of ecosystem respiration in 2011 was lower than in the previous year; the peaks maxima occurred in DOY 30 (2.1), the $2^{nd}$ occurred on DOY 180 (2.3), and the third on DOY 256 (2.33).

Annual *variations*

During the period of study the site was a small carbon sink. Annual fluxes ranged between $-78.80gCm^{-2}\ y^{r-1}$ in 2010 to $-130.85gCm^{-2}\ y^{r-1}$ in 2012. The difference in NEE between the relatively wet year in 2010 and the severe dry year of 2011 was approximately $-10gC\ m^{-2}\ y^{r-1}$. Annual budget of carbon uptake ranged from $221.3gC\ m^{-2}$ in 2010 to $215.9gC\ m^{-2}$ in 2012, annual carbon uptake decreased in 2011 to $131.3gC\ m^{-2}$. Ecosystem respiration ranged from 142.5 $gC\ m^{-2}$ in 2010 to 85.05 $gC\ m^{-2}$ in 2012, annual ecosystem respiration in 2011 to 65.83 $gC\ m^{-2}$.

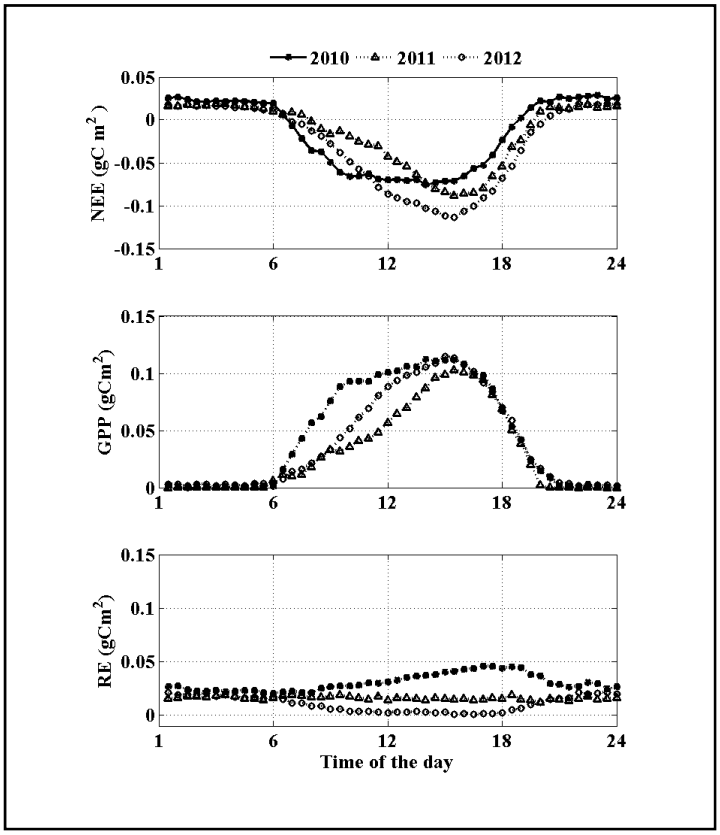


**Figure 11** Diurnal variation of carbon, latent and sensible heat during 2010-2012

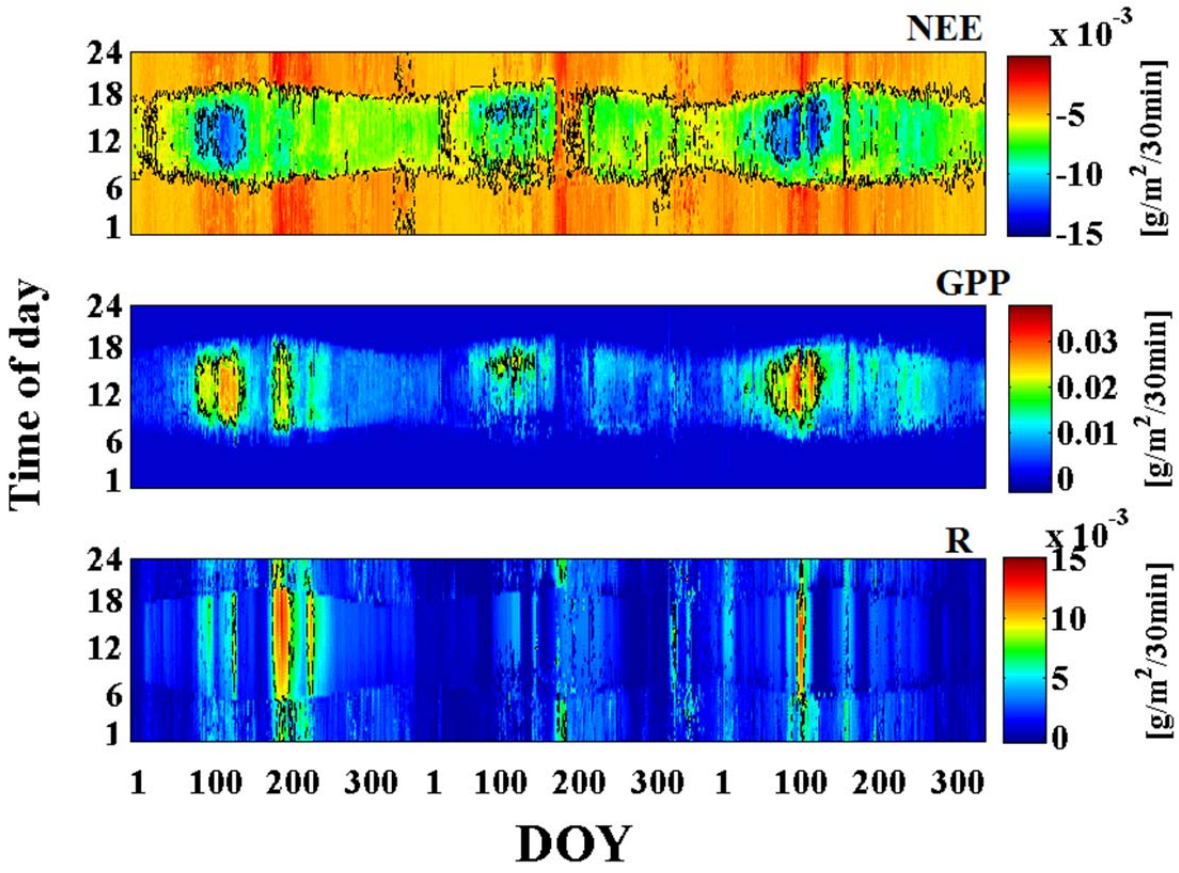


**Figure 12** Time series of net ecosystem exchange, gross primary productivity, and respiration.

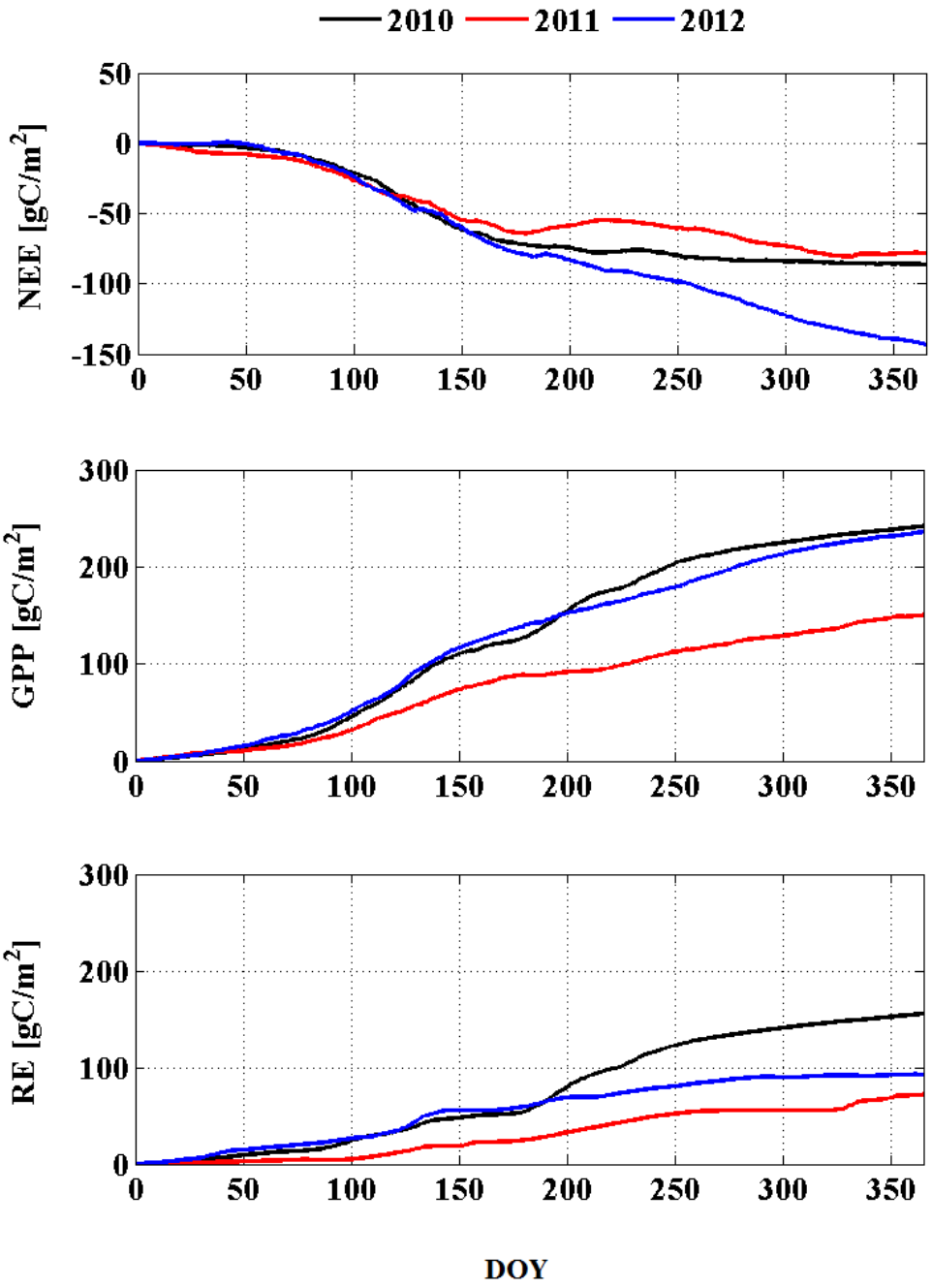


**Figure 13** Annual cumulative of ecosystem fluxes.

**Table 2** Summary table

| | | 2010 | 2011 | 2012 |
|---|---|---|---|---|
| **Carbon [$g\ m^{-2}\ yr^{-1}$]** | *NEE* | -78.80 | -65.47 | 130.85 |
| | *GPP* | 221.3 | 131.3 | 215.9 |
| | *R* | 142.5 | 65.83 | 85.05 |
| **Air Temperature [°C]** | *Mean* | 16.38 | 17.38 | 16.27 |
| | *Min* | -9.80 | -24.40 | -10.10 |
| | *Max* | 38.60 | 37.90 | 38.00 |
| **Precipitation [mm]** | *Total* | 191.5 | 98.4 | 138.6 |
| | *Num of Days* | 32 | 29 | 37 |

### 2.3.3 Biophysical drivers of ecosystem fluxes

The overall variance explained by using the random forest analysis ranges from 60% to 98%.The analysis of variables of importance of top ranked predictors of ecosystem fluxes of carbon, were selected by using the highest increase percent of mean square error that was above 20%. This is an indication that after multiple permutations each response variable had two to five predictors whose mean square error is still high enough to control the response of ecosystem fluxes. Results of the sensitivity test to estimate how many predictors explained most of the variance of ecosystem fluxes indicates that about 85% and 95% of the variance of R, GPP and NEE is explained by the interaction of five top predictors, whereas, only three top predictors explained 82% and 93% of the variance of sensible heat and latent heat flux (Table 3).

Results from the variable of importance of the random forest analysis indicates that ecosystem fluxes of carbon were controlled by the interactions of temperature (air and soil temperatures at 10cm depth), energy component (either net radiation, photosynthetic active radiation, or soil heat radiation), greenness index, and water availability from the soil as estimated as volumetric water content, and vapor pressure deficit. Although, these variables are the primary controls of ecosystem fluxes, their relative importance differs among ecosystem fluxes of carbon (Figure 18).

The analysis of the partial dependence plots (Figure 18) indicate that thresholds of the biophysical controls that stimulate carbon uptake in the system is mainly controlled by Soil temperature at 10cm depth, air temperature between 15°–25°C; photosynthetic active radiation higher than 500 umol/ $m^2$/day; greenness index above 60, volumetric water content at 10cm

depth above 0.8$m^3/m^3$; and, a critical threshold lower than 1KPa. Ecosystem respiration responds positively to a wider range of air and soil temperature between 10° and above 30°C; also, when net radiation is above 80 $W/m^2$/day and greenness index around 40 and above 120.

**Table 3**. Coefficient of determination ($R^2$) of random forest predictions and observed response variables.

| ***Predictor*** | ***NEE*** | ***GPP*** | ***R*** |
|---|---|---|---|
| ***#of Predictors*** | | | |
| 1 | 0.42 | 0.44 | 0.20 |
| 2 | 0.52 | 0.57 | 0.56 |
| 3 | 0.62 | 0.88 | 0.78 |
| 4 | 0.82 | 0.92 | 0.84 |
| 5 | 0.94 | 0.96 | 0.85 |

n= 1095

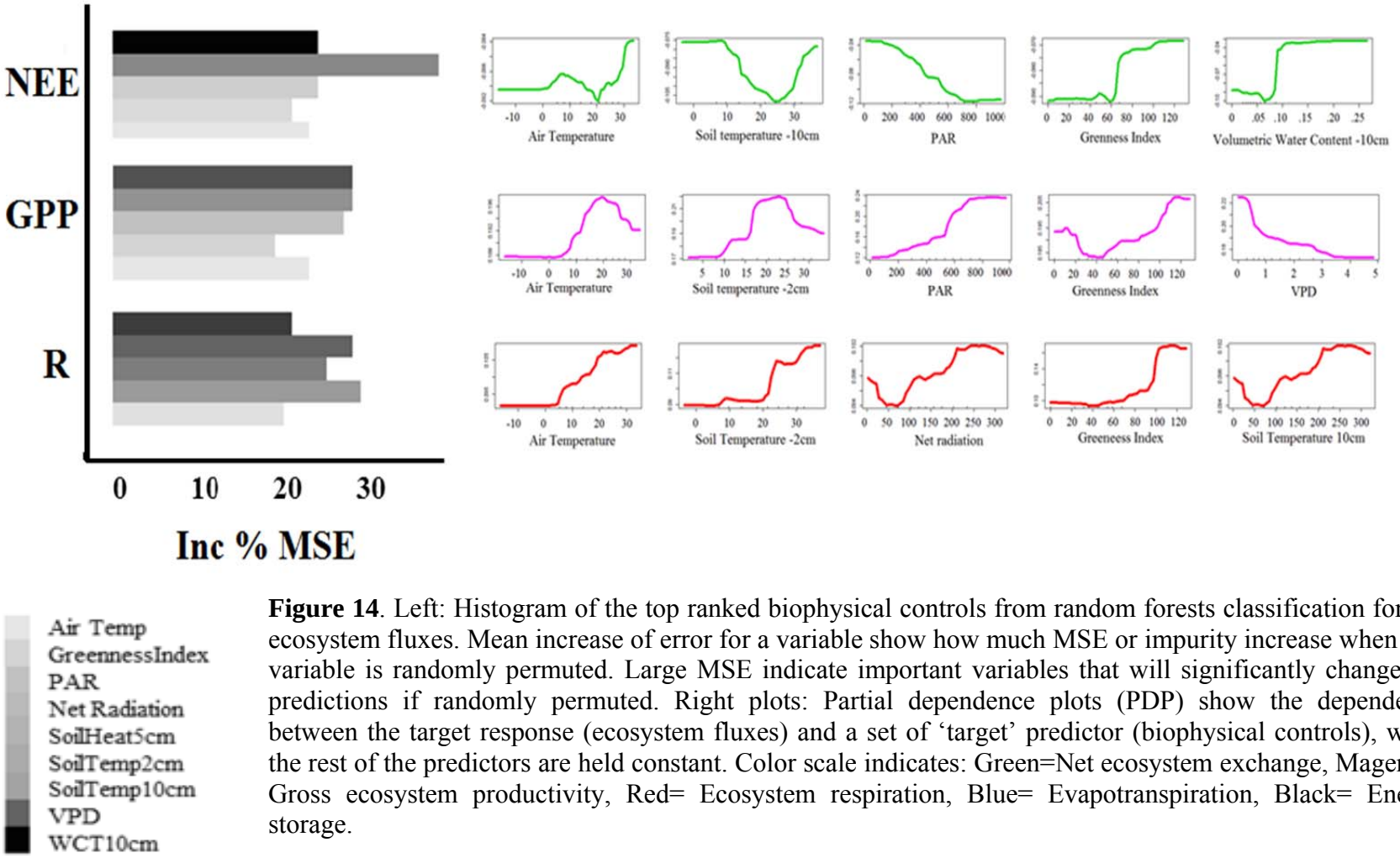


**Figure 14**. Left: Histogram of the top ranked biophysical controls from random forests classification for net ecosystem fluxes. Mean increase of error for a variable show how much MSE or impurity increase when that variable is randomly permuted. Large MSE indicate important variables that will significantly change the predictions if randomly permuted. Right plots: Partial dependence plots (PDP) show the dependence between the target response (ecosystem fluxes) and a set of 'target' predictor (biophysical controls), when the rest of the predictors are held constant. Color scale indicates: Green=Net ecosystem exchange, Magenta= Gross ecosystem productivity, Red= Ecosystem respiration, Blue= Evapotranspiration, Black= Energy storage.

#### *2.3.2.1 Random forest validation*

Response curves of the biophysical drivers of NEE showed a non-linear relationship between them. Results from the deterministic model shown the $r^2$ of the predicted NEE versus observed NEE values ranged from 0.5 to 0.93, corresponding to 1095 observation to 36 observations respectively (Table 4). Results from 2013 as independent data set to validate the model were $r^2$=0.7 for monthly data, and $r^2$=0.26 for daily data

**Table 4** Summary of deterministic models

| | ***Daily*** | ***Monthly*** |
|---|---|---|
| p-value | <0.001 | <0.001 |
| $R^2$ | 0.5054 | 0.9347 |
| Norm of Residuals | 11.6667 | 0.4756 |
| X1 | 5.1202 | 5.4200 |
| X2 | 6.9792 | 7.0796 |
| X3 | 351.2201 | 292.6700 |
| X4 | 11.0159 | 12.0100 |
| X5 | 4.5694e-04 | 0.0014 |

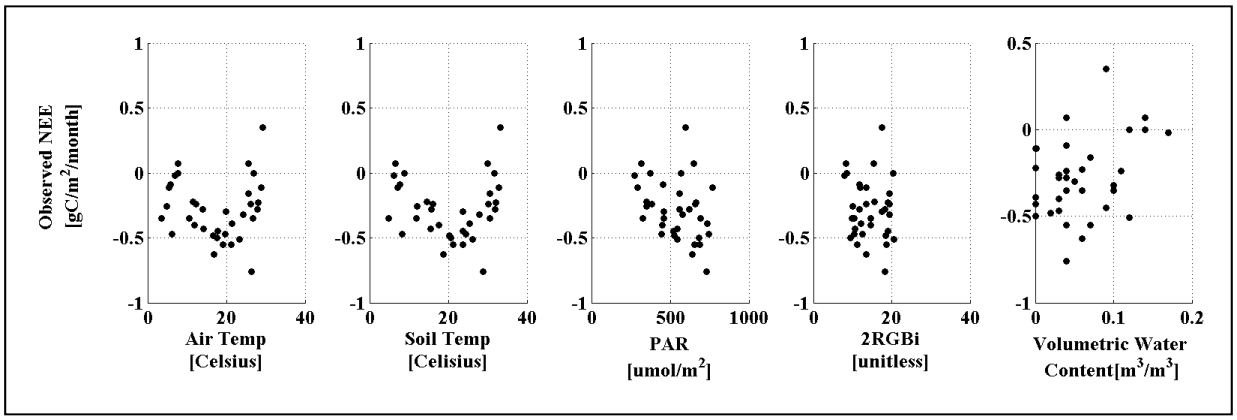


**Figure 15** Response curves of NEE and biophysical variables 2013 data

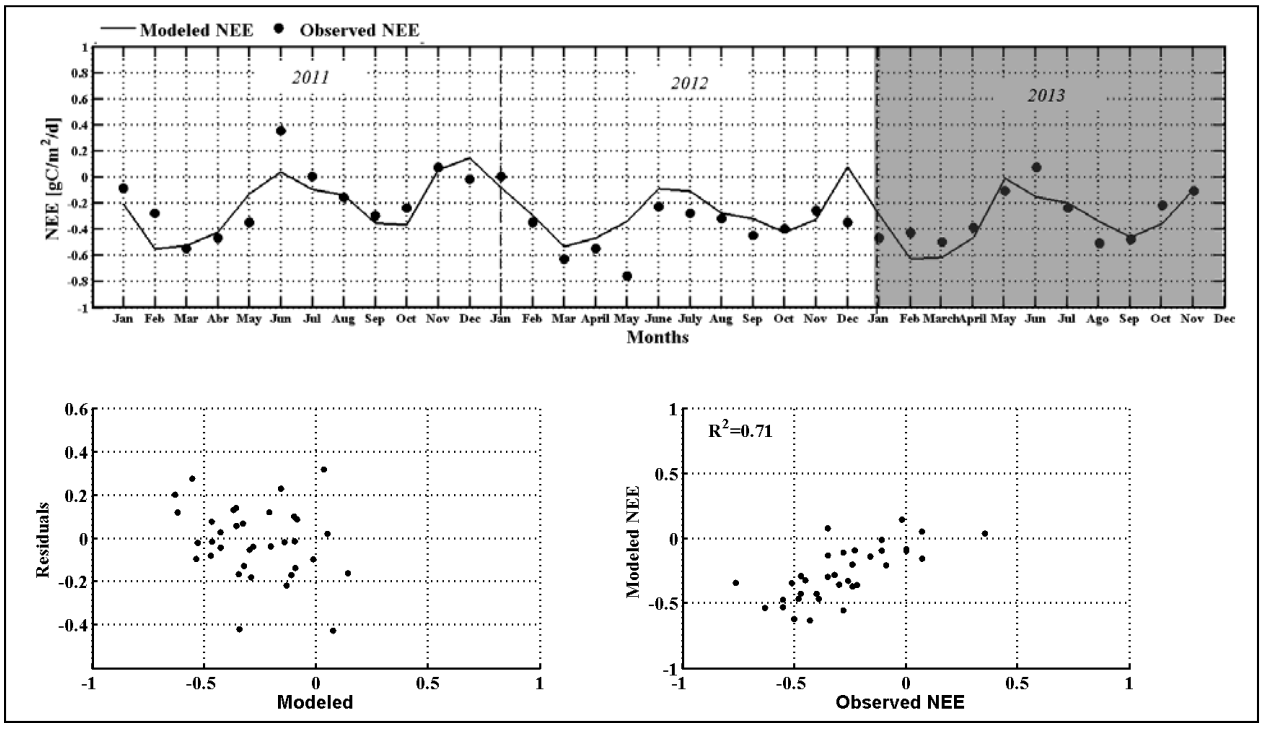


**Figure 16** Assessment of the observed and Modeled NEE. Shaded grey area denotes 2013 as the independent data set used to test the model.

## 2.5. DISCUSSION

This study was structured in two main sections 1) Characterizing microclimate, and ecosystem fluxes in the Shrublands representative of the Northern Chihuahuan desert, and 2) Identifying biophysical controls of ecosystem fluxes of carbon, water, and energy using statistical modeling.

Local climatology indicated the study area received 40% less precipitation during the period of study than the long term average rainfall recorded at the Jornada Experimental Range between 1915 and 1995 (Wainwright 2006). On a regional perspective, the study area received a mean annual of 142mm, this represents about 40% less precipitation than the mean annual received at Santa Rita Experimental Range (340 mm/yr) and Walnut Gulch Experimental Watershed (345 mm/yr), these regions represent the Sonoran desert and the transition zone between Sonoran and Northern Chihuahuan desert, respectively (Cavanaugh *et al.* 2011); JER annual precipitation estimates were about 58% below the annual estimates for the Sevilleta Experimental Range (244 mm/yr), region representative of the Northern Chihuahuan desert (Anderson-Texeira *et al.* 2011). The analysis of mean temperatures suggested the period of study was 1.9 °C above the long-term record annual mean temperature between 1915 and 1993 recorded at JER. On a regional basis, the mean annual estimates of temperature were 3°C below the annual mean temperature of the Sonoran desert (20°C) and overall mean annual temperatures estimates at the Sonoran –Chihuahuan desert transition zone and the Chihuahuan desert were consistent with the area of study oscillating on ~17°C (Anderson-Texeira *et al.* 2011; Cavanaugh *et al.* 2011).

Unlike desert grasslands of the Jornada Experimental Range that were characterized as sources of carbon (~143 $gCm^{-2}yr^{-1}$) between 1996 to 2001 (Gutschick & Snyder, 2006). Desert shrublands of the JER were a consistent sink of carbon during 2010 to 2012 with a total 3year cumulative of -428.5$gCm^{-2}$. This three year cumulative NEE is equivalent to mean annual estimates of NEE for Pinon Juniper woodland of New Mexico Elevation Gradient (Anderson-Texeira *et al.* 2011). Although, there was a significant difference on NEE among years (from -98 $gCm^{-2}yr^{-1}$ to -191.5 $gCm^{-2}yr^{-1}$); these values are above those reported from Sarcocaulescent shrublands of the Sonoran Desert (-39 to -52$gCm^{-2}yr^{-1}$) during 2002-2003 (Hastings *et al.* 2005), Californian grasslands (-88 gCm-$2yr^{-1}$) (Xu & Baldocchi, 2004), and desert shrublands of the New Mexico Elevation Gradient (-30 to -50 $gCm^{-2}yr^{-1}$).

The random forest tree analysis has not been used in micrometeorology studies; however, results from it underpinned the top predictors of NEE, GPP and R in desert shrublands are similar to those identified in other arid and semiarid regions, in which temperature and water availability in different partitions of the ecosystem and the atmosphere are the primary controls of ecosystem fluxes (Anderson-Texeira *et al.* 2011; Shao *et al.* 2013b; Thomey *et al.* 2014). Although the results suggest that ecosystem fluxes have similar biophysical controls, their top ranked importance, based on the increase of percentage mean squared error, is different. This has implications for further modeling, in which less than five predictor variables can be used to model the response of fluxes. The partial dependency plots indicated that Shrublands of the Northern Chihuahuan desert are predominantly above the critical zone of vapor pressure deficit at which any C4 plants would be able to withhold enough water to survive extreme conditions for long periods of time (Marshall & Woodward 1985). Seasonal changes appeared in general

when the vegetation is switching on/off photosynthesis during the growing season (mid-May through mid-September). Similar to other shrublands in western US described by Yufei *et al.* (2010), there is a bimodal maximum uptake distributed at the beginning of the growing season (early-May) and at the peak of the monsoon season (mid -August). Our records indicate the drought in 2011 represented 70 days delay of active growth during the period of study, this difference accounted for more than half of the carbon uptake recorded during 2012. Despite 2010 received the largest amount of precipitation, the system acted as a modest carbon sink of -78.80 $gCm^{-2}$ $y^{r-1}$. This suggest that there are other mechanisms beside precipitation and temperature that control net ecosystem exchange in/out the system (M. C. Duniway 2010; Yufei *et al.* 2010; Shao *et al.* 2013a). It seems that 2010-2011 winter precipitation was enough to support plant activity until early spring 2011. However, since water availability was limited due to the shift in precipitation timing and magnitude, the system was unable to support new/adult growths of existing species as usually occurs during summer precipitation in the Northern Chihuahuan desert (Robertson *et al.* 2010). Therefore, an important decrease in carbon sequestration occurs during the usual peak growing season. In turn an increase in respiration occurs, thus the system shifts to a small sink of carbon up to -30 $gCm^{-2}$ $y^{r-1}$. Summer precipitation supported carbon sequestration bringing the total annual cumulative to -65.47 $gCm^{-2}$ $y^{r-1}$ in 2011. The following c2012 the system received a small amount of winter precipitation (~5 mm), enough to supply moisture in the system to recruit new growths that started leafing out at the beginning of the growing season as soon as temperatures increased at the end of winter 2012. Summer rainfall promoted the growth of deeper rooted shrubs and fobs. Essentially, because of fairly constant and evenly distributed rain events throughout the year, the system acted as the largest sink during the period of study (-130.85 $gCm^{-2}$ $y^{r-1}$).

## 2.6 CONCLUSIONS

Local climatology indicates a decreasing trend of increasing precipitation and decreasing temperature in the JER. Annual precipitation at the study site was substantially below the long term mean annual precipitation estimated for both Sonoran and Chihuahuan desert of the Santa Rita Experimental Range and Sevilleta Experimental Range, respectively.

Shrublands of the Northern Chihuahuan Desert were larger sinks of carbon than other arid and semiarid areas of the Southwest desert. The three year cumulative carbon sink was equivalent to annual cumulative estimates for Pinon Juniper woodland of New Mexico Elevation Gradient.

Net ecosystem exchange of $CO_2$ is greatly affected by hot and dry conditions which inhibit the accumulation of significant carbon stocks in desert shrublands. The ratio of respiration: gross primary production increases with temperature and decreases with increasing soil moisture and cooler soil temperatures in deeper soil profiles.

The quadratic model was able to validate the predictive capacity of the variables of importance of ecosystem fluxes. This model is a great tool to explore possible changes in ecosystem fluxes response to specific changes of their drivers. More robust models are suggested to predict net ecosystem exchange. Some limitations of the study, the predictive potential of the partial dependency plots assumes the system will remain in steady state, therefore more robust modeling technique are suggested to decrease uncertainty if predictive values when change is input into the ecosystem

## Suggestions for future research

Studies that focus on the implication of vertical distribution of soil moisture, phenology and carbon uptake are necessary to better understand the thresholds that trigger larger carbon uptake of this ecosystems, and how they compare with other deserts of the Southwest Desert region. A very comprehensive analysis in a similar system was studied in Santa Rita Experimental Range by Martinez (2011).

## Acknowledgement

This study could have not been possible without the contribution of fellow lab mates. Plot phenology data was collected by Libia Gonzalez and Christine Laney. Greenness index was derived from PhenoCam.m phenology analyzer packaged developed by Geovanny Ramirez.

# Chapter 3: Effects of extreme climatic events in land-atmosphere exchange of carbon, water and energy in desert shrublands of the Chihuahuan desert

## 3.1 ABSTRACT

This study leveraged 4-years of continuous data collection of ecosystem properties and processes in a shrubland of the Northern Chihuahuan desert to explore how extreme temperature changes and drought conditions impact land-atmosphere exchange of carbon dioxide. Specifically the study: 1) Identified and quantified extreme events in the 4-year study period relative to long term climatic records; 2) Assessed how these events impacted land-atmosphere exchange of carbon; 3) Determined how important ecosystem impacts from the identified extreme were relative to cumulative seasonal and annual fluxes. Results were discussed with a mindset for interpreting how an increased frequency of extreme events that are expected with climate change may impact ecosystem function of comparable desertified landscapes in the future. Long term climatic records of the JER were calculated using 30-year data (1983-2013) of temperature and precipitation obtained from the Jornada Basin Long-Term Ecological Research (LTER) project. Four extreme events were defined for the 30-year period: Wet, extreme drought, cold anomaly and warm anomaly. The assessment of the relative importance of extreme events to seasonal and annual fluxes was done by selecting the days identified as extreme events. Random Forest analysis was used to analyze the relative importance of extreme events to control ecosystem fluxes under "Normal" and "Non-Normal" conditions. Results indicated the even though extreme events are erratic in occurrence and duration (from days to 2-months), their incidence have important implications on regulating ecosystem fluxes because they modify seasonal patterns of their biophysical controls; Hence, regardless of the length of the event, it will have important effects on the annual cumulative of ecosystem fluxes. Extreme events correspond to 18% of the total number of days of the analysis, and those events account for 20% of the total 4-yr cumulative NEE.

## 3.2. INTRODUCTION

Meteorological phenomena that are known to impact ecosystem properties and processes in dryland regions include temperature extremes (Small 2001), drought (Cipriotti *et al.* 2008; Schwalm *et al.* 2012), floods (Trenberth *et al.* 2003), snow, wildfires (Ansley & Castellano 2007; Betts & Dias 2010), and wind storms (Nicholson 2011). The occurrence and duration of these stochastic phenomena can vary from hours (e.g. rainfall), days (e.g. cold events), and weeks, months or years (e.g. drought). Moreover, cumulative impacts from concomitant extreme events have increasingly been recognized for their capacity to dramatically alter ecosystems (Rich *et al.* 2008; Hamerlynck and Huxman 2009; Sura 2012) whereby the combined impact from multiple co-occurring phenomenon can be greater than the sum of the component impacts (Peters *et al.* 2013; Ponce Campos *et al.* 2013).

Recent shifts in wet-dry climatic patterns of Western North America have been documented over the last two decades (Seager 2007; Mokhtari *et al.* 2013). Shifts in these trends have been attributed to the denominated turn of the century drought that occurred from 1999 to 2004 as a consequence of the El Niño–Southern Oscillation (ENSO) of 1997-98. The turn of the century drought was characterized as the most severe extreme five-year average Palmer Drought Severity Index event since 1200 and its effects triggered the unfolding drought from 2004 to date (Seager *et al.* 2007). Precipitation projections estimate western North America is undergoing an imminent transmission warmer and drier climate, thus current shifts of wet/dry periods consist the beginning of the drier hydro-climate period of the 21st century (Schwalm *et al.* 2012).

The protracted occurrence of extreme climatic events had been documented in western North America over the last 30 years. In the warm desert region (Sonora, Mojave, and Northern Chihuahuan desert) ecosystems dynamics is driven by pulse precipitation events (Huxman *et al.* 2004; Sponseller 2007; Wohlfahrt *et al.* 2008), the emphasis on studying extreme events has been restrained to assessing the effects of drought on carbon uptake (Scott *et al.* 2010; van der Molen *et al.* 2011; Schwalm *et al.* 2012), evapotranspiration (Charney 1975), survival of grass seedlings (Cipriotti *et al.* 2008). Few of them have examined cold, wet events (Peters *et al.* 2011), had important effects in reducing biomass and aboveground net primary production (Peters et al. 2012), losing fertile soil due to wind and water erosion, depleting soil recharge, and modifying rain use efficiency by plants (Bowling et al. 2011).

The unprecedented freezing event experienced in western North America in February of 2011 (NOAA 2011) risen interrogatives about the impact of other climatic extreme events on a systems that are undergoing an imminent transition towards warmer and drier climate (Seager *et al.* 2007). Due to the importance and implication of extreme climatic events in ecosystems goods and services, there is an increasing interest in improving detection and attribution of climate change and climate extremes from local to global scales (Mirle *et al.* 2013).

Some authors indicate that a limitation to the assessment of extreme events on dryland ecosystem properties and processes has been due to the scarcity of long term studies coupled with high frequency continuous measurements especially in desertified landscapes relative to other biomes. However, recent studies have aided elucidating ecosystem responses to the protracted occurrence of extreme events. For instance the eco-physiological response and

adaptation of shrubs to extreme conditions under lab conditions suggest freezing enhances shrublands resilience to drought (Maderos & Pockman 2011); whereas heat and water stress inhibits the capacity of the system to store carbon build-up (Hüve *et al.* 2011). Drought intensifies respiration rates over carbon uptake rates (Anderson-Texeira *et al.* 2011; Maderos & Pockman 2011) and pulse events of precipitation promote recruitment of new species of grasses, and positively feedbacks carbon uptake (from soils, vegetation), primary productivity (Bowling *et al.* 2011; Munson *et al.* 2013), carbon sink capacity, primary production, and latent heat (Schwinning & Sala 2004; Sponseller 2007; Bowling *et al.* 2011; Schwalm *et al.* 2012).

Due to the long term record of data sets, Jornada experimental range provides a great framework to investigate the occurrence of past, present extreme climatic events in the region. To date, there has not been a comprehensive study that implements a quantitative analysis to identify extreme climatic events and also investigates the effect of the occurrence of isolated or combined effects of extreme climatic events in the underlying processes of ecosystem dynamics. This study leverages 4-years of continuous data collection of ecosystem properties and processes in a shrubland of the northern Northern Chihuahuan desert to explore how extreme temperature changes and drought conditions impact land-atmosphere exchange of carbon dioxide, water, and energy. Specifically the study:

1) Identify and quantifies extreme events in the 4-year study period relative to long term climatic records

2) Assesses how these events impacted land-atmosphere exchange of carbon;

3) Determines how important ecosystem impacts from the identified extreme are relative to cumulative seasonal and annual fluxes.

Results are discussed with a mindset for interpreting how an increased frequency of extreme events that are expected with climate change may impact ecosystem function of comparable desertified landscapes in the future.

## 3.3 METHODS

### 3.3.1 Study Area and measurements

The study was conducted on the ecological station of Systems Ecology Lab, University of Texas at El Paso (SEL-UTEP). The station is located on the Jornada Basin Long Term (JER) site in Southern New Mexico (32.5655 N, -106.6598 W). The area is dominated by a mixed creosote bush (Larrea tridentata) and honey mesquite (Prosopis glandulosa) shrubland. Creosote bush is an evergreen, drought-resistant C3 perennial shrub (Peters et al. 2006). Honey mesquite is a deciduous, thorny, long lived C4 shrub that is characterized by very deep and laterally extensive root systems (Peters et al. 2006). Other species found at the site include tarbush (Flourencia cernua), the grass bush muhly (Muhlenbergia porter), fluff grass (Dasyochloa pulchella), as well as a variety of forbs. The shrub average canopy height is approximately 2.0 m.

Environmental measurements collected from the SEL-UTEP ecological station during 2010-2013 were recorded The open path eddy covariance system consists of 22 instruments distributed on a 10m height tower. Instrumentation consists of a three dimensional sonic anemometer (CSAT3-SONIC CSI), an infrared gas analyzer (IRGA, LI-7500 Li-COR Inc) located at 5m height, a four-component net radiometer situated 20m to the east of the main eddy

covariance tower at a height of 3m (CNR1- Kipp and Zonen), a photo-synthetically active radiation sensor (PAR-LITE - Kipp and Zonen) located at 10m height, a temperature and humidity sensor (HMP45C-L - CSI) at 5m height, a barometer (CS106 –CSI) located inside an enclosure about 1.30m height, a 2D anemometer (03002-L -CSI)at 10m height, a tipping bucket rain gauge (TE525-L), eight probes to measure soil temperature and volumetric water content (ECTM – decagon), and four soil heat flux plates (HFP01 Hukseflux CSI). Soil instruments are distributed into two subsystems of soil profiles installed to capture underground temperature, volumetric water content, and heat from underneath a mesquite and bare soil. These profiles are located at 2cm, 10cm, 15cm and 20 cm depth. All data is collected and stored in a Campbell Scientific CR3000 data logger. The system is powered by a 300W 10-panel solar array. The solar panels are mounted on an aluminum structure located 35m north and downstream of prevailing winds at the EC tower. The panels face south to maximize battery recharge. The system uses four 12VDC sealed deep cycle batteries, and the load is regulated through a morning start ProStar 15 Amp 12/24 charge controller. Data files are stored on a 2GB card and are retrieved remotely using an internet connection. This connection is established by a Virtual Private Network that passes via a point to point Wi-Fi connection that links an antenna situated at 9m on the eddy covariance tower to the headquarters of the JER from where it then routes to UTEP servers through hardwired Ethernet. The system also provides a 500m Wi-Fi bubble from an Omni-directional antenna situated at 5m on the eddy tower and connects multiple wireless devices associated with the local sensor network at the study site. Flux calculations were computed with EddyPro TM 4.1 software. Then, a moving average window of 5 days was used to reject spikes following the method described by (Lee *et al.* 2004). Additionally, to eliminate the influence of the stable lower boundary conditions, all flux data recorded with u* less than 0.1ms-1 were

discarded. Gap filling and flux partitioning was done following Lasslop et al.'s (2010) method. Day and night time separation was based on a threshold of photosynthetic photon flux density. Ecosystem respiration output from the Lasslop et al. (2010) method was used to estimate gross primary production using Equation 1 as described by (Reichstein *et al.* 2012a). Data collection and data processing were validated using the eddy covariance portable system and their MATLAB flux processing routine during August 2012. Standard sign convention for NEE is used to indicate NEE>0 equals a net loss of $CO_2$ to the atmosphere (source) and NEE<0 indicates $CO_2$ uptake by ecosystem (sink). The results obtained with the use of the eddy covariance system represent the average functioning of land-atmosphere interactions within the footprint area. The footprint analysis was done using a combination of the footprint models from (Kormann et al. 2001) and (Kjun *et al.* 1997), built within EddyPro 4.1.0 (LICOR 2011). The 90% daytime footprint contribution distance reached a yearly average of 370m.

### 3.3.2. Identification of extreme events and data analysis

This section focused on identifying and quantifying the occurrence of extreme events in the 4-year study period relative to long term climatic records. A combination of two widely used methodologies based on anomaly detection of air temperature (Dominguez *et al.* 2010) and hydrological drought index (Fuchs 2012) was used to identify the occurrence of four critical extreme events of interest for Western North America: 1) Drought, Wet, Cold , and Warm. . Long-term air temperature and precipitation from 1983 to 2013 data were obtained from the daily summary climatic data of the JRN-LTER project (Anderson 2013).

*Anomalies of temperature: Cold and warm extreme events*

The climatic "normal" temperature for the Jornada region was calculated by estimating the seasonal pattern of air temperature between 1983 and 2013. Analysis 30-year climate series is considered by the World Meteorological Organization (WMO) as an adequate standard period to filter out Inter-annual variation, but also short enough to detect longer climatic trends (Arguez & Vose 2011). The seasonal temperature pattern was estimated by obtaining the mean daily temperature over the 30-year period; hereon this will be referred as "*normal temperature*" (Figure 22). Then, anomalies of temperature were calculated by subtracting the observed temperature from the normal temperature (Figure 22). Cold and warm extreme events were defined when actual mean daily temperature fell outside the $98^{th}$ tail of the probability density function of anomalies of the temperature over the 30 years (Sura 2012; Mirle *et al.* 2013). A similar method for identifying climatic anomalies is used by the International Governmental Panel on Climate Change (IPPC 2007). This method was applied over the 30 years period; however special emphasis was done to 2010-2013to be able to compare with ecosystem fluxes.

*Drought Index: Drought and relative-Wet extreme events*

The standardized precipitation- evapotranspiration index (SPEI) has been shown to be an optimal measure of drought intensity and duration for ecosystem studies (Diehl & Lutz 2010, ) and incorporates monthly surplus or deficit moisture (precipitation minus potential evapotranspiration (PET)); therefore SPEI is more sensitive to and representative of drought stress, intensity, and duration (Diehl & Lutz 2010). SPEI also provide a strong comparative context to other studies using similar indices (Scott, R., et al. 2010). The drought index was

calculated using the R package SPEI version 1.6 (Begueria and Serrano 2013), where positive values above 2 indicate exceptionally wet months and values below 0 denote dry conditions. Dry conditions are categorized as abnormally dry (D0:-0.5 to -0.7), moderate drought (D1:-0.8 to -1.2), severe drought (D2:-1.3 to -1.5), extreme (D3:-1.6 to -1.9), and exceptional drought (D4:-2.0 or less) (National Drought Mitigation Center, 2011).

The assessment of the relative importance of extreme events to seasonal and annual fluxes was done by selecting the days identified as extreme events above defined. Those dates were extracted from the ecosystem flux time series data-set to quantify seasonal, annual and overall 4-year cumulative per event. Furthermore, to analyze the relative importance of extreme events to control ecosystem fluxes under "Normal" and "Non-Normal" conditions, the random fores analysis described on chapter 2, was performed. Normal conditions were defined by removing the corresponding extreme events dates from the time series data-set of NEE. The time series with the corresponding extreme events dates were denominates a "Non-Normal". An estimation of the 4-yrs cumulative NEE of, "Normal", "Non-Normal" and per event cumulative NEE was done. This analysis was coded using Matlab software.

## 3.4 RESULTS

### 3.4.1 Climatology and identification of extreme events in the Jornada

The analysis of the 30-year mean annual temperature suggests a decreasing tendency of precipitation with increasing temperature (Figure 18). However, this is a non- linear trend with time, in fact there is an extreme occurrence of wet/dry years. The 30-year mean annual temperature was 17.74°C with a standard deviation of 4.52°C. The minimum annual temperature was 14.76°C in 2008, and the maximum annual temperature was 19.3°C in 1997. The 30-year mean annual precipitation was 269mm. The minimum recorded value for completed year was 91.7mm, which occurred in 2003, with a maximum annual precipitation of 434.4mm in 1991. During the four year study period 2011 and 2010 were above the 30-year mean annual temperature at 17.7°C and 18.5°C respectively. Mean annual temperature for 2012 and 2013 were slightly below it, at 17.30°C and 17.1°C respectively (Figure 22). Mean annual precipitation for the study period was below the 30-year mean, and but the lowest and highest mean annual precipitation was recorded in 2011 (98mm) and 2013 (280mm) respectively

The 2nd percentile of the probability density function for anomalies of daily air temperature estimated for the 30-year record occurred when air temperatures departed more than -7.54°C from 30-year mean daily air temperature. This threshold was used to flag cold anomalies. In the last 30 years, 206 days of cold anomalies occurred and 38 of these fell within the four year study period. There has not been precedent of cold anomaly as that reached on February 2011, which was -22.57°C. In fact, the minimum cold anomaly occurred in 1984 and reached -17.5°C (Figure 19B). The 98th percentile of the probability density function of anomalies of temperature was 6.47°C; this was the threshold to estimate warm anomaly events.

A total of 190 days of warm anomalies occurred in the last 30-years and 23 days occurred during the study period. The maximum anomaly for mean daily temperature in the 30-year period was 12°C during 1988, and the maximum during the four year study period was 9.73°C on December 20, 2010.Overall, cold anomalies occurred with higher frequency than warm anomalies during the period of study (Figure 19C).

Analysis of the 30-year record of standardized precipitation and evapotranspiration index (SPEI) detected an increase of drought conditions since 1993. Over the 30-year record for SPEI the most exceptional drought period was recorded between 2001 and 2003 (Figure 20A). Although exceptional drought conditions did not occur during the study period, higher than normal frequency of abnormally dry to severe drought conditions prevailed, such conditions characterized Extreme drought, D3 on SPEI scale. D3 conditions were present in April 2011 and July 2013 (Figure 20B). Wet periods have significantly decreased during the last 30-years period. During the last four years there were some wet periods depicted by the SPEI, however these are not as wet periods as periods during the early 1980's where the maximum SPEI was 2.12 in April 1984. With the expectation to be able to represent wet periods in a dry environment, a threshold of SPEI above 1 was established to select wet events during the last four years (Figure 20B). Overall, the analysis of SPEI over the last 30-years suggested that the frequency of drought conditions is higher than wet events in the region (Figure 20C).

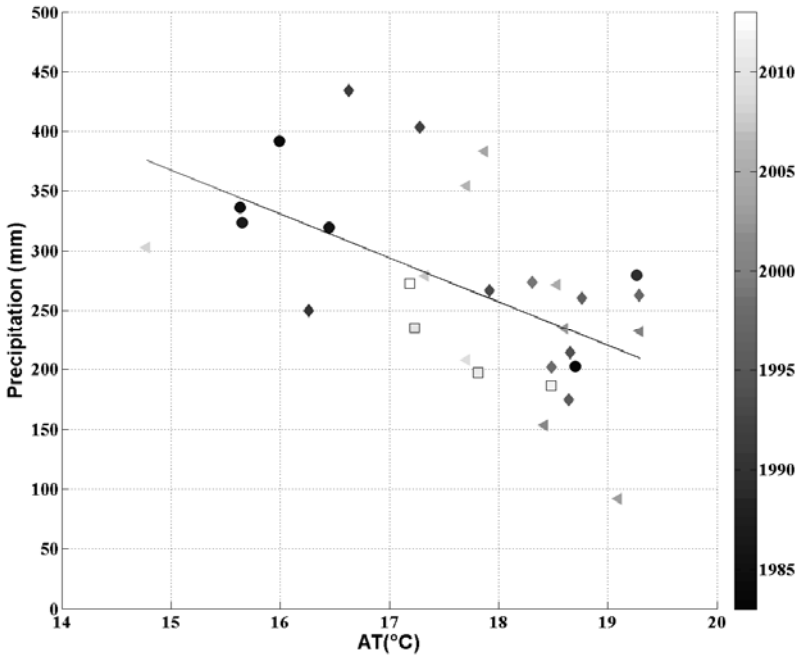


**Figure 17** Scatter plot of 30-year mean annual precipitation versus mean annual air temperature. Darker color scale denotes older years and lighter colors denote recent records. . Symbols represent decades: circle: 1980's; diamond: 1990's; triangle: 2000's; square: 2010's. Best fit correlation shown in black P-value=<0.001; $r^2$=0.34.

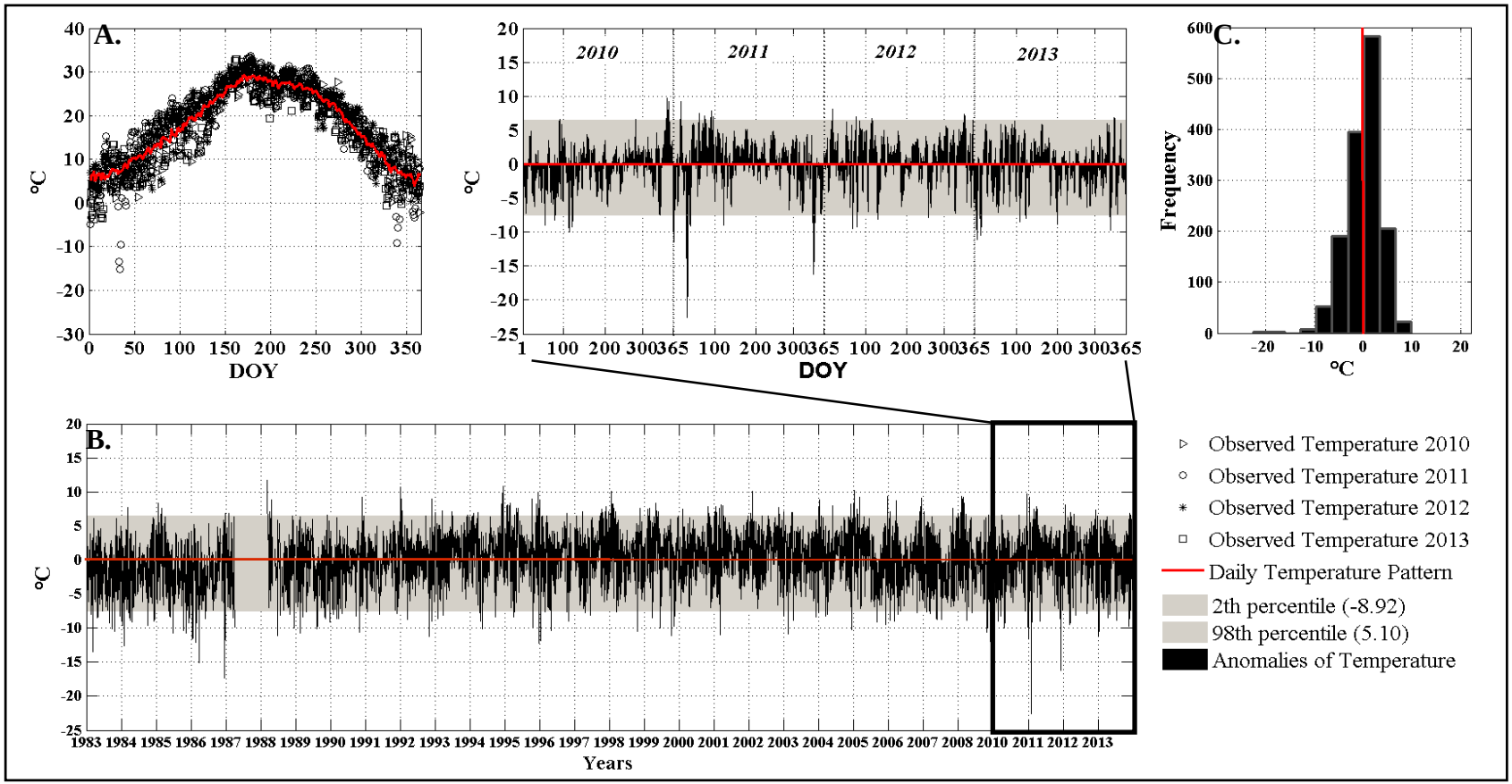


**Figure 18** A) 30-year anomalies of temperature estimated from 1983-2013 temperature data. Red bold line shows the seasonal pattern of temperature estimated from daily mean air temperatures of 30-year period. Observed mean daily temperature values of 2010 (triangles), 2011 (circles), 2012 (asterisks), 2013 (squares). *B)* Anomalies of temperature during 2010-2013. B) Anomalies of temperature during 2010-2013. Shaded grey areas denote the 2nd and 98th percentile tails of the probability density function. *C)* Histogram of frequency distribution of anomalies of temperature.

Note: Daily mean temperature data was obtained from summary climatic JRN-LTER project. No data was available for 1984.

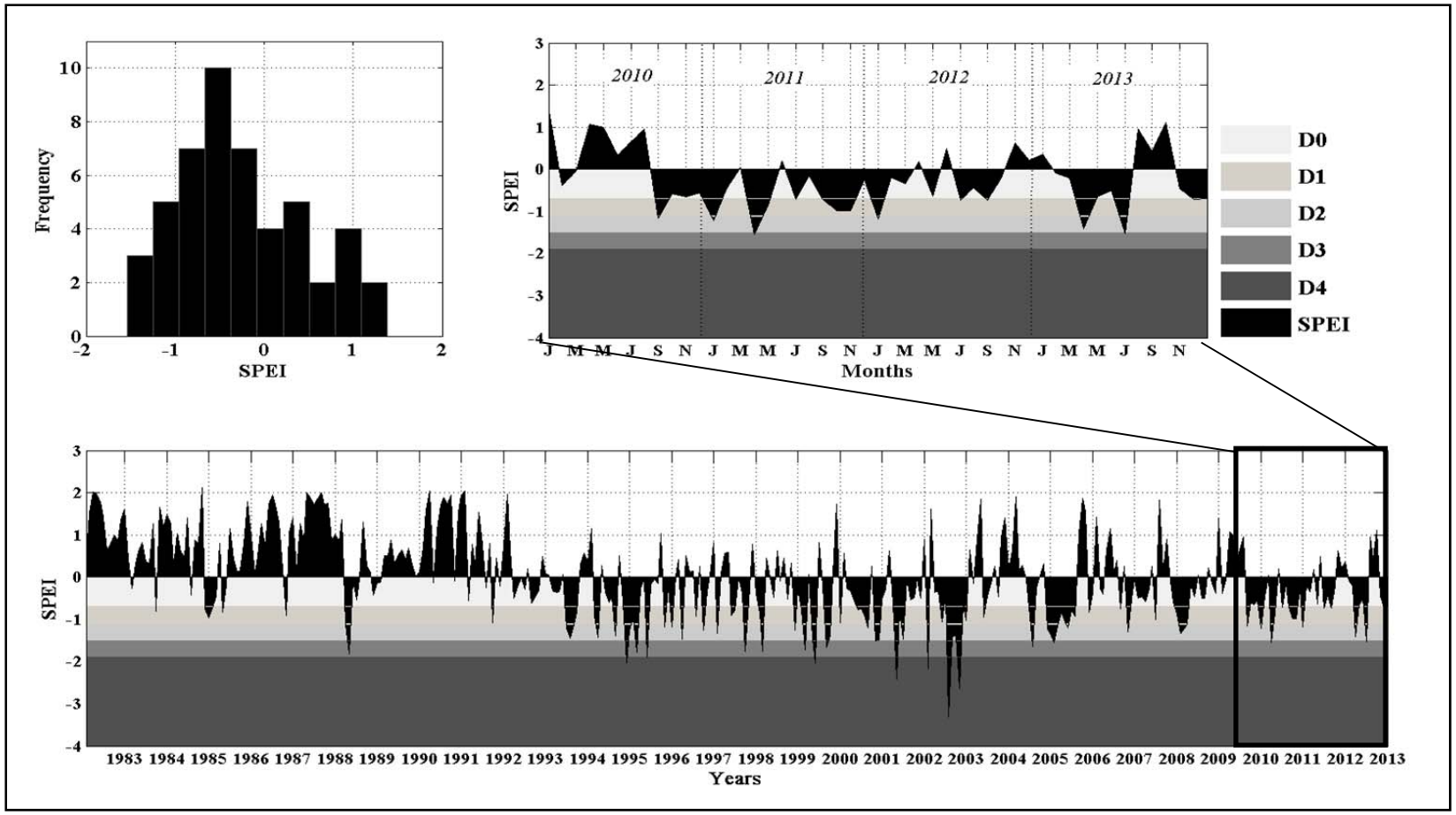


**Figure 19** A) 1-month Standardized Precipitation and Evapotranspiration Index (SPEI) calculated for 1983-2013. A) 1-month Standardized Precipitation and Evapotranspiration Index (SPEI) calculated for 1983-2013. Shaded areas denote: D0-Abnormally dry, D1-Moderate drought, D2-Severe drought, D3-Extreme drought, and D4-Exceptional drought. B SPEI of the 2010-2013 study periods. C) Histogram of frequency distribution.

In summary, anomalies in daily air temperature and monthly SPEI values suggested that the occurrence of cold anomalies and drought is higher than warm anomalies and wet periods at the JER (Table 5). Hereafter, the events are referred as: 1) Cold anomaly, 2) Warm anomaly, 3) Drought, and 4) Wet. Each of these events is defined below:

A *Cold anomaly* is defined as days in which the anomaly of temperature reached values below the 98th percentile (98th percentile=5.1°C) from normal temperature. *Warm anomaly* refers to days in which the anomaly of air temperature reached values above the 2th percentile (2th percentile= -8.92°C.) from the normal temperature. Severe drought refers to days when SPEI reached values equaled or fell below-1.25. Wet represents days in which SPEI reached values equal or above 1.

The presence of extreme events constituted 14% of days (n=1460) in the study period. Cold anomalies ranged from a few days to a week in duration and that amount was equivalent to 2% of days in the study period. Cold anomalies of 2011 and 2013 reached sub-freezing temperatures whereas those identified in 2010 and 2012 primarily occurred in early spring and summer and were above freezing. Warm events represented 1% of the study period and typically occurred in winter or early spring (Figure 23). Even though abnormally dry and moderate drought prevailed throughout the period of study, severe drought was recorded in only two months of 2011 and 2013. These signified 4% of the total days of extreme events (Figure 23). Wet periods of 2010 and 2013 represented 6% of the total days with the presence of extreme events. Although three months were identified as wet conditions by the SPEI (Figure 20B), this conditions are not identified as extreme wet conditions in the 30-year period.

However, wet conditions are selected as a reference to compare effects of wet periods in the 4-yr period of study.

**Table 5** Dates with presence of extreme events during 2010-2013

| *Event* | *Dates* | *Total Days* |
|---|---|---|
| Cold anomaly | 02/23/10 | 7 |
| | 03/20/10 | |
| | 04/22/10-04/23/10 | |
| | 04/30/10-05/02/10 | |
| | 12/31/10-01/02/11 | 15 |
| | 02/03/11-02/04/11 | |
| | 02/09/11-02/10/11 | |
| | 05/02/11 | |
| | 12/02/11-12/07/11 | |
| | 03/09/12-03/10/12 | 6 |
| | 03/20/12 | |
| | 05/09/12-05/10/12 | |
| | 09/08/12 | |
| | 01/03/13-01/05/13 | 10 |
| | 01/13/13-01/16/13 | |
| | 05/03/13 | |
| | 07/18/13 | |
| | 11/24/13-11/25/13 | |
| | ***Total:*** | ***38*** |
| Warm anomaly | 03/03/10 | 9 |
| | 10/01/10 | 8 |
| | 12/15/10-12/21/10 | |
| | 01/18/11-01/19/11 | |
| | 03/03/11 | |
| | 03/17/11 | |
| | 04/02/11-04/03/11 | |
| | 04/06/11 | |
| | 12/06/11 | |
| | 01/20/12 | 8 |
| | 03/17/12 | |
| | 04/24/12 | |
| | 12/03/12-12/07/12 | |
| | 01/06/13 | 3 |
| | 12/03/13-12/04/13 | |
| | ***Total:*** | ***28*** |
| Severe drought | 03/01/11-03/90/11 | 30 |
| | 05/10/13-06/09/13 | 30 |
| | ***Total:*** | ***60*** |
| SPEI - Wet | 01/01/10-01/31/10 | 60 |
| | 03/31/10-04/30/10 | |
| | 10/01/13-11/30/13 | 30 |
| | ***Total:*** | ***90*** |

*n=1460 days*

### 3.3.5 Assesses how these events impacted seasonal and cumulative annual fluxes of NEE, GPP and R

During the 4-year study period the study site was a small sink of carbon (-458.44gC/$m^2$/4yrs *see* Chapter 1). During this period, 906gC/$m^2$/4-yr and 448.41gC/$m^2$/4-yr of NEE was partitioned to GPP and respiration respectively. Smaller magnitudes of net ecosystem uptake (-28.24 gC/$m^2$/28days, and -21.97 gC/$m^2$/60days) occurred during warm events and drought respectively (Figure 21). Similar correspondence occurred with gross primary production and respiration. Essentially, cold anomalies and wet events have higher rates of GPP (82.79 gC/$m^2$/38days, 74.74 gC/$m^2$/90days) and R (39.18 gC/$m^2$/38 days, 30.71 gC/$m^2$/90days). Then, warm anomalies and drought accounted for small rates of GPP and R; especially respiration rates were the lowest (14.91 gC/$m^2$/ 28days) during warm events. Cumulative GPP always exceeded respiration, although rates vary per extreme event and the 4-year total.

The first half of 2010 was marked by the subsequent occurrence of extreme events that included the two highest rainfall events received during the study period. Cold anomalies and warm anomalies were also registered (Figure 22a, b, c). On an annual scale, the combined effect of these conditions resulted in a total annual cumulative of NEE of -80 gC/$m^2$/$yr^{-1}$, GPP of 210 gC/$m^2$/$yr^{-1}$, and respiration rates of 145gCm-$^2$$yr^{-1}$ (Figure 23a).

The transition between 2010 and 2011 was characterized by a series of alternate extremes from 8 days of warm anomalies to 15 days of cold anomalies followed by 30 days of extreme drought. All of them occurred during the first 150 days of 2011. The rapid response of ecosystem fluxes was manifested in reducing the uptake capacity until the system became a small source of carbon between DOY 196 to 205 (Figure 22a, b, c). These results suggest that the combined effect of these unprecedented extreme conditions may led to a substantial decrease of the annual budgets of NEE (60 $gCm^{-2}yr^{-1}$); in fact the annual cumulative of GPP, respiration, was reduced

to almost half the budgets reported the previous year to 120 $gCm^{-2}yr^{-1}$, 60 $gCm^{-2}yr^{-1}$, (Figure 22b).

During 2012 18 days of extreme event conditions were recorded including 8 warm days and 10 days of cold anomalies and these were distributed relatively evenly throughout the year. The largest annual sink of carbon during the 2010-13 study period was recorded in 2012 with a total annual NEE of -135 $gCm^{-2}yr^{-1}$. GPP, latent heat and sensible heat fluxes were very similar to those measured in 2010 (210 $gCm^{-2}yr^{-1}$, latent 7000 $W/m^2$., and sensible heat of 2.310x4 $W/m^2$ respectively) However, respiration rates were significantly smaller than those found in 2010 and higher than those documented in 2011 (90$gCm^{-2}yr^{-1}$) (Figure 22c).

In 2013, there were 73 days of extreme event conditions documented and these were distributed relatively evenly throughout the year. There were 10 days of cold, 3 warm days, 30 days with drought, and 30 wet days. The combination of cold anomalies event with subfreezing temperatures followed by drought resulted in a significant decrease in the carbon sequestration capacity during the growing season. During the following days, the system became a small source of carbon, very similar to the drought conditions of 2011 (Figure 22a). The total annual cumulative of NEE was -110 $gCm^{-2}yr^{-1}$; during this year GPP of 250 $gCm^{-2}yr^{-1}$, were the highest rates recorded for the overall 4-year period; Respiration rates were 120 $gCm^{-2}yr^{-1}$.

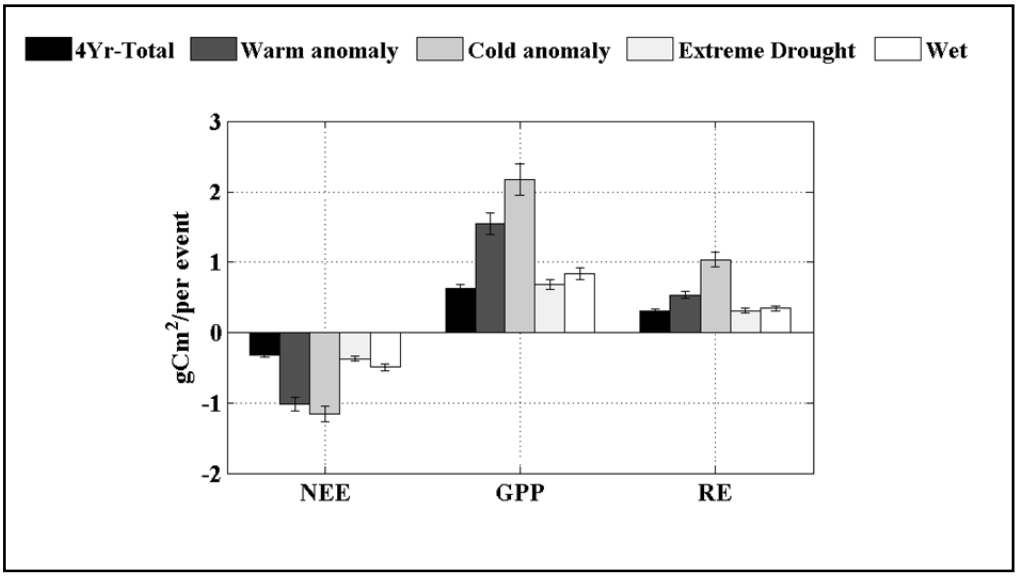


**Figure 20** Proportion of ecosystem fluxes during each extreme event during 4yr period

**Table 6** Contribution of cumulative ecosystem fluxes during extreme events, normalized by the number of days of their occurrence.

| *Total fluxes/ # of days* per event | *NEE* $gC/m^2$ | *GPP* $gC/m^2$ | *R* $gC/m^2$ |
|---|---|---|---|
| Warm/28 | -1.00 | 1.54 | 0.53 |
| Cold/38 | -1.14 | 2.18 | 1.03 |
| Drought/60 | -0.36 | 0.68 | 0.31 |
| Wet/90 | -0.49 | 0.83 | 0.34 |

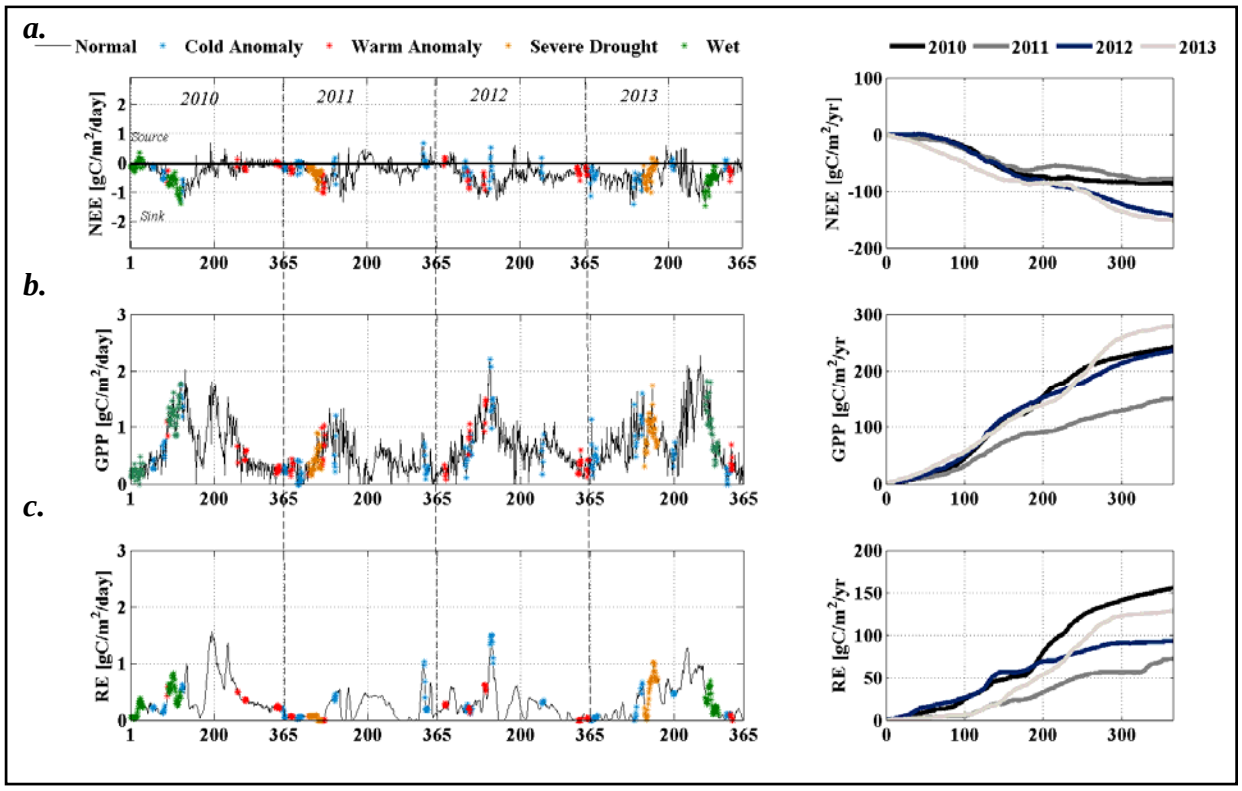


**Figure 21** Time series of ecosystem fluxes color coded for the occurrence of extreme events

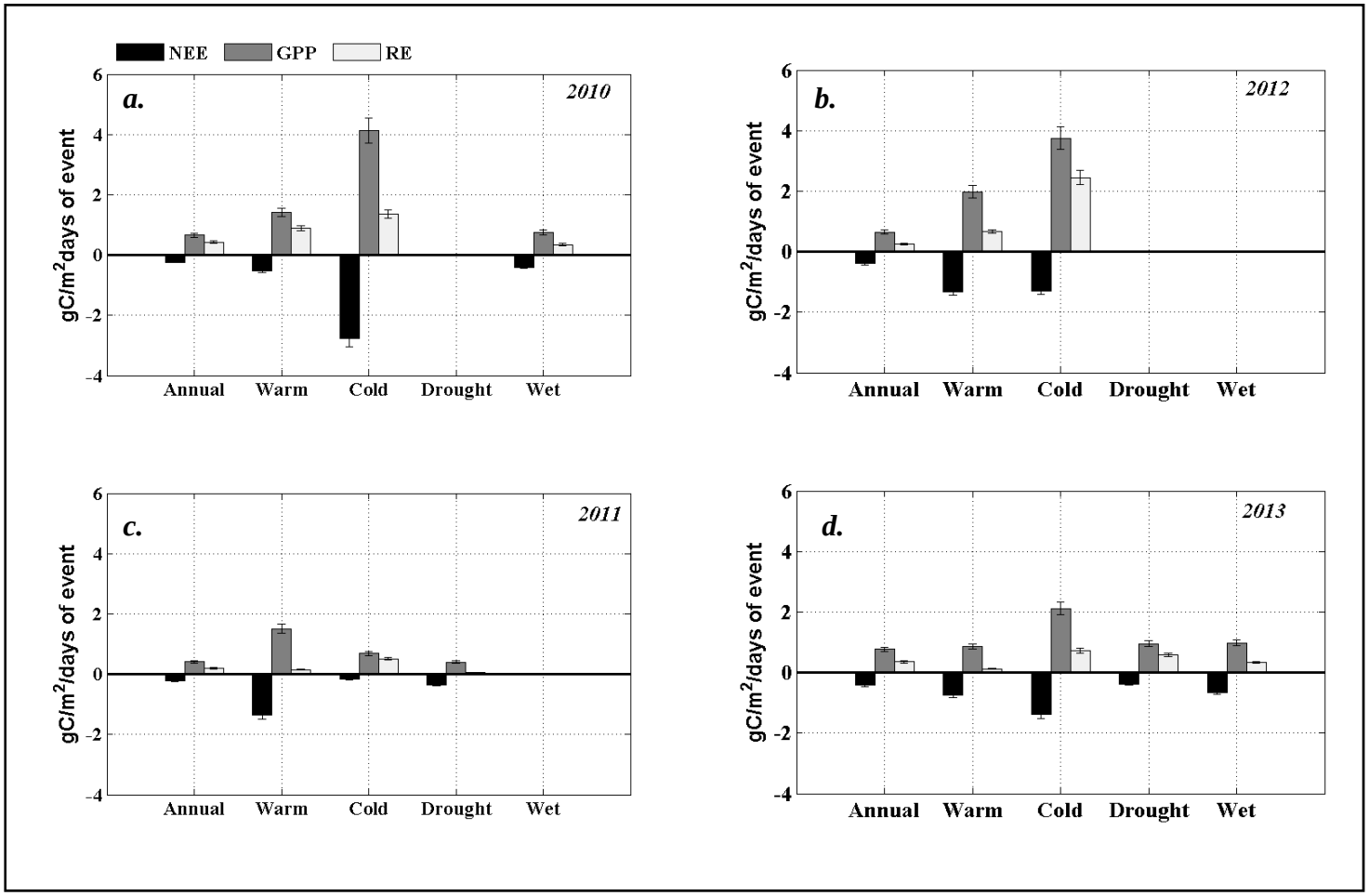


**Figure 22** Proportion of ecosystem fluxes during each extreme event per year during 2010-2013. Bars are normalized by the number of days per event as listed on table 6.

**Table 7** Contribution of cumulative ecosystem fluxes during extreme events per year, normalized by the number of days of their occurrence.

| Year | Event | NEE gC/m$^2$/#of days/ event | GPP gC/m$^2$/#of days/ event | R gC/m$^2$/#of days/ event |
|---|---|---|---|---|
| **2010** | Warm | -0.52 | 1.40 | 0.89 |
| | Cold | -2.77 | 4.13 | 1.36 |
| | Drought | 0.00 | 0.00 | 0.00 |
| | Wet | -0.41 | 0.76 | 0.35 |
| **2011** | Warm | -1.35 | 1.51 | 0.15 |
| | Cold | -0.17 | 0.68 | 0.51 |
| | Drought | -0.35 | 0.40 | 0.05 |
| | Wet | 0.00 | 0.00 | 0.00 |
| **2012** | Warm | -1.32 | 1.98 | 0.67 |
| | Cold | -1.29 | 3.74 | 2.45 |
| | Drought | 0.00 | 0.00 | 0.00 |
| | Wet | 0.00 | 0.00 | 0.00 |
| **2013** | Warm | -0.75 | 0.86 | 0.12 |
| | Cold | -1.39 | 2.12 | 0.73 |
| | Drought | -0.38 | 0.96 | 0.57 |
| | Wet | -0.65 | 0.98 | 0.33 |

### 3.3.5 Assess the impact of cumulative annual fluxes of NEE with and without the effect of extreme events

The 4yrs period of study compress 1460days. This time series is identified as Non-normal because it includes dates with occurrence of extreme events. The cumulative NEE under Non-Normal conditions was equivalent to -390.40 g/$m^{-2/}$4yrs. The period estimated as Normal comprised 1,208 days and a difference of ~60 gC/$m^{-2}$ of cumulative NEE was quantified under Normal conditions (-319.50 g/$m^{-2/}$4yrs) (See figure 24).

The analysis of the relative importance of each event over the 4-yr cumulative of NEE showed that the lowest difference of cumulative NEE (~40 gC/$m^{-2}$) was found when subtracting cold anomalies; followed by a ~20 gC/$m^{-2}$ difference of cumulative NEE when subtracting warm anomalies (-363.30 gC/$m^{-2}$/4yrs), finally the smallest difference of ~15 gC/$m^{-2}$ was found when subtracting drought conditions (-375.32 gC/$m^{-2}$/4yrs) (Table 8).

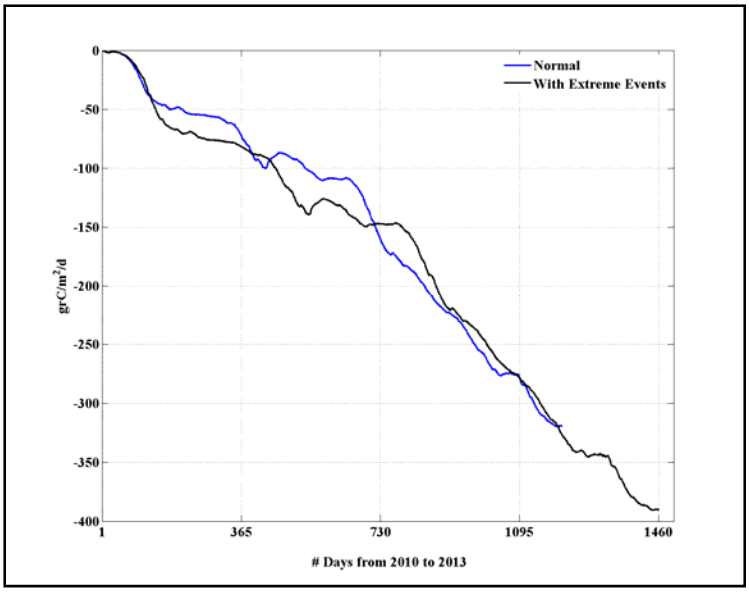


**Figure 23** Cumulative NEE during the four years period. Black line represents daily cumulative NEE during 4-yrs (n=1460), and blue line represents 4-yrs without extreme events (n=1208).

**Table 8** Annual cumulative of ecosystem fluxes with and without extreme events

| | *Num Days* | *NEE* $g/m^{-2}/4yrs$ |
|---|---|---|
| Normal (without Extreme Events) | 1,208 | -319.50 |
| With Extreme Events | 1,460 | -390.40 |
| Without warm anomaly | 1,374 | -363.30 |
| Without cold anomaly | 1,330 | -351.80 |
| Without drought anomaly | 1,399 | -375.32 |

*Analysis of the random forest analysis under Normal conditions*

The variables of importance output from the random forest analysis suggest that under normal conditions the main drivers of NEE are: Soil temperature at 15cm depth, net radiation, volumetric water content 2 and 1, (15cm and 5cm respectively), and photosynthetic active radiation. GPP and R are primarily controlled by vapor pressure deficit and volumetric water content 2 (15 cm depth). GPP however, is controlled by PAR, VWC1, and ST1; whereas R is controlled by VWC1, 2GRBi, and ST2 (Figure 25). The partial dependency plots suggest the thresholds of ecosystem fluxes are:

<NEE when, soil temperature <25°C, VWC1 between 0 – 0.10 $m^3/m^3$, PAR above 600umol/$m^2$, net radiation < 50watts/$m^2$.

>GPP when VPD >6,PAR>600, VWC1 and 2 >20 $m^3/m^3$, ST1 =25°C

>R when VPD >6, VWC1 and 2 >20 $m^3/m^3$, 2GRBi =30, ST2 >20°C

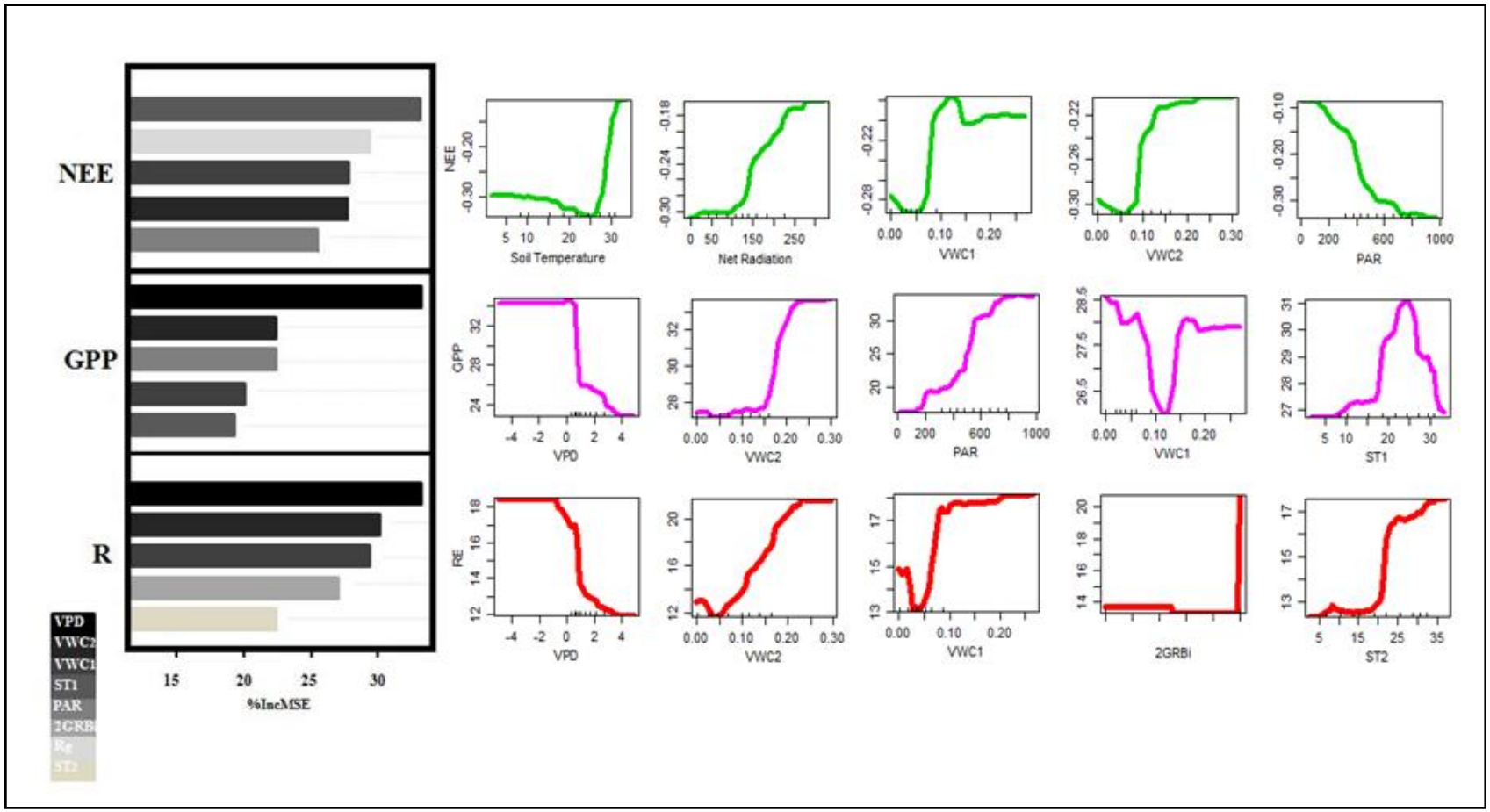


**Figure 24**. Left: Histogram of the top ranked biophysical controls from random forests classification for NEE, GPP, and Ecosystem respiration. Mean increase of error (*MSE*)for a variable show how much *MSE* or impurity increase when that variable is randomly permuted. Large *MSE* indicate important variables that will significantly change the predictions if randomly permuted. Right plots: Partial dependence plots (PDP) show the dependence between the target response (ecosystem fluxes) and a set of 'target' predictor (biophysical controls), when the rest of the predictors are held constant. Color scale indicates: Green=Net ecosystem exchange, Magenta= Gross ecosystem productivity, Red= Ecosystem respiration.

## 3.5. DISCUSSION

The study identified and quantified extreme events in the 4-year study period relative to long-term climatic records. It also, determined the importance of the identified extreme events relative to cumulative annual fluxes. Lastly, it estimated the difference of 4yr cumulative NEE and evaluated the controls of ecosystem fluxes under normal vs. non-normal conditions.

### *Climatology*

The analysis of the climatology and the standardized precipitation-evapotranspiration index of the last 30-years indicated that similar to other regions of western North America, the JER is undergoing a trend towards drier and warmer climate (Seager *et al.* 2007). The mean annual temperature in the last 30 years was 3°C above the long-term annual temperature and precipitation was 73mm below the long term maximum precipitation estimated by Wainwright (2006). Specifically for the period of study from 2010 to 2014, the JER experienced the lowest mean annual precipitation of the last 30-years in 2011 (98.9mm), but still above the long-term record of 70mm in 1974.

### *Cold anomalies*

Cold anomalies had precedent in western North America in 1983, 1989, 2003, 2006, 2008, and 2010 (Federal Energy Regulatory Commission 2011). However, the cold anomaly event of February 2011 was the coldest of the region on record. The event was caused by an intense arctic air mass that was moved into southern New Mexico and far West Texas by a strong upper level high pressure ridge across western Canada and the Arctic Ocean (NOAA 2011). Despite the magnitude of the event, the analysis of ecosystem fluxes did not show significant reduction in the carbon sequestration capacity. These results agree well physiological studies that suggest *Larrea tridentata* can withstand sustained freezing temperatures and maintain relatively high rates of photosynthesis rates are maintained under temperatures of -24C

(Medeiros *et al.* 2012). In fact, the subsequent cold anomalies increased the carbon sequestration capacity of the system. Snow increases albedo (Davidson & Wang 2004) and if it melts, can wets soil layers deeper than the surface, therefore stimulating photosynthesis and the subsequent green-up of the shrub canopy (Sanchez-Mejia 2013). However, Plants are very sensitive to changes in temperature (Martin *et al.* 2010), thus timing of cold anomalies demonstrate to be important, because when cold anomalies occur at leaf bud or leaves of their lifecycle, the system shifted to a small source of carbon.

*Warm anomalies*

Warm anomalies were infrequent and ranged from one to three consecutive days. Their occurrence led to heat stress that inhibited photosynthesis and promoted increased respiration mainly in winter. Their cumulative effect may lead to dehydration and substantial decrease in the accumulation of carbon stocks (Anderson-Texeira *et al.* 2011). Similar effects have been reported in other shrublands in the US southwest (Hüve *et al.* 2011).

*Drought*

The estimation of the hydrological drought by the SPEI indicated the unfolding of a drier state of the region since 1993. Recent studies in the US southwest show evidence that these conditions have been triggered and exacerbated by the increasing intensity of El Niño–Southern Oscillation (ENSO) of 1992-93 and 1997-98 (Seager *et al.* 2007). The latter, with greater magnitude, had remarkable impact on water supply and storage in the region, causing an unprecedented drought since the last 800 years. In the 30-year period of analysis, the turn of the century drought was depicted in the 1-month SPEI as exceptionally drought conditions between 2002 and 2003. Severe drought conditions were experienced sporadically in subsequent years (2004, 2005, 2011, and 2013). This study focused on severe drought periods that prevailed in 2011 and 2013. Severe drought had repercussion on the carbon sequestration capacity of the system, especially in 2011. Although, the study site remained a small carbon sink during the

peak of the severe drought conditions depicted by the SPEI, its effects were not perceived until 1 to 2 months later, when respiration rates favored GPP, and the system became a small source carbon. Similar patterns were reported by Anderson-Texeira et al (2011) for shrublands of the Sevilleta –LTER. Conversely sensible heat flux rates held constant seasonality throughout the 4-years, with higher rates on cold events, with the exception of 2011, where warm events represent two times higher rates than cold anomalies and drought.

*SPEI-Wet*

The overall period of study did not have exceptionally wet conditions. In fact, the 30-years data revealed a substantial decrease in precipitation since 1983. The SPEI reflects values of water supply slightly higher than the demand of water for this period. Thus, in this study the denominated wet period is not a direct reflection of wet conditions caused by precipitation pulses in relationship with the carbon sequestration capacity of the system.

*Extreme events and annual cumulative fluxes*

Annual cumulative fluxes shown differences in the period of study, this are attributed to the occurrence of extreme events; as it has been demonstrated that extreme events contribute to a small but significant amount to the variability of carbon balance (Zscheischler, J., et al 2014). These results suggest the occurrence of extreme events have important implications of a multiyear cumulative net carbon uptake in the system. Extreme drought conditions had the biggest impact on reducing carbon sink capacity of the system. These results suggest that the interaction of precipitation and evaporation are critical to inhibit/promote carbon sink capacity of the system, similar to other regions of the Chihuahuan desert reported by Texeira, et al (2010).

Future directions to complement this study are to parameterize drivers of ecosystem fluxes under normal conditions using the deterministic model described on chapter 2. This

evaluation will be able to compare normal vs. non-normal biophysical drivers and their relative impact on net ecosystem exchange.

### 3.6 CONCLUSION

Even though extreme events are erratic in occurrence and duration (from days to 2-months), their incidence have important implications on regulating ecosystem fluxes because they modify seasonal patterns of their biophysical controls Hence, Regardless of the duration length of the event, they have important effects on the annual cumulative of ecosystem fluxes.

Inter-annual variability showed important differences in carbon uptake especially during years when severe drought was documented. The severe drought of 2011 decreased the sink capacity of the system and was also reflected on the carbon sequestration of 2012; the system recovers on 2013. Conversely, sensible heat flux presented small variations in magnitude per year.

If the current trends toward drier and warmer climate continue, it is likely shrubs withhold under these conditions. The success of shrubs under these conditions will increase desertification rates; because C3 plants are less adapted and will be displaced by the more resilient and adapted shrubs.

**Acknowledgements**

30-year climatology data sets were provided by the Jornada Basin Long-Term Ecological Research (LTER) project. Funding for these data was provided by the U.S. National Science Foundation (Grant DEB-1235828)

# Chapter 4: Assessment of the effectiveness of scaling carbon dioxide and water vapor fluxes through integrating spectral and flux measurements in a shrubland ecosystem

## 4.1 ABSTRACT

This study aimed at evaluating the effectiveness of scaling ecosystem fluxes of carbon using a range of optical sampling methods employed in desert shrublands. Specific activities were explore the relationship between ecosystem fluxes and a range of spectral indices derived from hyperspectral a robotic tram system and phenocams. Specifically, the research questions were 1) Can land-atmosphere fluxes of carbon be adequately modeled using a range of ground-based remotely sensing methods; 2) which spectral indices most closely correlate with ecosystem fluxes of carbon, water and energy, why and when; and 3) do spectral indices capture Inter-annual variability of ecosystem fluxes in a desert shrubland? This study provided a comprehensive exploratory analysis of the feasibility of modeling GPP using a range of spectral indices derived from two spectral platforms. Results indicate that spectral indices derived from hyperspectral remote sensing and phenocams have the capacity to model GPP in desert shrublands. Specifically Volgeman and SR03 were better correlate with GPP, specially during wet conditions. Estimating GPP from either spectral indices was less successful. A more detailed characterization of leaf level physiological processes of C4 shrublands to variability of environmental drivers needs to be further investigated.

## 4.2 INTRODUCTION

The impact of global change at large spatial scales is assessed primarily from global terrestrial models derived from remotely sensed products (Turner *et al.* 2005). Estimation of photosynthetic activity derived from reflectance and fluorescence is used to develop global models of terrestrial gross primary production (GPP)(Schaefer *et al.* 2012), net primary production (NPP), light use efficiency (LUE) (Cheng *et al.* 2009), and phenology (Richardson *et al.* 2007). Remotely sensed products are also used to assess temporal dynamics in vegetation spectra (Campbell *et al.* 2011), woody plant density (Mark *et al.* 2008), patterns of carbon dioxide and water fluxes (Fuentes & Zhiyan Mao a 2006), ecosystem carbon uptake, albedo (Kim *et al.* 2006), and vegetation physiological status and diurnal and seasonal variability in photosynthetic efficiency (Middlenton 2010).

A range of remote sensing platforms have been used by several studies to couple and scale tower-based measurements of net ecosystem exchange of carbon, water and energy using spectral indices (Baldocchi *et al.* 2001; Fuentes & Zhiyan Mao a 2006; Gamon *et al.* 2011). A recent study by Balzarolo *et al.(* 2011) report the use of a dual-channel automatic system fixed to a tower is commonly used among the European community. The use of hyperspectral dual channel spectrometers mounted on robotic tram systems (Gamon *et al.* 1992; Goswami *et al.* 2011), rotating hemispherical spectrometers (Cheng *et al.* 2009), and phenocams have also been reported (Richardson *et al.* 2007; Kurc & Benton 2010). Phenocams have been recognized as a relatively low cost solution to spectrometers and their relative simplicity, low maintenance requirements and ease by which images can be automatically processed has underpinned their

now relatively broad scale use by the eddy covariance community striving to improve or automate plant to landscape scale phenology monitoring at their sites (Yang *et al.* 2014).

The use of these spectral platforms have provided scientist the ability to develop sophisticated models that have been parameterized by combining plant or ecosystem physiology and spectral measurements to derive spectral indices from hyperspectral measurements (Asner 1998; Goswami *et al.* 2011), and more recently greenness indices derived from phenocams (Richardson *et al.* 2007; Yang *et al.* 2014). Using such models, Scientists had characterized the relative importance of a range of plant functional types (Sims & Gamon 2002), leaf structures (Gamon *et al.* 1995; Huemmrich *et al.* 1999), and leaf developmental stages (Gamon *et al.* 1992; Campbell *et al.* 2011). Among them we find those sensitive to the relative importance of seasonal or other changes in leaf pigments such as Carotenoid content (Gitelson *et al.* 2002), Chlorophyll content (Carter, et at, 1994); Chlrophyll1A, 2A,1B, 2B content; Gitelson 1-5 (Gitelson & Merzlyak 1994, 1997); and indices such as Canopy greenness (Sims & Gamon 2002), Normalized difference vegetation index (Alfieri *et al.* 2007), pigments sensitive to changes in carotenoid, and conversion of xanthophyll-Phytochrome, Photochemical reflectance- (Gamon *et al.* 1992; Penuelas *et al.* 1995; Sims & Gamon 2002), estimating leaf area index through simple ratio; total chlorophyll content, (Volgeman, et. al. 1993), and plant water content (Claudio, H., et. al., 2006), among many others. Over the past decade especially, various greenness indices (e.g. NDVI, Gamon *et al.* (1995)) have been generally favored for monitoring plant health (Szilagy *et al.* 1998), due to their simplicity relative to other spectral indices, calculation potential using space borne platforms (Davidson *et al.* 2003), and general adequacy for modeling ecosystem phenology and physiology (Huemmrich *et al.* 1999). Phenocams deriver

greenness indices, or other fixed digital camera platforms, are calculated from a combination of red-green-blue (RGB) channel intensities derived from digital images. Among the most commonly used phenocam greenness indices in ecosystem studies are 2GRBi, Total RGB, and relative channel brightness (Richardson *et al.* 2007; Kurc & Benton 2010; Gonzalez, *et al.* 2011). Recent software developments have facilitated the otherwise labor intensive data processing of robotic tram line hyperspectral and phenocams platforms (Laney *et al.* 2013; Gonzalez, *et al.* 2011), These software tools provide a framework to evaluate the effectiveness of integrating remote sensed products with ecosystem flux data and a capacity to improve the representation of plant to landscape phenology in models to monitor broad scale ecosystem dynamics.

The challenge of integrating and developing models from spectral and greenness indices and ecosystem fluxes derived from tower-based measurements and scaling these to larger areas involves taking spatial and temporal processes at one scale to estimate information at larger spatiotemporal scales (Kim *et al.* 2006). For instance, tower-based flux measurements are restricted by spatiotemporal scales of about $<10^4$ to $10^6$ $m^2$ and hours to years, respectively (Castellvi *et al.* 2008; Burba & Anderson 2010) whereas remote sensing data typically provide coarser multi-temporal coverage providing the opportunity of scaling surface flux models from $>10^6$ to $10^{12}m^2$ and longer temporal periods spanning days to decades (Kim *et al.* 2006). The issue of scale-appropriateness or the scale of the spectral measurements relative to the spatial sample of eddy covariance is not yet well understood for a wide range of ecosystems, especially dryland landscapes (Asner 2001). The broader challenges that need to be addressed in order to move this field forward include improved methods or protocols for scaling flux estimates to advance cross-site comparison and up-scaling at regional levels (Balzarolo *et al.* 2011). Another

challenge is that desert shrublands are challenging ecosystems for deriving spectral products, because leaf area index is typically small, large expanses of sometimes reflective bare soil exists in shrub interspaces, and vegetation in these systems can respond quickly to phenological, climatic and other changes not readily captured at the scale of many remotely sensed products. Also, desert shrublands dominated by evergreen plants such as creosote bush, represent a challenge because they poses a relatively continuous sustained photosynthesis, therefore green-up signals and small carbon and latent heat fluxes are expected to be difficult to perceive with spectral derived products.

There are few comprehensive studies that characterize the effectiveness of using greenness indices to represent carbon uptake from C4 shrublands in the Santa Rita Experimental Range (Kurc & Benton 2010). This study intends to further explore the feasibility of two different spectral platforms to scale ecosystem fluxes. The rationale is that by improving accurate representation of spectral characteristics of desertified landscapes undergoing desertification process will improve ecosystem modeling that couple land-surface processes to the climate system, anthropogenic disturbances, among others (Richardson *et al.* 2013). To the best of my knowledge, currently there are only three similar hyperspectral systems with a mobile robotic cart actively operating in North America. Thus, this study provided a remarkable opportunity to evaluate the performance of semi-automated and phenocams coupled with flux tower estimation of ecosystem fluxes.

To date, few studies have assessed the relative accuracy of hyperspectral derived vs phenocam derived indices for modeling ecosystem fluxes in desert landscapes. The overarching

objective of this study is to use a range of optical sampling methods to evaluate representation of ecosystem fluxes of shrublands. Specific activities explore the relationship between ecosystem fluxes and a range of spectral indices derived from hyperspectral a robotic tram system and phenocams. Specifically, the research questions are 1) Can land-atmosphere fluxes of carbon be adequately modeled using a range of ground-based remotely sensing methods; 2) which spectral indices most closely correlate with ecosystem fluxes of carbon, water and energy, why and when; and 3) do spectral indices capture Inter-annual variability of ecosystem fluxes in a desert shrubland?

## 4.3. METHODS

### 4.3.1 Site description

The study site was located in the Jornada Basin Long Term (JER) site in Southern New Mexico (32.5655 N, -106.6598 W) in a shrubland representative of the northern Northern Chihuahuan desert. Vegetation at the site is dominated by creosote bush (Larrea tridentata) and honey mesquite (Prosopis glandulosa) shrubland. Creosote bush is an evergreen, drought-resistant C4 perennial shrub (Peters et al. 2006). Honey mesquite is a deciduous, thorny, long lived C4 shrub that is characterized by very deep and laterally extensive root systems (Peters et al. 2006). Other species found at the site include tarbush (Flourencia cernua), the grass bush muhly (Muhlenbergia porter), fluff grass (Dasyochloa pulchella), as well as a variety of forbs. Soils are classified as Ustic Calciargids (Northern Chihuahuan desert Rangeland Research Center 1980 Doña Ana Soil Survey).

### 4.3.2 Digital camera observations of plant phenology – Phenocams

Ground based observations of plant phenology were documented with a phenocam network that was mounted on top of a 10m tower (~8 m above the canopy) using three digital phenocams to cover a 170 degree view over the primary sampling area of eddy covariance instrumentation mounted to the same tower . The three phenocams (Microsoft Vx7000 with 1600 x 1200 pixel resolution) had a manually fixed focus for the specific experimental area. The phenocams were connected to a Belkin USB Plus 4-Port Hub (5V/2.6 A) mounted in a customized weatherproof camera enclosure, with a 36ft Tripp Lite U042-036 USB2.0 A/B repeater cable extension. Each phenocam took pictures hourly from 7:00AM to 7:00PM every day between March 2010 and December 31, 2013. Images were stored with a minimal compression factor in JPEG format and offer a visual record of plant to landscape phenological development. Daily images taken at 12:00PM were selected for the analysis. The analysis was embedded in a customized graphical user interface within MATLAB® 7.8.0 software that allows for the selection of regions of interest (ROI's) and the subsequent calculation of reflectance in the visible wavelength using R, G, and B channels. A specific ROI was selected in each of the three phenocams to correspond to the primary sampling footprint of the eddy covariance instrumentation (Figure 26). The lists of estimated indices are listed on table 9. This phenocam system is described in detail by Gonzalez (2011).

**Table 9** List of spectral indices derived from the phenocams used in this study as analyzed by custom MATLAB-coded phenology analyzer

| *Name* | *Definition* | *Formula* |
|---|---|---|
| nNDVI | Near normalized difference vegetation index | (green - red)/(green + red) |
| 2GRBi | Greenness index | (2green - red)/(green + red) |
| TotalRGB | Total RGB | R+B+G |
| Red band | Digital number (DN) of the red channel - an indicator of brightness | |
| Green band | Digital number (DN) of the green channel - an indicator of brightness | |
| Blue band | Digital number (DN) of the blue channel - an indicator of brightness | |
| green_pct | Percent of brightness attributed to the green channel as compared to total RGB | |
| blue_pct | Percent of brightness attributed to the blue channel as compared to total RGB | |
| red_pct | Percent of brightness attributed to the red channel as compared to total RGB | |

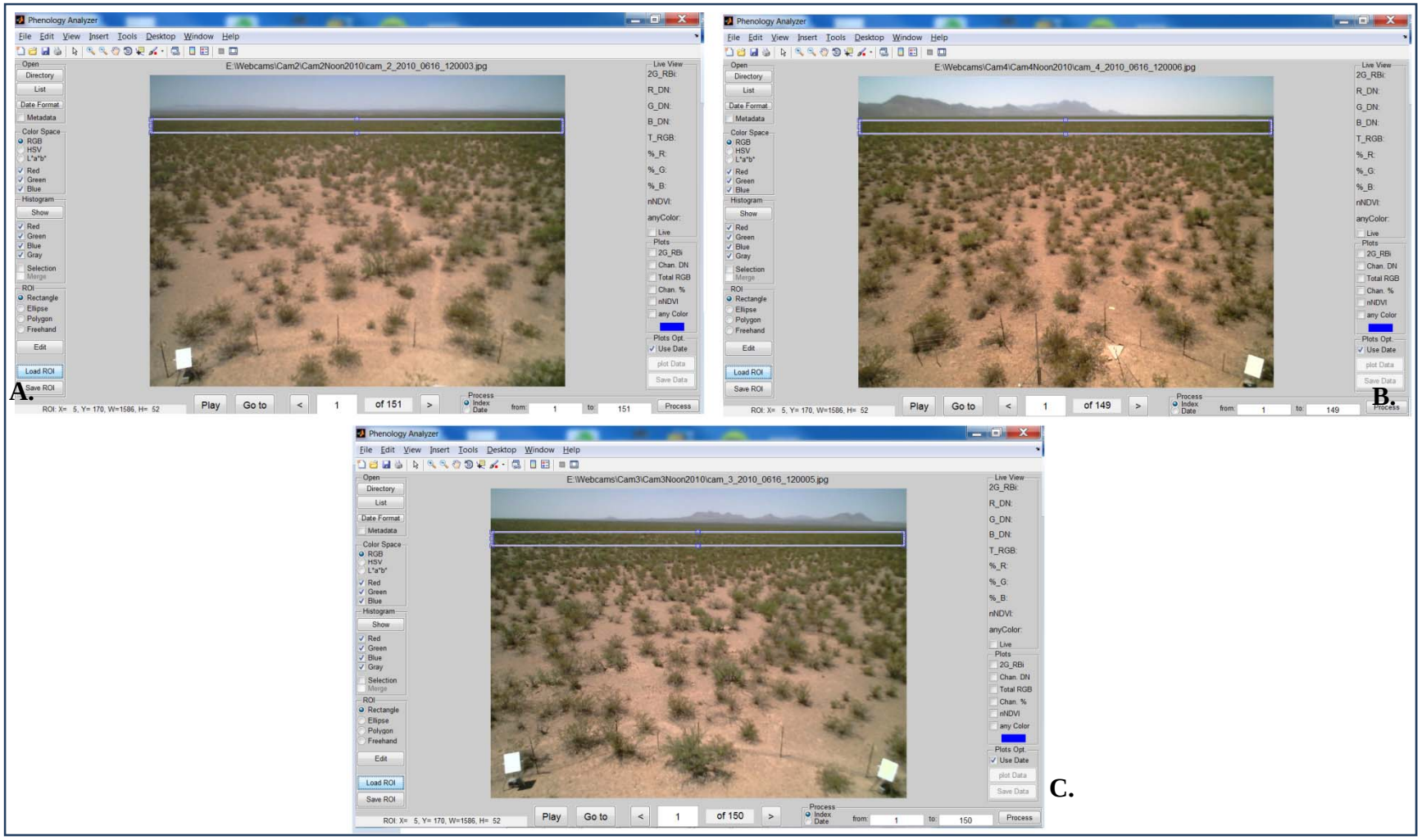


**Figure 25** The interface of MATLAB-coded Phenology Analyzer is presented above. Three digital cameras, and the ROI (denoted by the blue rectangle). A) Phenocam 2, B) Phenocam 3, and C) Phenocam 4.

### 4.3.3 Indices derived from a robotic Tram system

Hyperspectral reflectance measurements were made weekly using a robotic tram system similar to that described by Gamon et al. (2006) and Goswami et al. (2011). This customized system consists of a 110m east-west oriented tram rail system that provides platform upon which a robotic cart operates. A dual-detector field portable spectrometer with a nominal range of operation between 400 and 1000 nm (Unispec DC, PP Systems, Amesbury, MA, USA) is placed on the semiautonomous robotic cart, which is started manually and travels along the tramline to make measurements. A mechanical switch mounted on the base of the cart passes over crossbars situated every meter along the tramline triggering the spectrometer to make a measurement. The spectrometer simultaneously measures irradiance (incoming radiation from the sky) and radiance (outgoing radiation from the vegetation/ground). The two detectors are cross-calibrated using a white panel with 99% reflectance at the beginning and end of each tram run. Typically, three or four sampling runs are performed consecutively each week, and within two hours of solar noon. Data have been collected and processed by a number of graduate students at SEL since the spring 2010 (Figure 27). Derivation of spectral indices was performed using *rHyperSpec.r* a software application to analyze and visualize hyperspectral data in order to derive 67 spectral indices (Laney 2013, see Table 10 for a derived list of spectral indices).

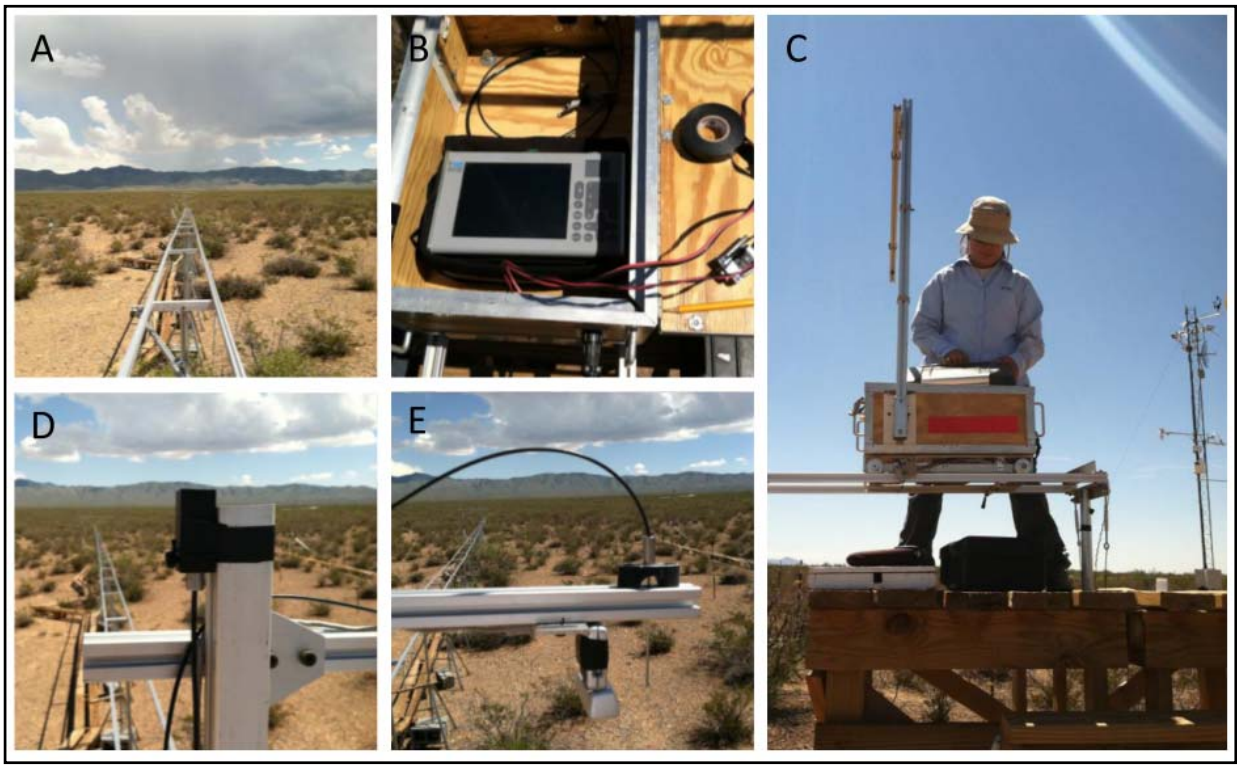


**Figure 26** The 110m long aluminum rail tramline and spectrometer setup at the SEL-Jornada research site. A. The rail extends 110 m from west (270°) to east (90°). B. The unispec DC spectrometer mounted in the robotic cart. C. A researcher prepares the semiautonomous robotic cart. D. The upward-facing fiber optic with cosine head. E. The downward facing fiber optic fitted with ferrule and hypo tube that limits the field of view 20°. A downward facing phenocam is also mounted adjacent to the downward facing fiber optic of the spectrometer.(Image from Laney *et al.* 2013)

**Table 10** List of spectral indices calculated from *rHyperSpec.r* (Laney *et al.* 2013). The compilation of spectra indices was generated by Fred Huemmerich. The expression column denotes the calculation for each index. R indicates reflectance follow by the correspondent wavelength.

| *Application* | *Name* | *Index Abbreviation* | *Expression* | *Reference* |
|---|---|---|---|---|
| Carotenoid content | Carotenoid 1 | cri1 | (1/R510)-(1/R550) | Gitelson AA, et. al. (2002) |
| | Carotenoid 2 | cri2 | (1/R510)-(1/R700) | Gitelson AA, et. al. (2002) |
| Chlorophyll content | Carter 1 | carter1 | R695/R760 | Carter, G.A., (1994) |
| | Carter 2 | carter2 | R695/R420 | Carter, G.A., (1994) |
| chlorophyll a, chlorophyll b, chlorophyll a + b, and total carotenoid content | Chlorophyll 1 A | chl1a | (R740^2)/(R675*R800) | |
| | Chlorophyll 1 B | chl1b | (R740^3)/(R675*R695*R800) | |
| | Chlorophyll 2 A | chl2a | (R685^2)/(R675*R800) | |
| | Chlorophyll 2 B | chl2b | (R685^3)/(R675*R695*R800) | |
| | Curvature Index | Curvature | (R675*R690)/(R683^2) | Zarco-Tejada, P. J., et. al. (2002) |
| | Datt 1 | datt1 | R860/(R708*R550) | Datt B (1998) |
| Chlorophyll content | Gitelson 1 | gitelson1 | (R800-R700)/(R800+R700) | Gitelson, A. A., (1994) |
| | Gitelson 2 | gitelson2 | (R750-R705)/(R750+R705) | Gitelson, A. A., (1994) |
| | Gitelson 3 | gitelson3 | (R750-R445)/(R700-R445) | Gitelson, A. A., (2003) |
| | Gitelson 4 | gitelson4 | (1/R550)-(1/R750) | Gitelson, A. A., (2003) |
| | Gitelson 5 | gitelson5 | (1/R700)-(1/R800) | Gitelson, A. A., (2003) |
| | Greenness 1 | green1 | (R554/R675) | |
| Frost Damage | Modified Normalized Difference Vegetation Index | Mndvi | (R750-R705)/ (R750+R705-2*R445) | |
| Canopy greenness | MSR | Msr | (R750-R445)/(R705-R445) | D.A. Sims, (2002) |
| | Normalized Difference 1 | nd1 | (R682-R553)/(R682+R553) | S. Gandia, 2004. |
| | Normalized Difference 2 | nd2 | (R708-R546)/(R708+R546) | Yi et al 2007 |

| *Application* | *Name* | *Index Abbreviation* | *Expression* | *Reference* |
|---|---|---|---|---|
| Canopy greenness | Normalized Difference 3 | nd3 | (R750-R705)/(R750+R705) | D.A. Sims, (2002) |
| | Normalized Differential Vegetation Index 1 | ndvi1 | (R800-R680)/(R800+R680) | |
| | Normalized Differential Vegetation Index 2 | ndvi2 | (R800-R667)/(R800+R667) | |
| | Normalized Differential Vegetation Index 3 | ndvi3 | (R750-R667)/(R750+R667) | |
| | Normalized Differential Vegetation Index 4 | ndvi4 | (R774-R677)/(R774+R677) | |
| | Optimized Soil Adjusted Vegetation Index (OSAVI) | Osavi | 1.16*(R800-R670)/(R800+R670+0.16) | Rondeaux, G.,(1996) |
| Pigment to detect the use of light | Phytochrome 1 | phyt1 | R730/(R730+R652) | |
| | Phytochrome 2 | phyt2 | (R730-R652)/(R730+R652) | |
| | Phytochrome 3 | phyt3 | R724/(R724+R654) | |
| | Phytochrome 4 | phyt4 | (R724-R654)/(R724+R654) | |
| | Phytochrome 5 | phyt5 | R730/(R730+R666) | |
| | Phytochrome 6 | phyt6 | (R730-R666)/(R730+R666) | |
| Sensitive changes to carotenoid | Photochemical Reflectance Index 1 | pri1 | (R531-R570)/(R531+R570) | John Gamon et al 1992 |
| | Photochemical Reflectance Index 2 | pri2 | (R530-R550)/(R530+R550) | Sims DA, (2002) |
| | Photochemical Reflectance Index 3 | pri3 | (R531-R670)/(R531+R670) | Gamon, J.A., 1997 |
| | Photochemical Reflectance Index 4 | pri4 | (R531-R667)/(R531+R667) | |
| | Plant Senescence Reflectance Index | psri | (R680-R500)/R750 | Merzlyak MN, (1999) |

| Application | *Name* | *Index Abbreviation* | *Expression* | *Reference* |
|---|---|---|---|---|
| | Reflectance Phytochrome | Rphyto | R730/(R730+R665) | |
| | RFFR 1 | rffr1 | R730-R650 | |
| | RFFR 2 | rffr2 | (R730-R650)/(R685+R650) | |
| | RF Green | Rfgreen | R525-R550 | |
| | RF Red | Rfred | R690-R650 | |
| | RI | RI | (R678-R667)/(R678+R667) | |
| | Structure Independent Pigment Index | Sipi | (R800-R450)/(R800-R650) | Peñelas, J., 1995. |
| | Simple Ratio 01 | sr01 | R430/R762 | |
| | Simple Ratio 02 | sr02 | R550/R430 | |
| | Simple Ratio 03 | sr03 | R550/R650 | |
| | Simple Ratio 05 | sr05 | R685/R655 | |
| | Simple Ratio 06 | sr06 | R690/R655 | |
| | Simple Ratio 07 | sr07 | R705/R715 | |
| | Simple Ratio 08 | sr08 | R705/R930 | |
| | Simple Ratio 09 | sr09 | R708/R545 | |
| | Simple Ratio 10 | sr10 | R750/R550 | |
| | Simple Ratio 11 | sr11 | R750/R700 | |
| | Simple Ratio 12 | sr12 | R750/R705 | |
| Estimating LAI | Simple Ratio 13 | sr13 | R752/R690 | |
| | Simple Ratio 14 | sr14 | R775/R675 | |
| | Simple Ratio 15 | sr15 | R800/R650 | |
| | Simple Ratio 16 | sr16 | R800/R680 | |
| | Simple Ratio 17 | sr17 | R800/R750 | |
| | Simple Ratio 18 | sr18 | R860/R550 | |
| Total chlorophyll content | Vogelman Red Edge 1 | vog1 | R740/R720 | Vogelmann, J.E., 1993. |
| | Vogelman Red Edge 2 | vog2 | (R734-R747)/(R715+R726) | Vogelmann, J.E., 1993. |
| | Vogelman Red Edge 3 | vog3 | (R734-R747)/(R715+R720) | Vogelmann, J.E., 1993. |
| Plant Water Content | Water Band Index | Wbi | R900/R970 | Claudio, H., et al. (2006). |

### 4.3.4 Ecosystem fluxes

Eddy covariance measurements were used to quantify ecosystem exchange of water, energy and carbon dioxide during 2010-2013. The instrumentation consisted of a three dimensional sonic anemometer (CSAT3-SONIC CSI) and an infrared gas analyzer (LI-7500 Li-COR Inc). Manufacturer protocols for installation, maintenance, and calibration were followed and kept to assure proper system performance (Campbellsci 2004, 2005, 2009; Zonen 2004). The infrared gas analyzer was calibrated against gas mixtures with 500 ppm $CO_2$; the span for the water vapor was calibrated with a dew point generator (Li 610, Li-COR Inc). The instrument was zeroed using 99.99% nitrogen gas. With adherence to the protocol, 30 min fluxes were calculated from fast response instrumentation and independent measurements from slower response sensors were used to measure and calculate background meteorological variables. Flux calculations were computed with EddyPro TM 4.1 software. Then, a moving average window of 5 days was used to reject spikes following the method described by (Lee *et al.* 2004). Additionally, to eliminate the influence of the stable lower boundary conditions, all flux data recorded with u* less than 0.1ms-1 were discarded. Gap filling and flux partitioning was done following Lasslop et al.'s (2010) method. Day and night time separation was based on a threshold of photosynthetic photon flux density. Ecosystem respiration output from the Lasslop et al. (2010) method was used to estimate gross primary production using Equation 1 as described by (Reichstein *et al.* 2012a). Data collection and data processing were validated using the eddy covariance portable system and their MATLAB flux processing routine during August 2012. Standard sign convention for NEE is used to indicate NEE>0 equals a net loss of $CO_2$ to the atmosphere (source) and NEE<0 indicates $CO_2$ uptake by ecosystem (sink). The results

obtained with the use of the eddy covariance system represent the average functioning of land-atmosphere interactions within the footprint area. The footprint size is a combination of measurement height, atmospheric conditions such as wind speed and stability, and surface characteristics (Kjun et al. 2004). The footprint analysis was done using a combination of the footprint models from (Kormann et al. 2001) and (Kjun *et al.* 1997), built within EddyPro 4.1.0 (LICOR 2011). The 90% daytime footprint contribution distance reached a yearly average of 370m. The mire has a very stable and well-defined southwesterly wind direction distribution.

### 4.3.5 Statistical analysis

A random forest analysis was used to construct regression tree models for correlating the response of ecosystem fluxes (NEE, R, GPP) to spectral indices derived from hyperspectral and phenocam measurements. Random forest analysis is a machine-learning technique based on regression tree analysis (Cutler *et al.* 2007). In a standard regression tree analysis, response data are recursively split into groups based on the values of predictor variables. Tree models can represent complex, non-linear relationships between variables, because the same predictor variable can appear at multiple branch points (Cutler *et al.* 2007). However, tree algorithms tend to over-fit the data, and cross-validation is required to determine their predictive power. Standard regression trees are also inadequate as a solution for multicollinearity between predictors because each split is based on only a single predictor variable. When predictors are strongly inter-correlated, tree models select arbitrarily among them, which can lead to a loss of information and biological plausibility in the final tree (Karels *et al.* 2004). Random forest techniques allow the user to overcome these limitations. 1000 trees were generated based on bootstrapped samples (random sampling with replacement) drawn from the original dataset. Each tree used a randomly selected set of predictor variables. The mean squared error (MSE) was calculated for each tree by

comparing its predictions for the out-of-bag data set with observed values in order to generate an estimate of the percent of variance in the response variable explained by the tree. These values are averaged over the entire 'forest' of regression trees to produce a cross-validated estimate of model fit (Liaw & Wiener 2002a; Archer & Kimes 2008). In addition to its benefits when compared to standard regression tree models, the random forest algorithm is a robust alternative to more common multivariate techniques like multiple linear regression and other types of generalized linear models, which, although relatively simple to interpret, are highly sensitive to multicollinearity and require the explicit specification of interactions between variables at a cost of increased model complexity (Hastie *et al.* 2011). In contrast, random forest models are relatively insensitive to the distributions of predictor variables. The characteristics of random forest models make them particularly well-suited to complex analyses with large numbers of potentially important predictor variables. However, like any statistical model, random forest models can generate spurious results, and should ideally only use predictor variables with strong *a priori* justification (Cutler *et al.* 2007; Strobl *et al.* 2007).

***Model Structure***

Ten random forest models were constructed to investigate which spectral and phenocam indices most closely correlate with ecosystem fluxes of carbon, water and energy, why and when. Nine spectral indices from Phenocams and sixty seven spectral indices derived from Hyperspectral reflectance collected from the robotic tram system. Five additional RF models were constructed to include all spectral indices from the combination of both platforms. For each RF model 1000 regression trees were generated. These models used the model-averaged percent variance explained, which can be interpreted similarly to the $r^2$ value of a multiple regression

model. All random forest modelling was conducted using the random forest package in R (Liaw & Wiener 2002b). Missing values were excluded from the models, yielding a sample size of 1146 observations for phenocams RF models and 148 observations for hyperspectral random forest models. The number of observations correspondent to each year were 30 observations in 2010, 47 observations in 2011, 39 observations in 2012, and 30 observations in 2013 (See table 11). The top spectral predictors of ecosystem fluxes were selected and subsequent linear regression plots were used to determine the correspondence between predicted and observed values.

***Variable of importance***

The variables of importance of spectral indices and ecosystem fluxes were evaluated by comparing predictor variables importance metrics in each model. Model-averaged variable importance estimates can be generated using out-of-bag data (Archer & Kimes 2008), and can be interpreted heuristically in much the same way that Akaike weights (Dalgaard 2008) are used when results are averaged across multiple generalized linear models (Burnham & Anderson 2002). To calculate variable importance, out-of-bag values for a given variable and trees are randomly permuted, and the tree mean squared error (MSE) is then estimated using both the original and the permuted out-of-bag data set. The resulting percent increase in MSE reflects the predictive power of that variable compared to random chance. Model-averaged variable importance values reflect the mean influence of a given variable on model fit, regardless of which other variables are included. Because they are generated stochastically, model-averaged variable importance values can vary slightly between model runs. As a result, the rank order of variables with similar importance may vary on a run-by-run basis, which can complicate the

interpretation of model output. However, if the top-ranked variables in a random forest result have substantially higher importance values than all others, their position generally remains unchanged from run to run. This was the case in the analyses performed herein, thus the top predictor variables from each model and for each response variable was identified, and selected as the main predictor. The goal was to identify spectral indices that were better correlated with ecosystem fluxes. The process followed to integrate Spectral data and ecosystem fluxes are described in a concept map depicted in Figure 28.

***Exploring relationships between top predictors and response variables***

Further exploration of correlations between top predictors and response variables were performed by using time series and correlation plots wherein predictors with the highest MSE as depicted on the variable of importance plots of the random forest analysis were selected. Selected variables were designated as primary responses of ecosystem fluxes. Scatter plots and linear best fit function were extracted using Matlab Statistical toolbox.

**Table 11** dates of hyperspectral measuraments from 2010 to 2013

| Year | Julian Day | Year | Julian Day | Year | Julian Day | Year | Julian Day | Year | Julian Day |
|---|---|---|---|---|---|---|---|---|---|
| 2010 | 145 | 2011 | 6 | 2011 | 222 | 2012 | 151 | 2013 | 96 |
| 2010 | 152 | 2011 | 13 | 2011 | 229 | 2012 | 159 | 2013 | 124 |
| 2010 | 159 | 2011 | 21 | 2011 | 236 | 2012 | 165 | 2013 | 137 |
| 2010 | 166 | 2011 | 32 | 2011 | 243 | 2012 | 174 | 2013 | 151 |
| 2010 | 173 | 2011 | 41 | 2011 | 250 | 2012 | 179 | 2013 | 158 |
| 2010 | 180 | 2011 | 49 | 2011 | 257 | 2012 | 185 | 2013 | 165 |
| 2010 | 187 | 2011 | 54 | 2011 | 266 | 2012 | 200 | 2013 | 172 |
| 2010 | 194 | 2011 | 63 | 2011 | 271 | 2012 | 207 | 2013 | 179 |
| 2010 | 201 | 2011 | 70 | 2011 | 274 | 2012 | 214 | 2013 | 186 |
| 2010 | 208 | 2011 | 77 | 2011 | 281 | 2012 | 228 | 2013 | 193 |
| 2010 | 223 | 2011 | 84 | 2011 | 285 | 2012 | 234 | 2013 | 204 |
| 2010 | 229 | 2011 | 90 | 2011 | 292 | 2012 | 242 | 2013 | 210 |
| 2010 | 236 | 2011 | 98 | 2011 | 306 | 2012 | 251 | 2013 | 219 |
| 2010 | 244 | 2011 | 105 | 2011 | 316 | 2012 | 258 | 2013 | 226 |
| 2010 | 250 | 2011 | 112 | 2011 | 327 | 2012 | 265 | 2013 | 240 |
| 2010 | 258 | 2011 | 119 | 2011 | 334 | 2012 | 279 | 2013 | 261 |
| 2010 | 264 | 2011 | 125 | 2011 | 341 | 2012 | 286 | 2013 | 268 |
| 2010 | 278 | 2011 | 133 | 2011 | 355 | 2012 | 293 | 2013 | 275 |
| 2010 | 286 | 2011 | 140 | 2012 | 6 | 2012 | 300 | 2013 | 282 |
| 2010 | 292 | 2011 | 147 | 2012 | 21 | 2012 | 307 | 2013 | 289 |
| 2010 | 300 | 2011 | 154 | 2012 | 39 | 2012 | 314 | 2013 | 298 |
| 2010 | 306 | 2011 | 162 | 2012 | 53 | 2012 | 321 | 2013 | 303 |
| 2010 | 314 | 2011 | 168 | 2012 | 60 | 2012 | 328 | 2013 | 312 |
| 2010 | 321 | 2011 | 173 | 2012 | 75 | 2012 | 335 | 2013 | 319 |
| 2010 | 327 | 2011 | 180 | 2012 | 81 | 2012 | 342 | 2013 | 326 |
| 2010 | 335 | 2011 | 187 | 2012 | 95 | 2012 | 356 | 2013 | 354 |
| 2010 | 344 | 2011 | 196 | 2012 | 102 | 2013 | 7 | | |
| 2010 | 348 | 2011 | 204 | 2012 | 109 | 2013 | 18 | | |
| 2010 | 356 | 2011 | 208 | 2012 | 116 | 2013 | 46 | | |
| 2010 | 363 | 2011 | 215 | 2012 | 131 | 2013 | 60 | | |

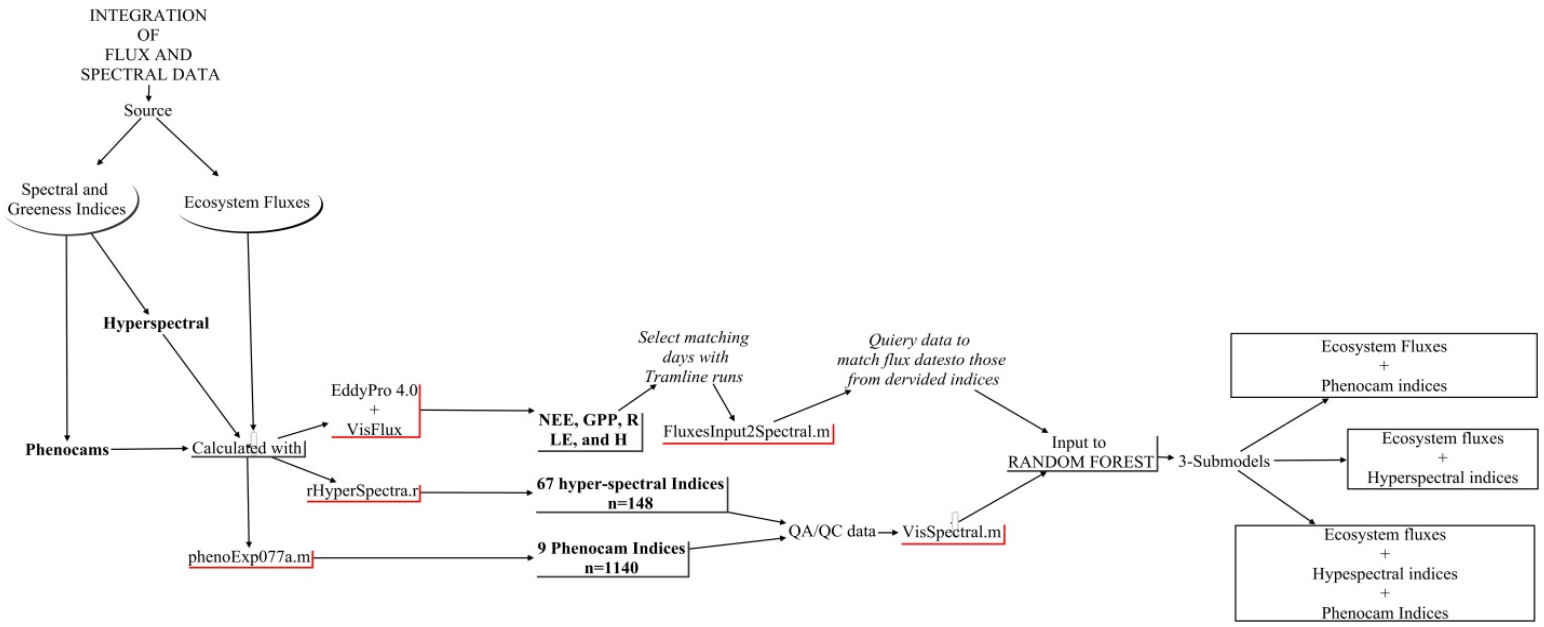


**Figure 27** Concept map explaining the data flow and methods used

## 4.4 RESULTS

A total of 1140 days of phenocam images were used in this analysis from which nine greenness indices were derived. A total of 148 days of hyperspectral data were collected from which 67 spectral indices were derived. All these measurements were distributed thought the four years of the period of study and their captured seasonality of ecosystem fluxes (Figure 4).

### 4.4.1 Phenocams and ecosystem fluxes

The 2GRBi and pctGreen greenness indices depicted seasonal patterns similar to those reported for shrublands of the Northern Chihuahuan desert; with a growing season between DOY~120 to ~250 (Figure 29). Inter-annual variability on growing season was depicted by indices, especially 2GRBi and pctGreen.

Results from the random forest analysis indicated that the 2GRBi and pctgreen were the greenness indices that explained more variability of Gross primary productivity (20% to 40%) (Table 12). NEE and R were not correlated to any of the derived greenness indices. A comparison of time series of 2GRBi and pctGreen shows that both indices represent trends of canopy development during the growing season of the year (Figure 30).

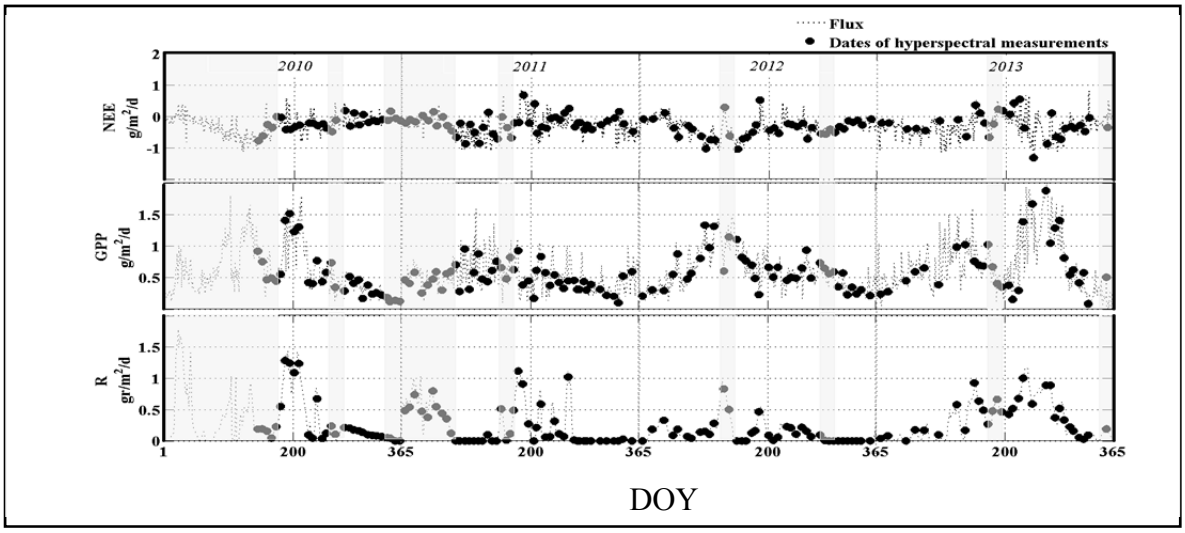


**Figure 28** Time series of ecosystem fluxes and corresponding dates of hyperspectral measurements shown as dark circle. Missing dates of indices derived from phenocams are shown by the shaded area.

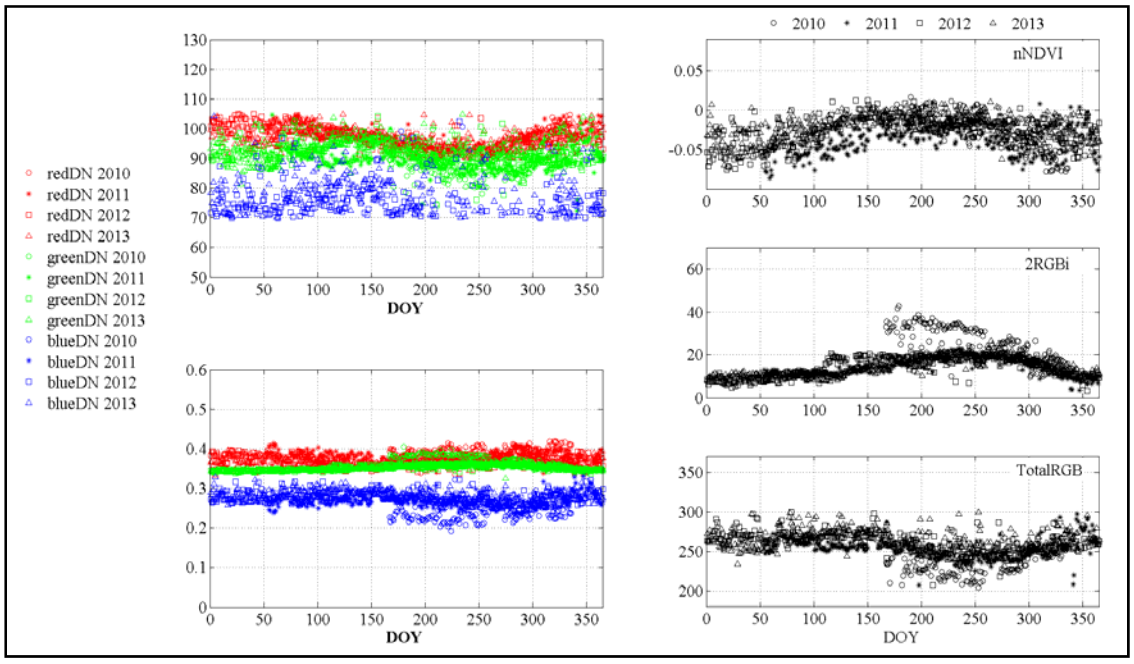


**Figure 29** Greenness indices estimated from Phenocams during 2010-2013

**Table 12** Summary of correlations between ecosystem fluxes and greenness indices

| ***Ecosystem Fluxes*** | *Greenness Indices* ***(Phenocams)*** **n=1140** | |
|---|---|---|
| | **$R^2$** | **Index** |
| NEE | 0.05 | pctG, 2GRBi |
| **GPP** | **0.26** | **2GRBi, redDN** |
| RE | 0.10 | pctG, 2GRBi |

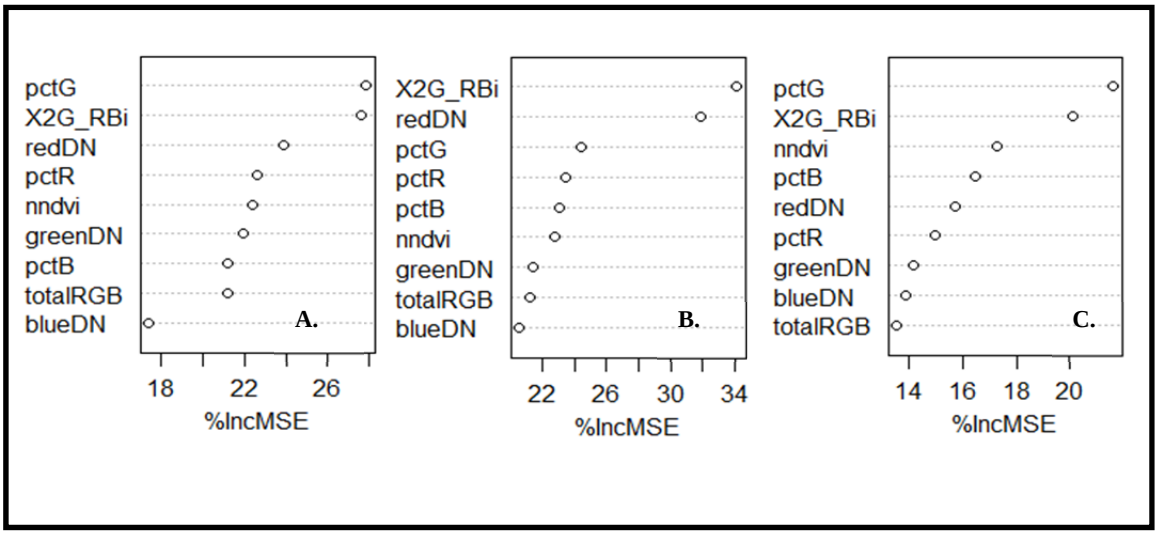


**Figure 30** Variable of importance of ecosystem fluxes of A) NEE, B) GPP, C) R,

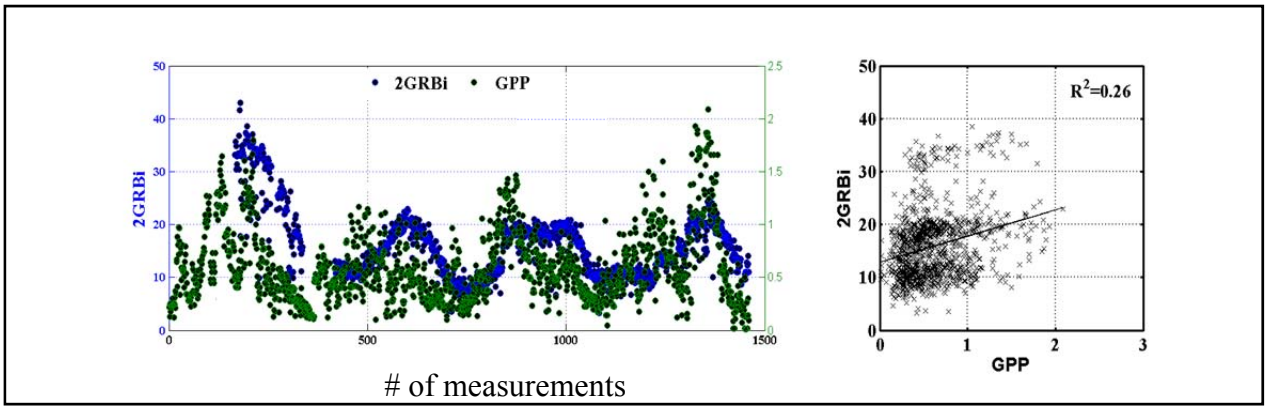


**Figure 31** Time series of 2GRBi and GPP in $gCm^{-2}d^{-1}$, LE in $Wm^{-2}d^{-1}$. The relationship between gross primary productivity (GPP) and Latent heat (LE) with 2GRBi is plotted on the scatter plots.

### 4.4.2 Hyperspectral indices and ecosystem fluxes

Random forest models suggest that hyper spectral indices explained between 40% and 45% of the variance of GPP, and only between 05 and 10% of the variance of NEE and R (Table 12). The relative variables of importance selected were based on the highest MSE output from the random forest analysis per ecosystem flux identified top predictors of GPP (Figure 33). Sub-models were constructed to test the predictive ability of spectral indices to estimate each ecosystem flux. The highest variance depicted by the analysis was related to GPP, where 40% to 45% of the variance was explained by an assembly of spectral indices that included spectral properties at the edge of green (550-570 nm), red (620-750 nm), and infrared (800nm) portions of electromagnetic spectrum. These indices are related to chlorophyll content, carotenoid levels, xanthophyll pigments, and leaf area index.

**Table 13** Summary of variance explained with hyperspectral indices

| **Ecosystem Fluxes** | *Spectral Indices* ***(Hyperspectral)*** n=148 | |
|---|---|---|
| | **$r^2$** | **Index** |
| NEE | 0.05 | Pri1, datt1,nd1, pri4, |
| **GPP** | **0.40** | **Pri1,Gitelson5,Gitelson 4, sr03** |
| R | *0.10* | Green, vog1, sr03 |

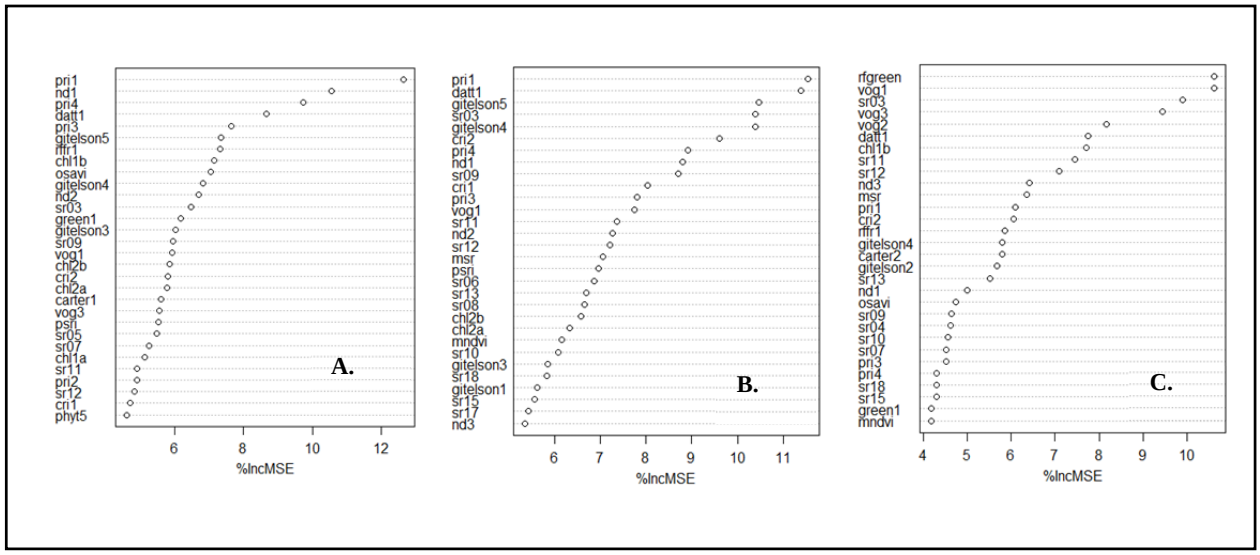


**Figure 33** Variable of importance of ecosystem fluxes of A) NEE, B) GPP, C) R

### 4.4.3Exploring relationships between spectral and greenness indices and ecosystem fluxes

The predictability of ecosystem fluxes improved when combining both spectral and greenness indices into the random forest analysis, which suggest that the combination of derived indices explained between 30% and 45% of the variance of GPP, H, and LE; and 10% of the variance of NEE and R. The relative variables of importance were selected based on the highest MSE output from the random forest analysis (Table 14, Figure 34).

**Table 14** Summary table of relative variable explained by ecosystem fluxes

| Ecosystem Fluxes | Combined Platforms (Hyperspectral and Phenocams) n=148 | |
|---|---|---|
| | **$R^2$** | **Index** |
| NEE | 0.10 | pri4,vog3,nd1,pctG |
| GPP | **0.40** | **datt1,vog1,sr03, 2GRBi** |
| R | 0.10 | rfgreen, 2GRBi, sr03 |

Sub-models were constructed to test the predictive ability of spectral indices to estimate each ecosystem flux. The highest variance explained by the analysis was for GPP where 40% to 45% of the variance was explained by an assembly of spectral indices that reflects from the green (510-550), edge of green (550-570 nm), red (620-750 nm), and infrared (800nm) portions of electromagnetic spectrum. These indices are related with chlorophyll content, carotenoid content, sensitive changes in carotenoid, conversion to xanthophyll's cycle pigment, and leaf area index. The simple ratio 03 and Vogelman Red Edge 1 were significantly correlated with GPP, especially with the peaks in GPP observed during 2010 and 2013. Although, 2GRBi was not recognized among the very top predictor of GPP; the best fit correlation is depicted for comparison purposes (Figure 35).

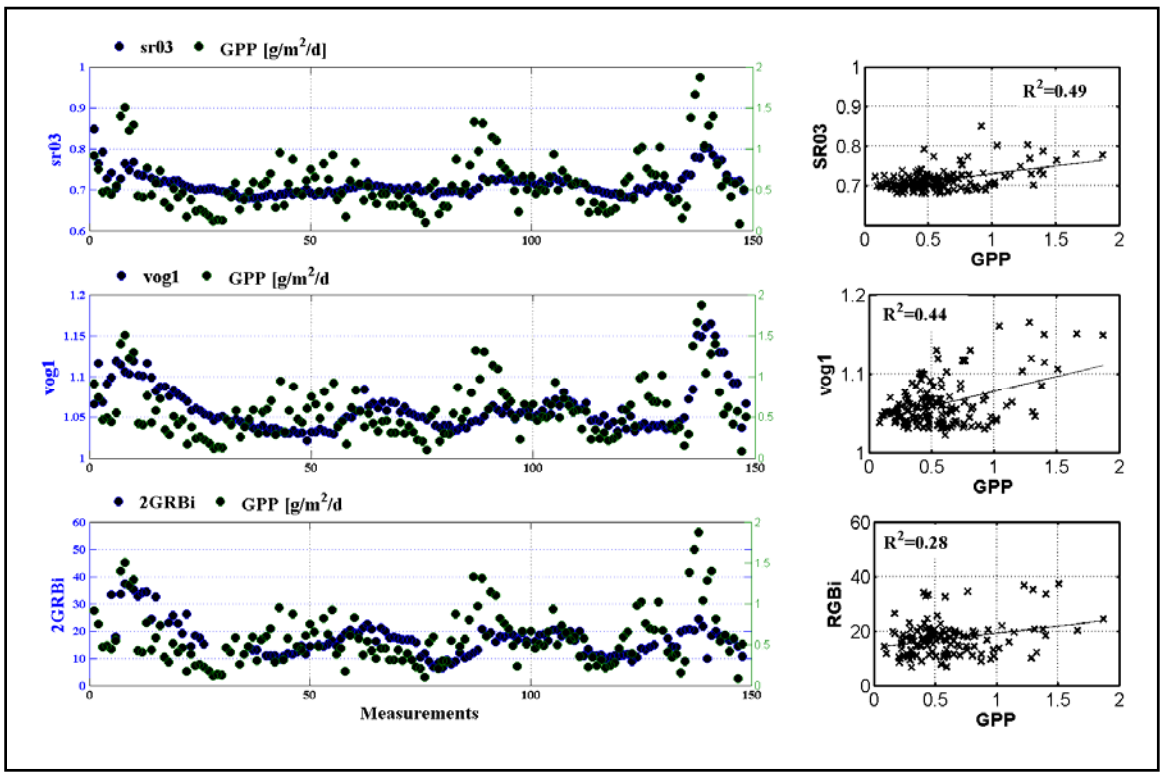


**Figure 34** Carbon uptake and latent heat and their relationship with spectral and greenness indices

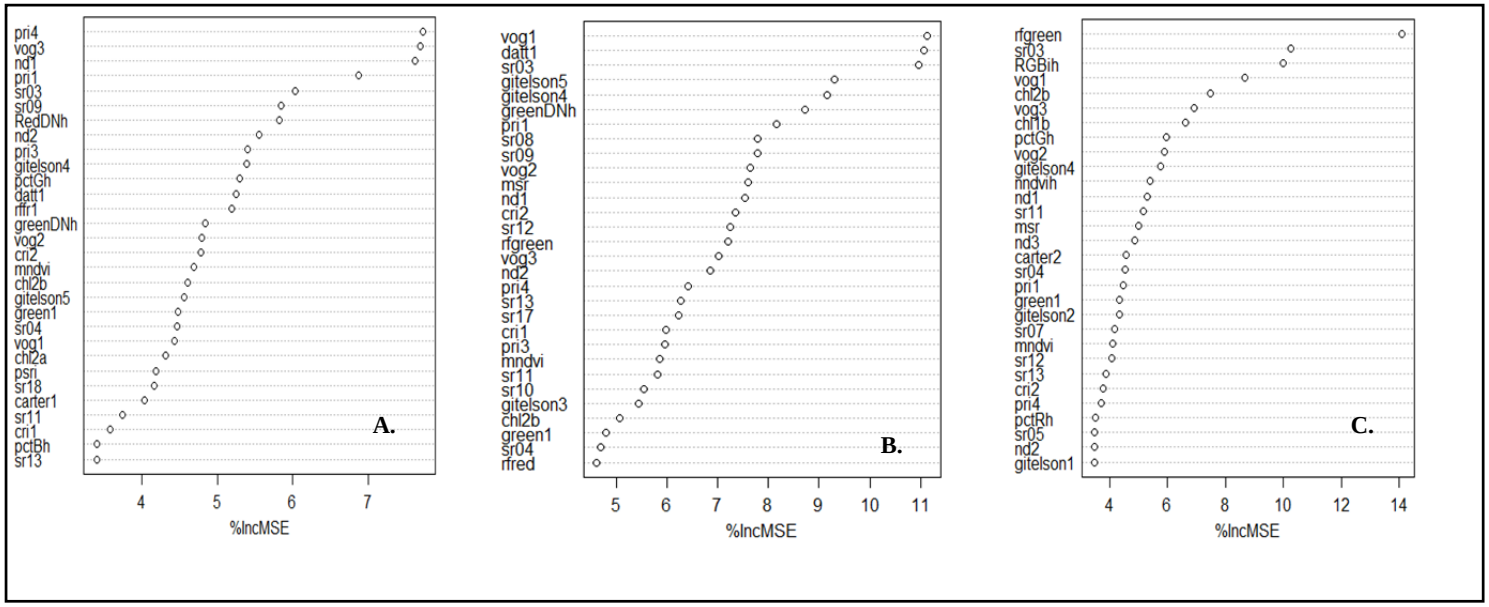


**Figure 37** Variable of importance for spectral indices derived from the robotic tram system and Phenocams

### 4.4.4 Inter-annual variability of ecosystem fluxes and relationships with spectral indices derived from phenocams and hyperspectral indices

The four years of the period of study presented remarkable differences in the annual budgets of GPP and precipitation (Table 15). The minimum temperature registered in 2011 was the lowest for the period of study. This seemed to have implications on shortening the number of days of carbon uptake period and the magnitude of uptake carbon from the atmosphere. The years with higher precipitation were 2010 and 2013, both years presented two peaks of carbon uptake periods that lead to overall longer and highest magnitude of carbon uptake (Table 15).

Random forest analysis showed that the highest variance explained for carbon uptake was found in 2010 and 2013; those years received the highest precipitation for the period of study. The top predictors associated to carbon uptake were vogelman red edge 1, vogelman red edge 2, 2GRBi, simple ratio 13, vogelman red edge 3 in 2010, and Normalized difference1, simple ratio 03, simple ratio 07, gitelson5, rffr1 in 2013. The vogelman red edge indices reflect the activity on the red edge of the electromagnetic spectrum (720-740nm); whereas the assembly of indices highly ranked in 2013 by the RF analysis spanned the red to infrared and green portions of the electromagnetic spectrum (553nm to 720nm). 2GRBi was only ranked as a top predictor in 2010.

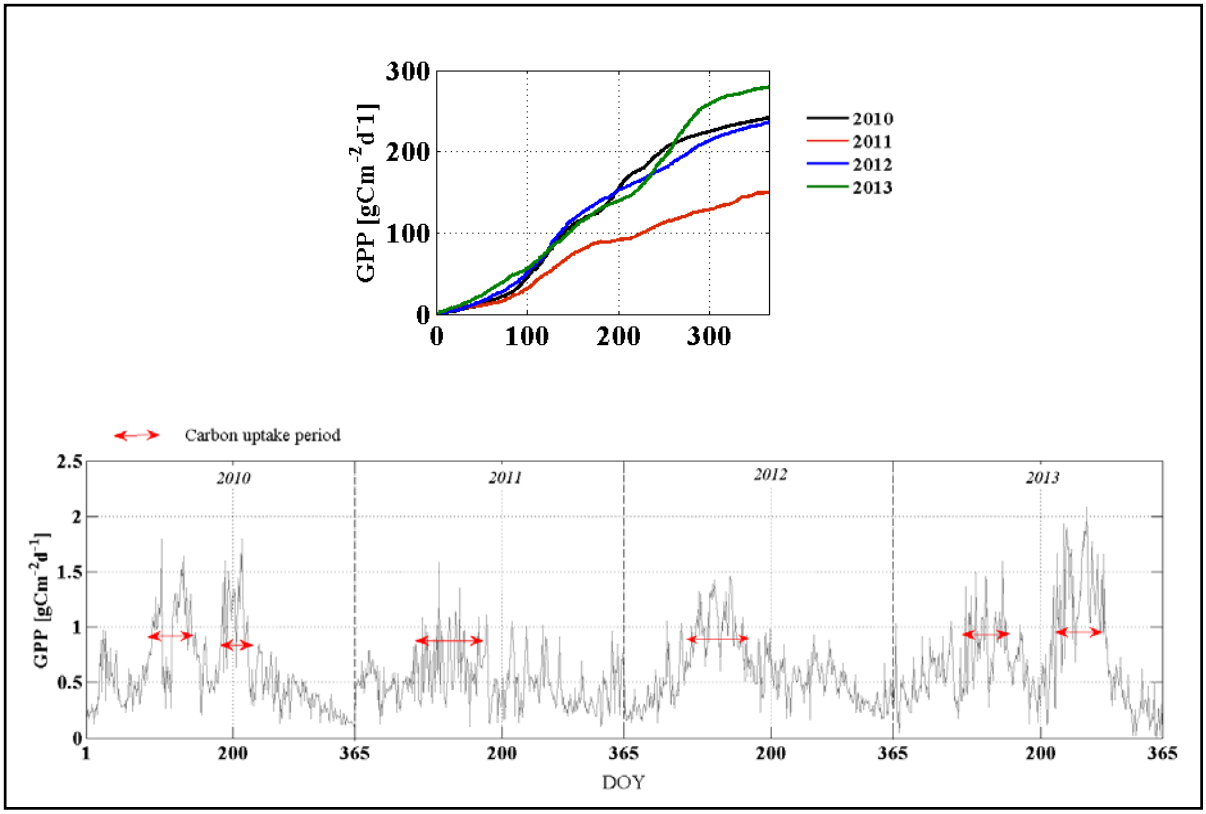


**Figure 38 A.** Annual cumulatives of GPP are shown. B. Time series of gross primary production. The red arrow represents the peaks of carbon uptake period..

**Table 15** Summary of the climatic conditions, carbon uptake dynamics, latent heat and sensible heat fluxes during the four year study period.

| | *2010* | *2011* | *2012* | *2013* |
|---|---|---|---|---|
| ***Climate Conditions*** | | | | |
| Total annual precipitation (mm) | 191.5 | 98.4 | 138.6 | 226.99 |
| Mean annual temperature (°C) | 16.38 | 17.38 | 16.27 | 16.58 |
| Maximum temperature (°C) | 38.6 | 37.90 | 38.00 | 40.25 |
| Minimum temperature (°C) | -9.80 | -24.40 | -10.10 | -11.23 |
| ***Carbon flux, Latent and Sensible heat*** | | | | |
| Carbon uptake period (# of days) | *95* | *86* | *74* | *109* |
| Carbon uptake start (day of year) | *90/184* | *92* | *92* | *99/229* |
| Carbon uptake end (day of year) | *148/221* | *178* | *166* | *152/285* |
| Carbon uptake ($gCm^{-2}yr^{-1}$) | 241.9 | 150.1 | 235.9 | 279.2 |
| | | | | |
| | | | | |

**Table 16** Inter-annual variance of ecosystem fluxes

| | Ecosystem Fluxes | $r^2$ | Index |
|---|---|---|---|
| *2010* *n=30* | NEE | 0.05 | RedDN, nndvi |
| | **GPP** | **0.30** | **Vog1, vog2, 2GRBi, sr13, vog3** |
| | RE | 0.05 | Vog1, 2GRBi, pctR, sr11, sr13 |
| | | | |
| | | | |
| *2011* *n=47* | NEE | 0.02 | Nndvi, greenDN, rff1 |
| | GPP | 0.10 | Datt1, cri2, chl2b, rffr1, vog1 |
| | RE | 0.05 | Pri4, sr06, nndvi |
| | | | |
| | | | |
| *2012* *n=39* | NEE | 0.05 | Chl2b, chl1b, Osavi,datt1, |
| | GPP | 0.10 | cri2, pri4,sr09 |
| | RE | 0.10 | Carter2, sr09, sr02, vog3, pri1, sr01, vog2 |
| | | | |
| | | | |
| *2013* *n=31* | NEE | 0.10 | Carter2, sr05, wbi, gitelson4, |
| | **GPP** | **0.25** | Nd1, **sr03,** sr07, **gitelson5**, **rffr1** |
| | RE | 0.10 | Rfgreen, pri1, sr09, nd02, pctG, carter2 |
| | | | |
| | | | |

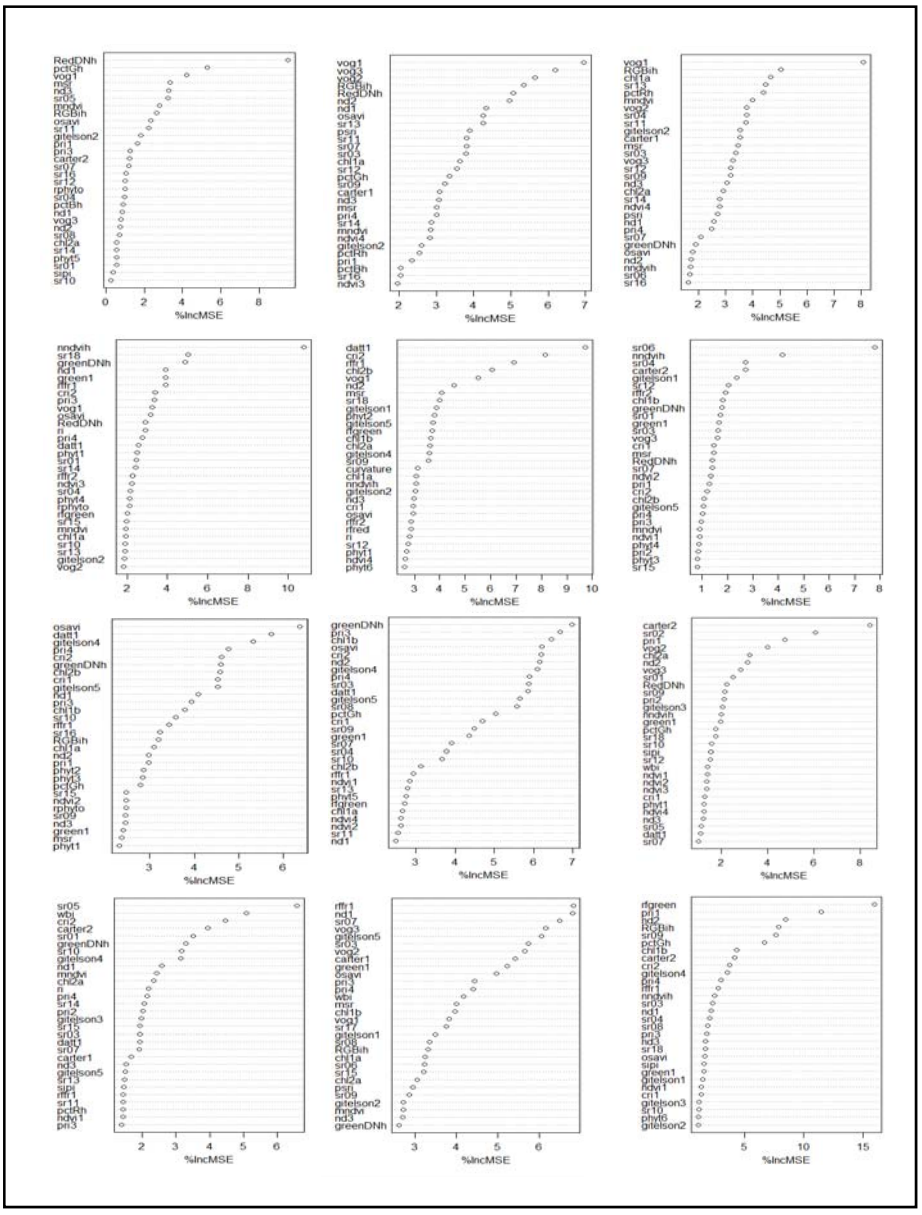


**Figure 39** Variable of importance plots of spectral indices derived from Hyperspectral and Phenocams and fluxes of NEE, GPP, R

Two of the top ranked spectral indices and one of the greenness indices were further evaluated to better understand which spectral index may be the best predictor under different conditions. Overall 2GRBi, rffr1, and volg1 had similar correlations with GPP in 2010 ($R^2$=0.46, $R^2$=0.47, and $R^2$=0.48, respectively). During years with lower precipitation (2011, 2012), these three indices had low correlations ($R^2$=0.01, and 0.08 respectively). 2013 was the year with higher precipitation (226.99 mm/yr), volg1 ($R^2$=0.42) had the strongest correlation with GPP, followed by rffr1 ($R^2$=0.35) and 2GRBi ($R^2$=0.28) (Figure 32).

A closer examination of seasonal trends in these three indices indicated that none of the spectral indices displayed a similar bi-modal peak to that shown for carbon uptake in the two years of higher precipitation (2010 and 2013). The analysis of annual carbon uptake and spectral indices (Figure 14) showed ~77 days in 2011 before the incipient peak of carbon uptake was represented by 2GRBi. In 2012 there were 120 days of delay on the peak of carbon uptake before 2GRBi capture green-up of canopy. The same delay is observed in spectral indices; however this delay only occurs for a maximum of 20 days. These results suggest that spectral indices are able to capture photosynthetic activity before this activity is reflected in the canopy color monitored by the phenocams.

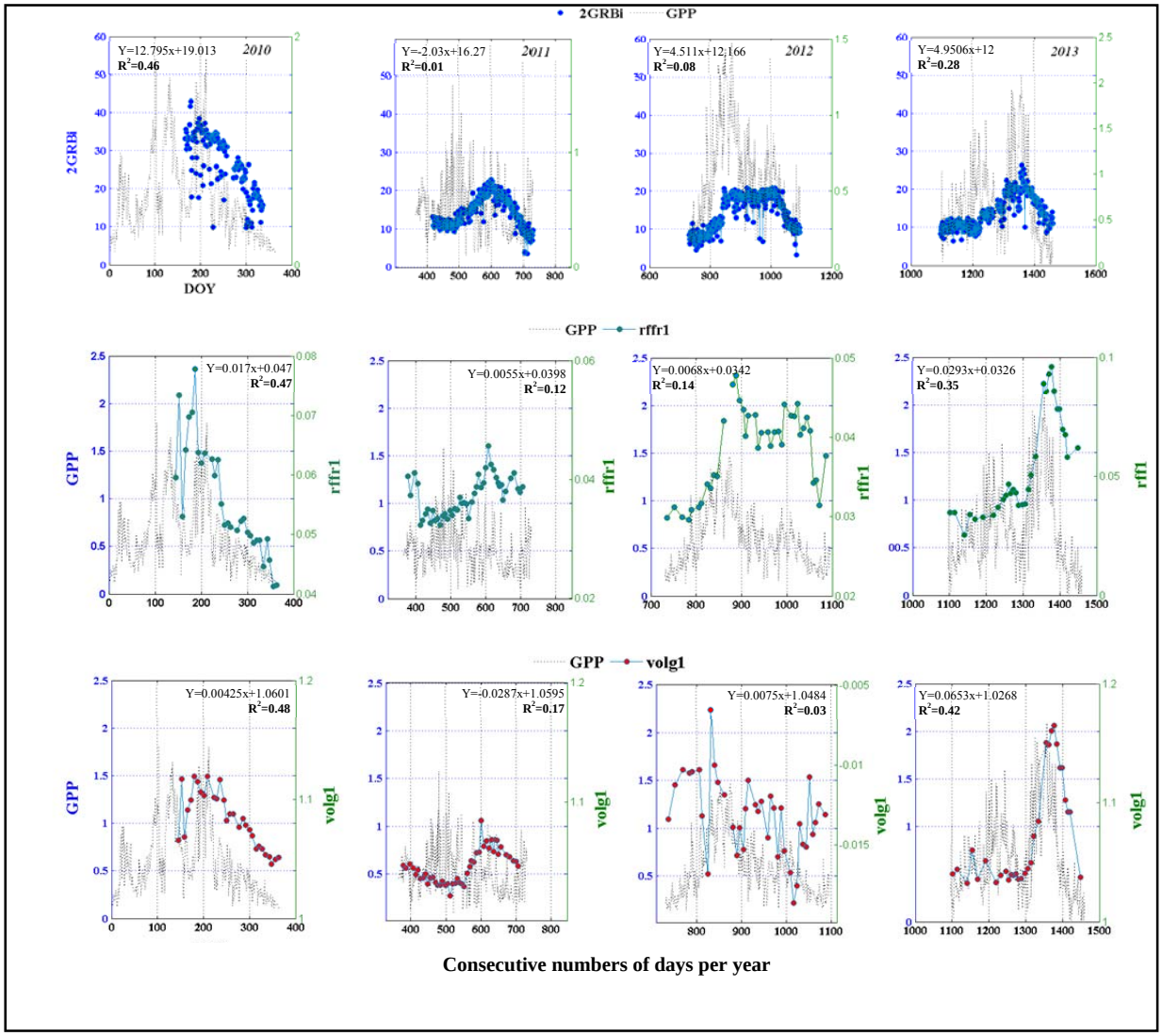


**Figure 32** Exploring the inter-annual relationships of top spectral predictors of carbon uptake

## 4.5 DISCUSSION

The overarching objective of this study was to assess the feasibility of modeling ecosystem fluxes of carbon in shrublands using a range of spectral and greenness indices derived from two spectral platforms. The questions driving the analysis were 1) Can land-atmosphere fluxes of carbon be adequately modeled using a range of ground-based remotely sensing methods; 2) which spectral indices most closely correlate with ecosystem fluxes of carbon, why and when; and 3) do spectral indices capture Inter-annual variability of ecosystem fluxes in a desert shrubland?.

This study demonstrated that both platforms have the ability to capture photosynthetic activity for the desert shrublands but only under specific conditions. The use of phenocams to monitor plant phenology and seasonal patterns of carbon uptake appears to be a reliable method for establishing an automatic, low cost monitoring system that allows for the prediction of ecosystem GPP in the desert shrubland study site; hence as Mizunuma *et al.* (2013) described, it has become a mainstream to monitor ecosystem phenology and facilitate scaling-up of net ecosystem fluxes. In this study, 2GRBi was the most strongly correlated indices with GPP derived from the phenocams. Studies performed in creosote shrublands by Kurc & Benton (2010), also reported the use of greenness indices derived from phenocams were sensitive to reflect carbon uptake peak during the growing season. In this latter study, 2GRBi was sensitive to inter-annual changes of carbon uptake; however, this study also found that in years with low precipitation, there appeared to be a delay between the beginning of peak of carbon uptake and 2GRBi seasonal peak. Similar findings were recently reported by Yang *et al.* (2014) ; and (Kurc & Benton 2010). This is attributed to complex processes at leaf level that are not directly

reflected by using canopy greenness.

The sampling range of the robotic tram line system provides a nominal spectral range (between 350nm to 1100 nm) that allows for the assessment of photosynthetic activity for ecosystems beyond the visible portion of the electromagnetic spectrum (Sims & Gamon 2002; Goswami *et al.* 2011). Data collection using robotic tram systems require substantial effort for both deployment and data processing. Spectral indices were highly correlated with GPP. The inter-annual variability of GPP was detected by spectral indices. Specifically, spectral indices that sense activity in the red edge of the electromagnetic spectrum were recognized as top predictors of carbon uptake during 2010 when precipitation was high. Whereas, different set of indices were recognized as top predictors of GPP during the 2$^{nd}$ wettest year of the period of study (2013); the assembly of indices encompasses photosynthetic activity in the red, green and blue portions of the electromagnetic spectrum. The fact that the top predictors of carbon uptake varied between years, suggests that similar to webcam derived spectral indices, hyperspectral indices are sensitive to detect photosynthetic activity of plants under different stress, especially water deficit.

## 4.6 Conclusions

The overarching objective of this study was to assess the feasibility of modeling ecosystem fluxes of carbon in shrublands using a range of spectral and greenness indices derived from two spectral platforms. The questions driving the analysis were 1) Can land-atmosphere fluxes of carbon be adequately modeled using a range of ground-based remotely sensing methods; 2) which spectral indices most closely correlate with ecosystem fluxes of carbon, why and when; and 3) do spectral indices capture inter-annual variability of ecosystem fluxes in a desert shrubland?.

This study provided a comprehensive exploratory analysis of the feasibility of modeling GPP using a range of spectral indices derived from two spectral platforms. Results indicate that spectral indices derived from hyperspectral remote sensing and phenocams have the capacity to model GPP in desert shrublands. Specifically Volgeman and SR03 were better correlate with GPP, specially during wet conditions. Estimating GPP from either spectral indices was less successful. A more detailed characterization of leaf level physiological processes of C4 shrublands to variability of environmental drivers needs to be further investigated.

**Acknowledgments**

This study would have not been possible without the support of many graduate students who collaborated with data collection and processing. Thanks to the efforts of Christine Laney, Libia Gonzales, Naomi Luna, and Geovanny Ramirez.

# Chapter 5: Designing and developing an end-to-end Cyberinfrastructure (CI) for studies using eddy covariance method.

## 5.1 ABSTRACT

## 5.2 INTRODUCTION

Understanding the movement of carbon, water, and energy between different earth subsystems and its relationship to global climate change represents one of the most pressing modern scientific challenges. Central to meeting this challenge is the development, deployment, and maintenance of technically advanced instrumentation from which large volumes of data are recorded and sometime telemetered before undergoing post processing and quality control before being used in analysis. The use of the Eddy Covariance method has become a recognized standard for measuring the vertical turbulence that drives the mass exchange of heat, water vapor, and carbon within the atmospheric boundary layer (Baldocchi *et al.* 2008). The eddy covariance method poses some challenges attributed to the complexity of the system design, implementation and processing of a large volume of data (Burba & Anderson 2010).

Globally, many sites employing eddy covariance methods to assess land-atmosphere carbon, water and energy exchange are associated with the FLUXNET network. FLUXNET is a global network of regional networks of eddy covariance towers and people who coordinate and share data for the purposes of improving regional and global analysis of observations (LBNL, 2014). At present, over 500 tower sites are operated on a long-term and continuous basis within FLUXNET (FLUXNET n.d.) and these sites span multiple countries, biomes and regions. However, each contributing tower is maintained by either a regional network (i.e. ) or by individual research groups. Although standardized protocols for data collection, tower maintenance (Campbellsci 2006), and data processing (LICOR 2011), software tools (Foken

2004; Clement 2010; Max Plank Institute 2012), and guidelines for best practices (Webb *et al.* 1980; Burba & Anderson 2010; Ubinet *et al.* 2012) have been developed by scientific community; the process of designing, implementing, collecting, processing and visualizing data is still regarded as a science in itself (Burba & Anderson 2010). These workflow components are computationally complex, not well tested in some biomes or climatic conditions, and are especially difficult to master for a non-expert user. At present, and despite widespread acceptance of the method for this field of science, there are no commercial or other off the shelf or end to end solutions for establishing an eddy covariance tower, collecting and processing data, quality checking and documenting these procedures, and analyzing and visualizing analyses to allow for easy inter-comparison of results. Subsequently, very few eddy covariance towers appear to be setup or operated in the same manner; new researchers in the field are required to consult with a range of experts in the field to gain consensus on advice offered; and a large proportion of the data processing requires a lot of manual processing, the integration of different data formats, software packages, and/or web based tools that are not yet interoperable. Hence, the most conspicuous challenges of Eddy Covariance are associated with uncertainty caused by systematic and random errors in the data set such as optimal sensor placement, instrument limitations, calibration errors, and site maintenance (Moncrieff *et al.* 1996). Additionally, issues associated with data analysis such as differences in processing routines, diversity of correction methods , the apparent lack of tools for customized analysis that fit to a specific ecosystem studies specifying when corrections should or should not be used (Moncrieff *et al.* 1996; Burba & Anderson 2010). Although many resources have been developed to assist the broader community, other networks and disciplines have developed or adopted new CI tools that can improve efficiency, interoperability and data discovery, integration and re-usability for similarly

complicated data collection, processing, and analysis routines (Jet Propulsion Lab, 1978; NCDC-NOAA, 2008; Stein, 2008).

### 5.2.1 Objectives

During the course of this dissertation, many of the challenges associated with establishing, and collecting, managing, processing, and analyzing data from an eddy covariance tower were encountered. The overarching objective of this chapter was to document a series of prototype tools that were developed to overcome some of these challenges. The tools presented below were developed with a mindset of creating an end-to-end framework for implementing and managing eddy covariance systems - ranging from site choice and design to refined data product delivery. Using a case study approach, the following cyberinfrastructure are presented:(1) an end-to end concept map that improves documentation of data provenance, identifies needs for interoperability, and shares knowledge for the intricacies of the eddy covariance method used at the site; (2) a quantitative method that optimizes site selection of an eddy covariance tower; (3) an interoperable work-flow driven software that enhances processing and visualization of eddy covariance data and derives data products typically expected by the community; (4) a tool for gap filling micrometeorological data; and (5) an evaluation of the accuracy of eddy covariance system used at the JER study site.

## 5.2 CASE STUDIES

### 5.2.1 Documenting the end-to-end Cyberinfrastructure for eddy covariance systems using concept maps

The aim of this case study is to conceptually map an end-to-end framework for designing and deploying an eddy covariance system to ensure that knowledge of the system design, workflow, and need for interoperability of data management components, and customization is captured. The use of concept maps and semantic abstract workflows is introduced as a method to document, structure capture concepts and relationships of data and methods in formal models that can be used to search, interpret, and reuse eddy covariance data within an information management system.

The context of this case study is built around the typical workflow for eddy covariance systems described by Burba and Anderson (2010), which represents best practice when implementing a tower-based eddy covariance system (Figure 42). This study extends Burba and Anderson's (2010) workflow by further deconstructing key components that enables a more robust knowledge-base to be developed. Although, the knowledge base described is customized to our specific tower site, it complies with the guidelines provided by the broader community at the network level to facilitate documenting, understanding, executing, interpreting, and sharing data sets from users with different levels of expertise (Burba & Anderson 2010).

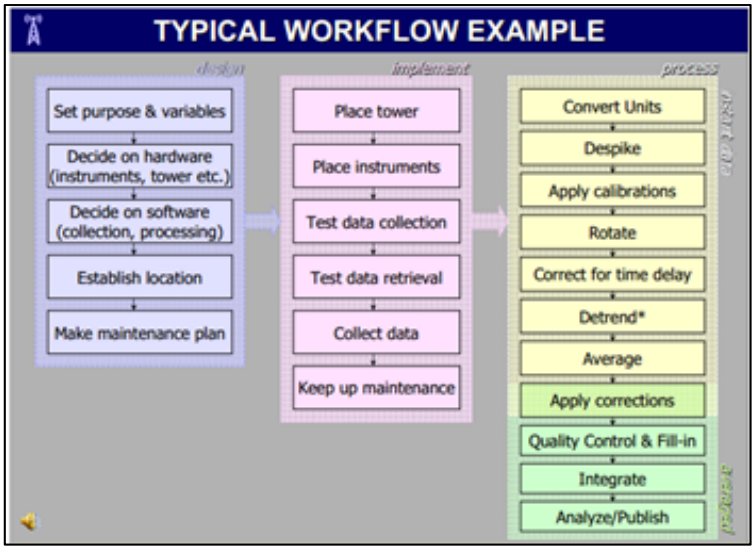


**Figure 33** Typical workflow of an eddy covariance system (Source: Burba and Anderson 2010).

The concept map was constructed using the software CmapTools, developed by the Institute for Human and Machine Cognition (IHMC 2014) CmapTools provides a toolkit to facilitate document, organize and structure knowledge through the development of concept maps and abstract workflows. In concept maps information flow moves from left to right where concepts, sources or sinks of information are enclosed in boxes, and relationships or methods linking those concepts are indicated by connecting a line that has arrows denoting information flow (Novak & Canias 2006). The overarching concept map of the end-to-end system used in the design, implementation, and data processing of eddy covariance system at the JER study site is depicted in Figure 43. Particular attention was given to deconstructing and documenting processes associated with site selection, data acquisition and transmission, data processing, data quality control /quality assurance, and gap filling and flux partitioning.

The concept map also includes an emphasis on hierarchical levels of data acquisition and processing where L0 data refers to raw data from instrumental or human observations; L1 data

refers to calibrated data generally from a single instrument, observer, or field sampling area, which may include information on data quality; L2 data refers to the combinations of level 1 data used to create a gap filled data; and L3 data refers to Level 1 and /or 2 data mapped to a uniform space\time grid. This hierarchical data product classification follows method described by (Beasley *et al.* 2010). Following generation of the overarching concept map, deconstruction of key steps and processes lead to the development of an additional more detailed concept maps and described below where relevant to a particular case study.

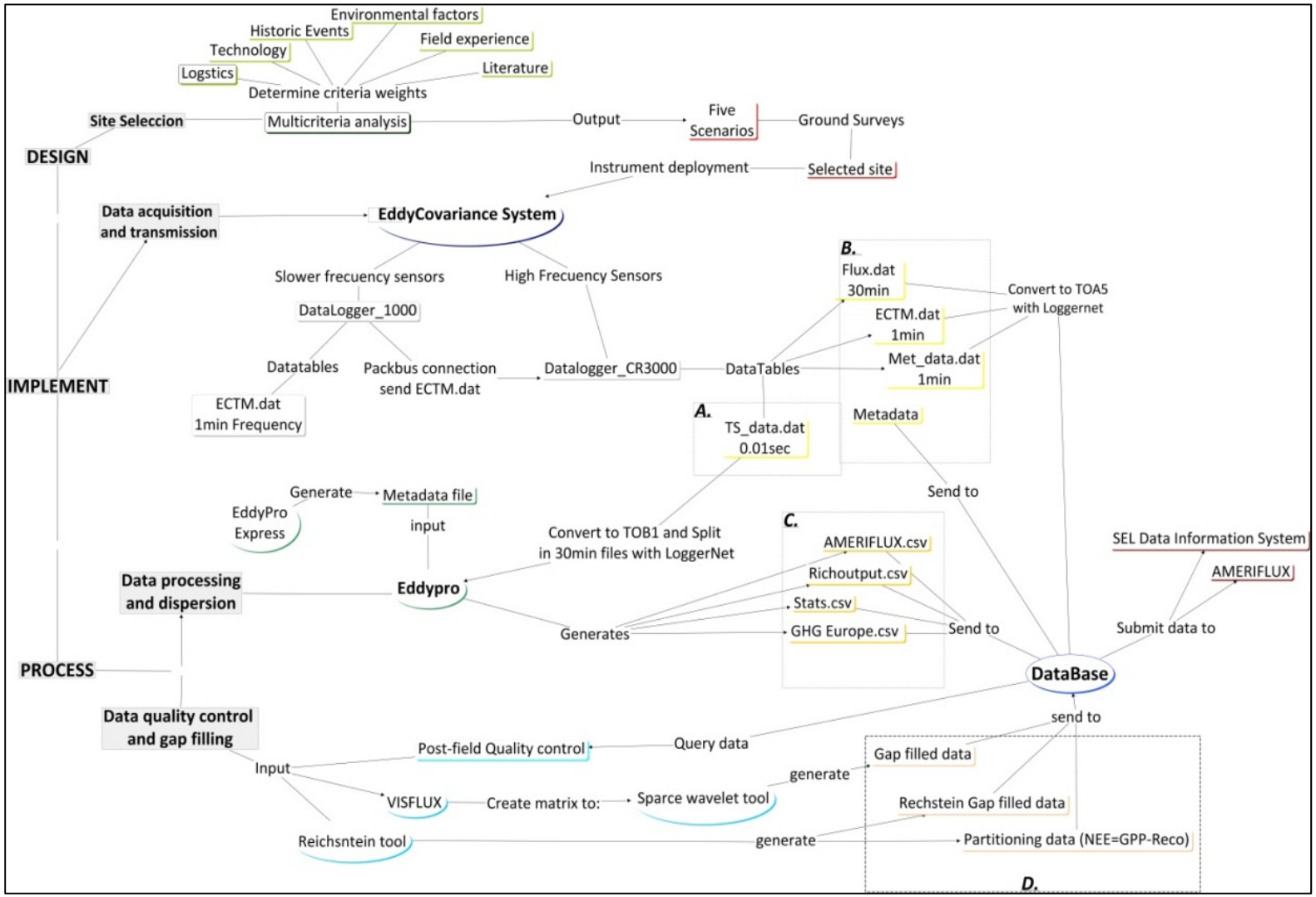


**Figure 34** Overarching concept map of the end-to-end system used in the design, implementation, and processing of eddy covariance data at the JER study site. A) L0 raw data from instrumental or human observations, B) L1 calibrated data from a single instrument, observer, or field sampling area, which may include information on data quality. C) L2 combinations of level 1 data used to create a gap filled data. D) L3 Level 1 and /or 2 data mapped on a uniform space-time grid. Hierarchical data classification follows the method described by Beasley et al. (2010).

### 5.2.2 Site Selection: Optimizing site selection of an eddy covariance tower

The selection of a site for deployment of an instrumented eddy covariance system is a critical decision of the implementation process (Moncrieff *et al.* 1996). Eddy covariance systems have specific requirements (Campbell n.d.; Ubinet *et al.* 2012). Currently, there appears to be no well-established and quantified methods optimize site selection for eddy covariance towers, which suggests that Cyberinfrastructure tools developed for such a role could benefit the greater research community employing eddy covariance methods. The specific case employed for this study focused on optimizing site choice for the JER eddy covariance tower based on constraints imposed by the eddy covariance method, logistics associated with maintaining an eddy covariance tower, and representiveness of landscapes within the region (Figure 44), that best fulfill instrumentation requirements and to reduce sources of random errors by characterizing potential flux footprints variations due to changes in wind speed and direction, topography, and other environmental variations.

Multicriteria analysis was used for this study because it allows for the comparative evaluation of the alternative scenarios. Multicriteria analysis has also been useful for selecting landing sites during space mission planning, and environmental other sampling problems (Fountoulis *et al.* 2003a). Three main criteria groups were defined (1. Logistics, 2. Technology, 3. Environmental factors) and a weight factor was assigned to each based on the defined desirable conditions for establishing an eddy covariance system. For example, the main criteria grouping was a preference for flat terrain, homogeneous canopy of shrubland ecosystem, footprint orientation relative to prevailing wind direction, wind speed above 1.5m/s, regionally and locally representative of the shrublands of the Northern Chihuahuan desert, also avoidance

of current and historical disturbance such as roads, and easy access for transport of heavy field equipment. Then, based on the defined criteria groups and the relative weight factors, the proper cumulative function is extracted. The summation of those grouped weight factors is 100%. The structure of this analysis is represented on Figure 45 and Table 16.

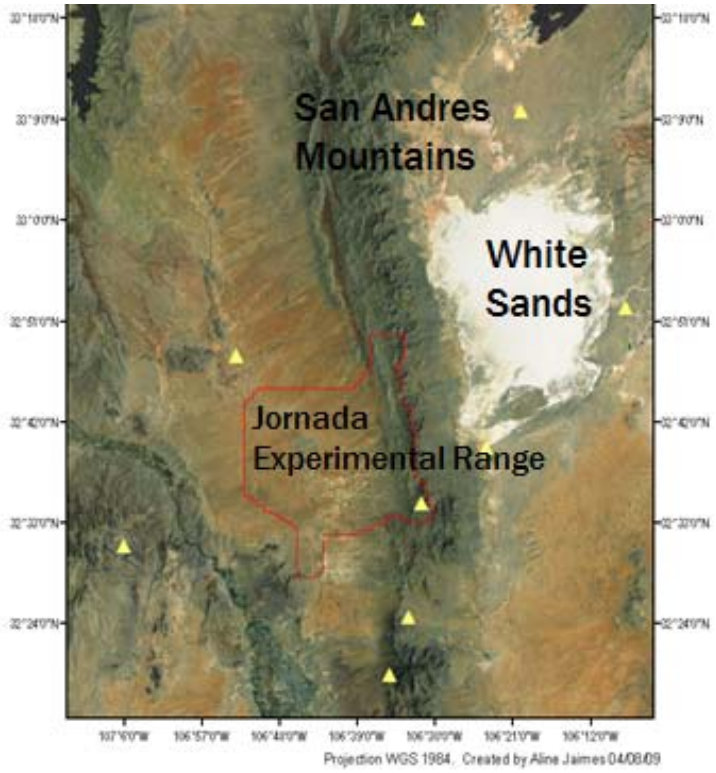


**Figure 35** Location of the Jornada Experimental range north of Las Cruces, New Mexico.

Based on the previous, the extracted cumulative function is the following:

$$F=0.60CG1+0.15CG2+0.20CG3+0.05CG4$$ (see Table 16)

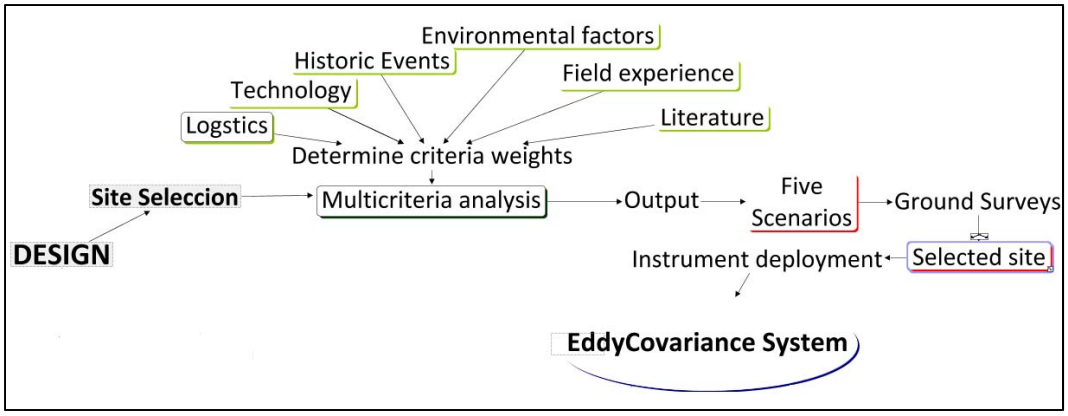


**Figure 36** Concept map of the site selection process. ****

**Table 17** Criteria groups and individual evaluation criteria groups and weight associated with each desirable condition.

| Criteria Groups (CG) | Individual Evaluation CG | Desirable conditions | *Weight* |
|---|---|---|---|
| Environmental features | Slope | Flat terrain | 0.20 |
| | Aspect | Homogeneous | 0.20 |
| | Wind speed | Non-stationary | 0.10 |
| | Wind direction | Instruments need to face predominant wind | 0.075 |
| | Canopy height | Homogenous canopy | 0.025 |
| | Vegetation type | Creosote | 0.20 |
| Logistics | Road conditions | Close to the site | 0.04 |
| Historic effects | Access distance | Not facing predominant wind | 0.06 |
| | Land cover change | Avoid historical disturbances | 0.10 |

The multicriteria analysis was implemented in a geographic information system (ESRI ArcGIS v4.1) by combining raster images using the weighted overlay tool. Model output was color coded raster layer that indicated optimal areas for potential site establishment, which were inspected through ground surveys (Figure 46) before a final choice was made. Ground inspection further assessed accessibility to the site, slopes bigger than 1m, canopy homogeneity, to derive a final location for the construction of the site.

This methodology can be implemented to other study sites where geographic information

data is available. The method is useful as a first assessment to narrow down large extensions of land that are appropriate to deploy eddy covariance system; the method can also be used to design different scenarios that can be defined on the criteria groups. A detailed model describing the application was reported on Jaimes *et al.(*2010). Specifically for eddy covariance community this method can be used to compare one or multiple footprints prior deploying sensors to the field.

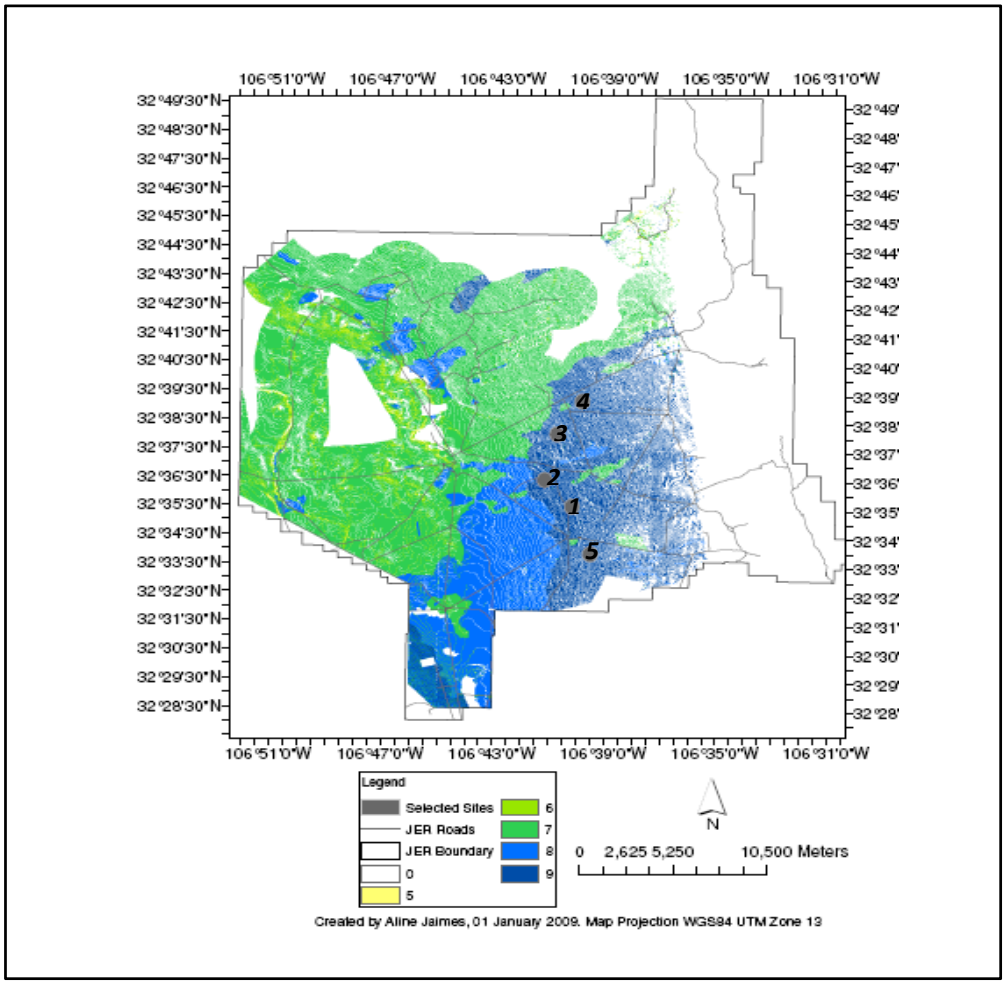


**Figure 37** Raster graphic illustrating the output of from multicriteria analysis during the site selection process for the study site on the JER. Grey circles show targeted areas. Grey circles represent selected sites in order of priority from 1 (highest) to 5 (lowest). The priority value was given with respect of distance to the mountains and accessibility to the sites within Creosote areas.

### 5.2.3 Data Processing: How an eddy covariance system can be interoperable and still use the available methods developed by the community?

A typical eddy covariance system operates continuously and collects data at a rate of up to 10 Hz. In order to compute accurate representation of land-atmosphere flux exchange, raw eddy covariance data needs to be retrieved, corrected and processed, gap filled, and partitioned. The scientific community has developed tools that aid computing specific parts of this process through the combination of different software platforms and web-based tools. For instance, LoggerNet provided by Campbell Scientific functions as the main datalogger support software, supports programming, communication and data retrieval between loggers and the PC, memory card (Campbellsci 2009). The software EddyPro (LICOR 2011) is a software application for processing eddy covariance data. A gap filling and flux partitioning tool implemented, supported, and maintained by the Max Plank Institute provides a web –based platform tool that implements an algorithm designed by Reichstein *et al.* (2005) to gap fill 30-min eddy covariance data. Flux partitioning is an implementation of the Lloyd-and-Taylor (1994) regression model to obtain ecosystem respiration (Reco) and gross primary production (GPP) (MPI 2012). Although these platforms are extremely helpful and have become commonly accepted by the community, they have been developed by sensor manufacturers, or independent research groups; therefore, they are not interoperable and still portions of this process need to be customized to each site.

The motivation of this case study was to develop a prototype tool to integrate a system were metadata; processing routines and data repositories can be integrated to assist parsing data through each commonly accepted software package and computational process outlined above. The process is depicted as a concept map in Figure 47. The methods used in this section are a combination of quality assurance and quality control of data, signal processing techniques, and time series analysis. The specific functions of these codes are to parse data from L0 to L3 level

products, filter data using quality control flags following method described by Foken (2004), performing quality control and quality assurance(Moncrieff *et al.* 1996), evaluating night flux and turbulence (Kaiman & Finnigan 1994), visualizing data as color maps, providing data table format input for gap filling procedure and flux partitioning, and reducing data to 30min, daily, weekly, monthly, yearly. These methods are implemented in a series of codes in MatLab R2012b. The ensemble of MatLab codes has been called VisFlux.

The implementations of VisFlux as a hub to parse, visualize, and reduce eddy covariance data was very successful to facilitate the execution of this process, but also along with the use of concept maps, facilitated the transfer of knowledge and reproducibility of the process available for continuing data processing. A recommendation is to be able to group these codes in a graphic user interface to facilitate execution of the process. The vision for this GUI is shown in Figure 48. The GUI has been designed and is under developing to incorporate a complete set of functions.

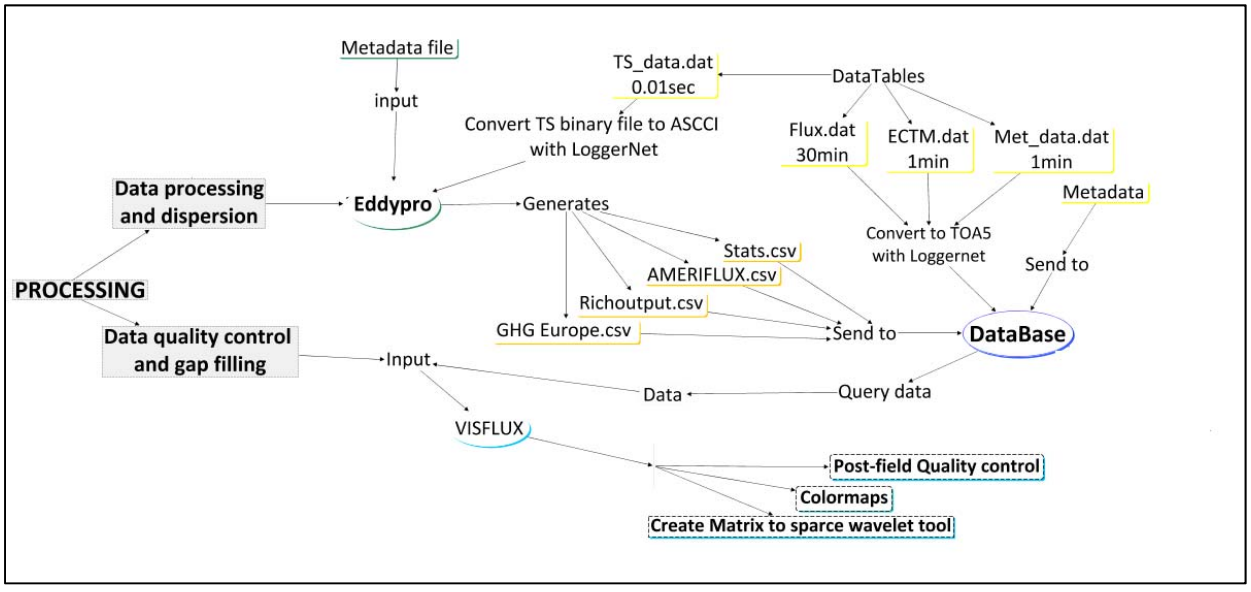


**Figure 38** Concept map illustrating the implementation of VisFlux used as hub between EddyPro and MPI Gap filling and flux partitioning web-tool.

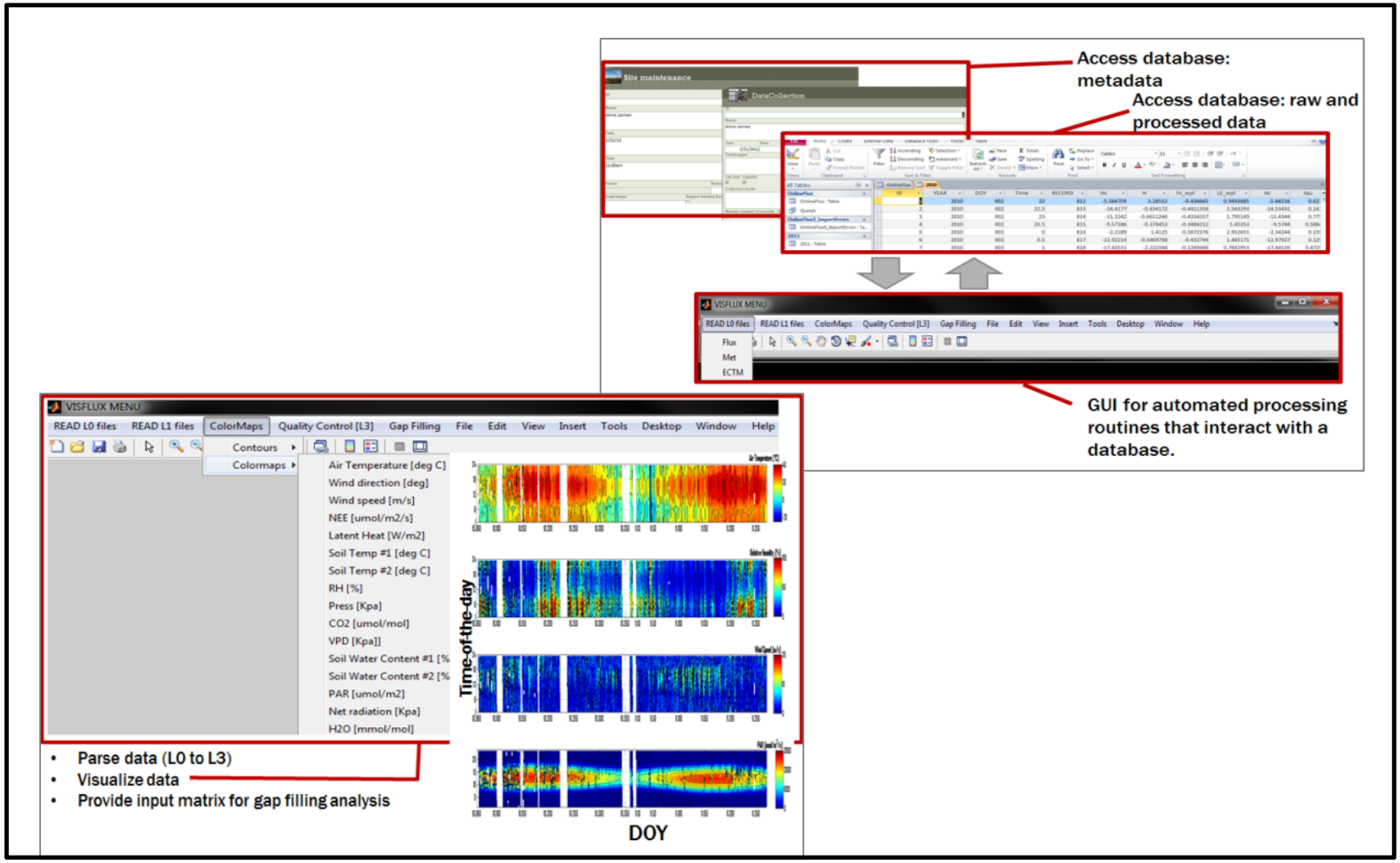


**Figure 39** Illustration of the prototyped graphic user interface to run VisFlux developed using MatLab R2012b

### 5.2.4. Gap filling: how sparse representation can aid gap filling in micrometeorological data?

Gaps in time series data set are a consequence of a range of factors that are not independent and can co-occur. These include data processing methods, instrument failure, bad calibration, or simply environmental variability. In most cases for eddy covariance methods, data is lost or rejected during one or several data processing routines. Consequently, gap filling procedures need to be applied in order to produce complete datasets from which reliable trends and conclusions can be determined. Several gap filling methods have been developed by the meteorological community. These methods include non-linear regression, kalman filtering, artificial neural networks, and mean diurnal variation. A comprehensive comparison of such methods can be found in Moffat *et al.* (2007).

The aim of this case study was to explore and evaluate the use of image Inpainting as a technique for gap filling eddy covariance datasets. Provided that data can be represented as a color map with days of the year and time of day along x and y axes respectively, very accurately representation of daily and temporal variability can be used. The question driving this case study was how sparse representation can aid gap filling in micrometeorological data?

In this case study the data set was considered as an image that contains redundant information due to smooth changes and nearly piece-wise constant structures present in the variables of interest (i.e., local correlations). Therefore, the target data encounters a sparse representation in the wavelet domain. This fact motivates exploration of sparcity as prior information in the data recovery process. A concept map that describes where this case study fits in the overall eddy covariance process is shown in Figure 49.

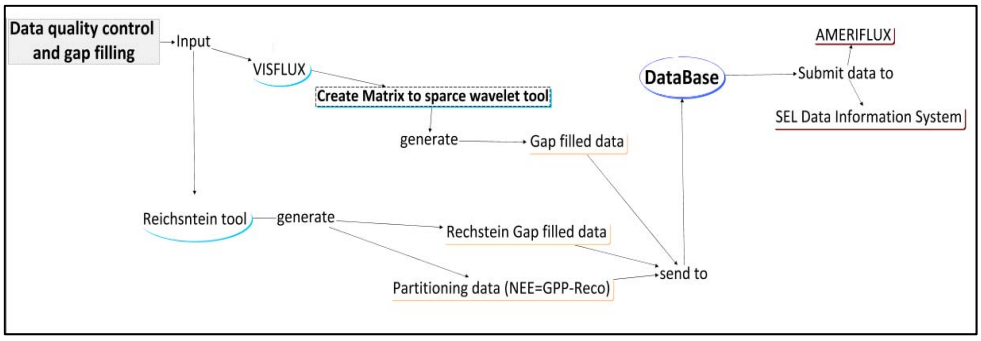


**Figure 40** Concept map representing the use of sparse wavelet tool within the eddy covariance process.

The method consists of using an image Inpainting algorithm based on the principle of sparse representation to incorporate the scarcity of structured images in the wavelet domain (see equation _).

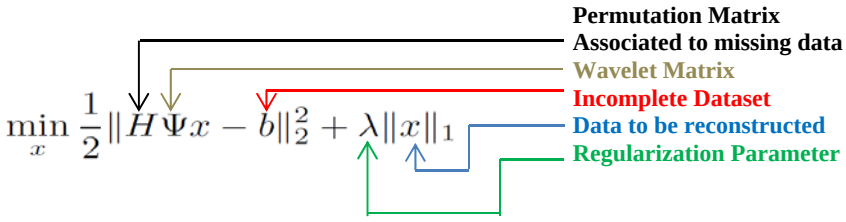


**Equation 2** Wavelet sparse algorithm

The wavelet sparse methods have proven application in image recovery (****). The application of the method to micrometeorological data is part of an application performed as a dissertation study of Ramirez, 2011 from the Computational Science Program at UTEP (Ramirez- 2011). To date, an evaluation of the performance of this algorithm for our JER eddy covariance datasets has been conducted using 36,864 half hourly measurements, spanning January 1 to September 13 2011. A total of 2,876 data points were missing or rejected during the processing of flux data during this period. A scalability assessment error was performed on this missing data that showed successful data recovery when up to 55% of data was missing (Figure 50). This first assessment is published in the IEEE International Conference on Image Processing

ICIP2012 (Ramirez *et al.* 2012). To date, this tool has been implemented as a Toolbox that executed from MatLab R2012b.

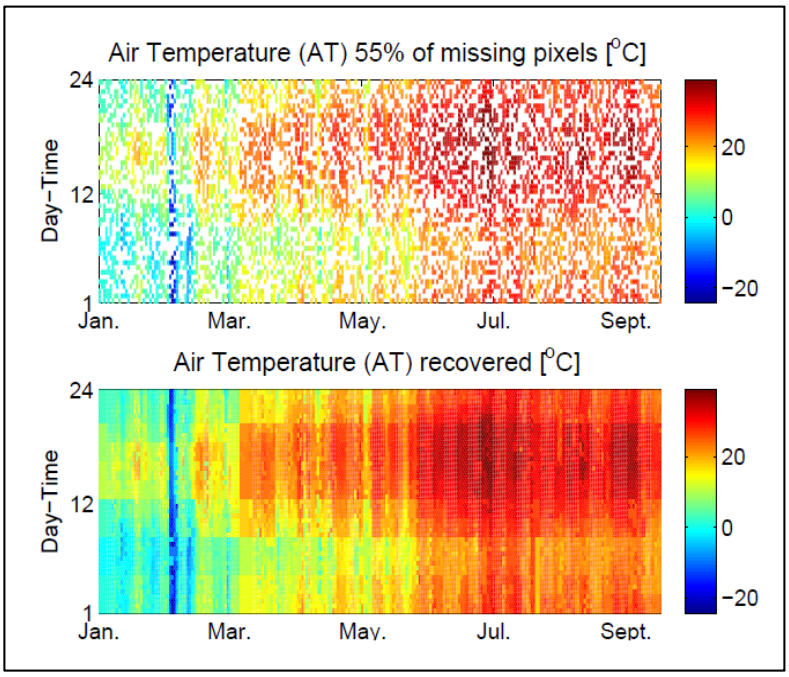


**Figure 41** Example of Image Inpainting method applied to a color map of Air Temperature. Random selection of 55% of the data is missing (upper panel), and Reconstructed dataset (lower panel)

To summarize, Image Inpainting is a useful resource to gap fill 30min meteorological data arranged in a matrix that incorporates regular patterns that can be recognized with sparcity in a wavelet domain. This method was successful in meteorological data that has seasonality that is recognized as structure in the wavelet domain. The method was not successful with ecosystem fluxes because they have more stochastic distribution throughout the year. The application of these techniques raises questions regarding the performance of Image Inpainting alongside other gap-filling tools currently used and accepted by the micrometeorology community (Falge et al. 2001, Lasslop et al. 2010). Answering this question is interesting for future work however it won't be included as part of this dissertation.5.2.5 Data Validation: How can the accuracy of eddy covariance system be evaluated?

Validating the performance of the eddy covariance system is an important step to ensure accuracy of the process and to enable trust in the sharing of data with the broader scientific community. This case study documents the evaluation and performance of the JER eddy covariance system that was conducted in collaboration with the AMERIFLUX QA/QC lab based in Oregon State University by Stephen Chan. Field data collection for the evaluation occurred during a 10 day site visit from 21$^{st}$ -31$^{st}$ August 2012. At this time, the AMERIFLUX Portable System (PS) was deployed to run parallel to the eddy covariance tower at the JER. During the 10 days of data collection regular visits to the site were made in order to monitor instrument performance and perform the highest level of site maintenance during the evaluation period. On the 9$^{th}$ day of the evaluation, the Infrared gas analyzer of our JER site was calibrated to match that from the portable system. High frequency data inter comparison utilized both EddyPro express and EddyPro Advanced. The calculated fluxes output from these analyses were sent to the AMERIFLUX QA/QC lab to be compared against AMERIFLUX data processing routines. The concept map on Figure 51 illustrates the process.

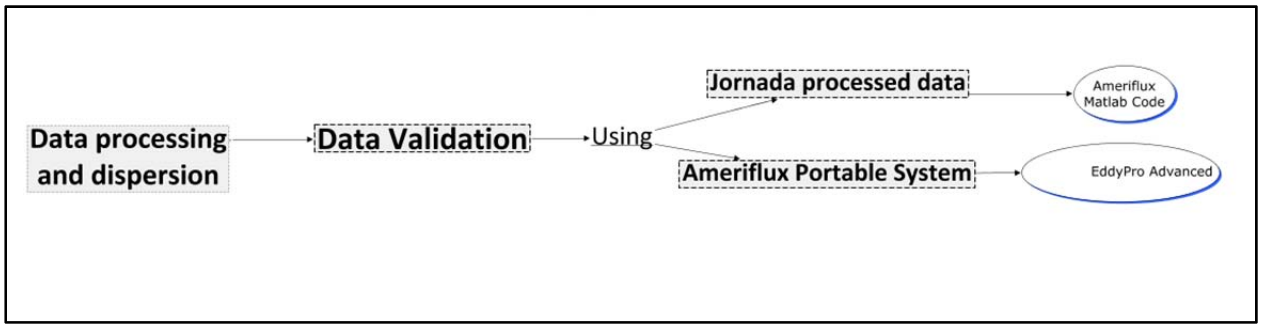


**Figure 42** Concept map of the data validation process.

Results of the inter comparison demonstrated good agreement between processing routines for sonic air temperature, barometric pressure, relative humidity, incoming shortwave

radiation, incoming long wave radiation, photosynthetic active radiation, wind direction, mean horizontal wind speed, water vapor, sensible heat flux, latent heat flux, friction velocity, and atmospheric carbon dioxide, see appendix 2 for a summary of report generated. The most conspicuous difference was found for carbon flux calculations. Further comparison of carbon fluxes calculated between EddyPro and Ameriflux QA/QC lab processing routines for DOY 238 showed disagreement (see figure 52). Further comparisons were performed by LICOR scientific specialist and Stephen Chan. The findings indicated the reason of these differences is due to the equation used to estimate spectral correction; AmeriFlux Matlab code used an approach described by Massman (2002) whereas EddyPro 4.1 uses the WPL correction developed by (Webb *et al.* 1980). In ecosystems with larger carbon fluxes these differences are negligible; however, since carbon fluxes in desert are smaller slight differences in spectral correction term are magnified in their impact on fluxes. However, based in the micrometeorological community these differences are understood as uncertainty of the eddy covariance method. It is important to notice that Ameriflux has since moved to using EddyPro as their primary processing software. Also, recent versions of EddyPro have incorporated multiple corrections options to address this issue.

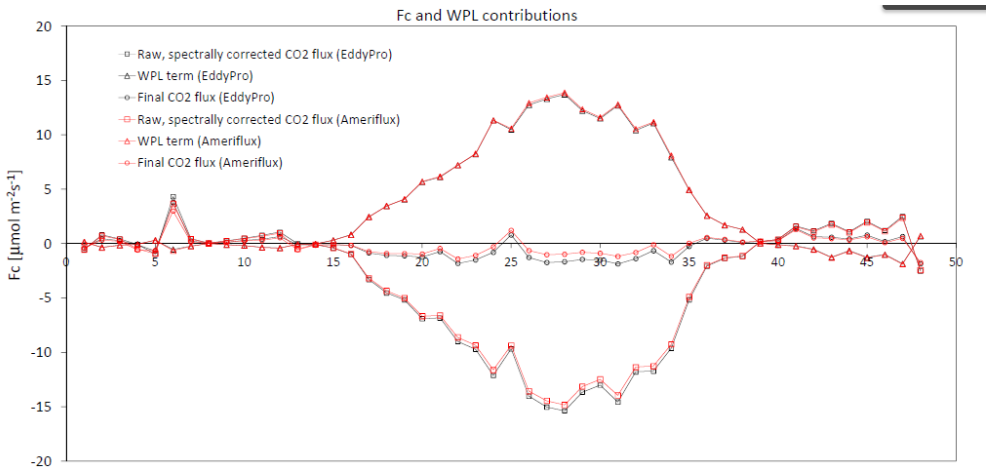


**Figure 43** Differences of methods were illustrated using day of the year 238 of 2012.

## 5.3 DISCUSSION

The end-to-end framework to complement various components of the standard work flow for eddy covariance systems through the exploration and developments of cases studies approach was successful as it allow the integration of different processes and methods designed and built by the flux community and also exported methods from other disciplines. This approach constitutes the first steps towards a more integrative approach from which other research groups from small labs can benefit.

The use of concept maps proved useful throughout the case studies presented above. In particular, they were useful tools for efficiently documenting, communicating, and sharing details related to the flow of information, processes, and data products at the JER site, which has the potential to facilitate knowledge transfer and ensure the continuation of the legacy dataset at this site (Salayandia *et al.* 2011). Utilizing and repurposing site selection algorithms used successfully by other disciplines proved useful for narrowing site selection by simultaneously incorporating a range of technical, logistic, and computational constraints (Jaimes *et al.* 2010a,

2010b). The design and development of VisFlux as a software tool for parsing, visualizing, and reducing eddy covariance data streamlined these processes. Image Inpainting was a useful resource for gap filling 30min meteorological data because the inherent seasonality is recognized by the algorithm as a structure in the wavelet domain (Ramirez *et al.* n.d.). The comparison of flux estimations with two independent paralel sensors provided certainty of our measurements.

## 5.4. CONCLUSION

In this study, prototype cyberinfrastructure (tools and methods) have been developed for the eddy covariance method employed at UTEP's study site on the Jornada Experimental Range. Through the use of case studies this chapter documents an end-to end concept map that improves documentation of data provenance, identifies needs for interoperability, and shares knowledge for the intricacies of the eddy covariance method used at the site; a quantitative method that optimizes site selection of an eddy covariance tower; an interoperable work-flow driven software that enhances processing and visualization of eddy covariance data and derives data products typically expected by the community; a tool for gap filling micrometeorological data; and an evaluation of the accuracy of eddy covariance system used at the JER study site.

# Chapter 6: General Discussion and Conclusions

Warm desert of North America are undergoing desertification (Scott, et al. 2014) and coupled with unprecedented increase in temperatures than any other region of the US (Drought Mitigation Center, 2014) make arid regions vulnerable to accelerate desertification process. Thus, understanding the rate at which this changes are occurring have important implications to estimate near future reduction of carbon stocks, land management, in these already water-stressed systems. The Mojave, Arizona and a portion of the Chihuahua desert, as part of the New Mexico Gradient, had been characterized over the last years to be able to quantify carbon stocks and ET related to monsoon. The presented study aimed at furthering our understanding land-atmosphere carbon exchange for a region representative Northern Chihuahuan desert shrubland dominated by creosote bush (*Larrea tridentata*) and honey mesquite (*Prosopis glandulosa*). Carbon exchange in this region had not been studied using FLUXNET and guidelines.

*The* key objectives addressed and underlying findings to each research questions are explained below:

**Research Objective 1**.was focus on characterizing the microclimate of the region during the period of study and assessing the temporal variability and controls of land atmosphere of carbon on a desert shrubland in the Northern Chihuahuan desert, using eddy covariance datasets spanning 2010-2012 and identified what environmental factors were associated with these, and how they impacted fluxes over multiple time periods.

Local climatology indicated the study area received 40% less precipitation during the period of study than the long term average rainfall recorded at the Jornada Experimental Range between 1915 and 1995 (Wainwright 2006). On a regional perspective, the study area received a

mean annual of 142mm, this represents about 40% less precipitation than the mean annual received at Santa Rita Experimental Range (340 mm/yr) and Walnut Gulch Experimental Watershed (345 mm/yr), these regions represent the Sonoran desert and the transition zone between Sonoran and Northern Chihuahuan desert, respectively (Cavanaugh *et al.* 2011); JER annual precipitation estimates were about 58% below the annual estimates for the Sevilleta Experimental Range (244 mm/yr), region representative of the Northern Chihuahuan desert (Anderson-Texeira *et al.* 2011). The analysis of mean temperatures suggested the period of study was 1.9 °C above the long-term record annual mean temperature between 1915 and 1993 recorded at JER. On a regional basis, the mean annual estimates of temperature were 3°C below the annual mean temperature of the Sonoran desert (20°C) and overall mean annual temperatures estimates at the Sonoran –Chihuahuan desert transition zone and the Chihuahuan desert were consistent with the area of study oscillating on ~17°C (Anderson-Texeira *et al.* 2011; Cavanaugh *et al.* 2011).

Unlike desert grasslands of the Jornada Experimental Range that were characterized as sources of carbon (~143 $gCm^{-2}yr^{-1}$) between 1996 to 2001 (Gutschick & Snyder, 2006). Desert shrublands of the JER were a consistent sink of carbon during 2010 to 2012 with a total 3year cumulative of -428.5$gCm^{-2}$. This three year cumulative NEE is equivalent to mean annual estimates of NEE for Pinon Juniper woodland of New Mexico Elevation Gradient (Anderson-Texeira *et al.* 2011). Although, there was a significant difference on NEE among years (from -98 $gCm^{-2}yr^{-1}$ to -191.5 $gCm^{-2}yr^{-1}$); these values are above those reported from Sarcocaulescent shrublands of the Sonoran Desert (-39 to -52$gCm^{-2}yr^{-1}$) during 2002-2003 (Hastings *et al.* 2005), Californian grasslands (-88 gCm-$2yr^{-1}$) (Xu & Baldocchi, 2004), and desert shrublands of the New Mexico Elevation Gradient (-30 to -50 $gCm^{-2}yr^{-1}$).

The random forest tree analysis had not been used in micrometeorology studies; however, results from it underpinned the top predictors of NEE, GPP and R in desert shrublands are similar to those identified in other arid and semiarid regions, in which temperature and water availability in different partitions of the ecosystem and the atmosphere are the primary controls of ecosystem fluxes (Anderson-Texeira *et al.* 2011; Shao *et al.* 2013b; Thomey *et al.* 2014). Although the results suggest that ecosystem fluxes have similar biophysical controls, their top ranked importance, based on the increase of percentage mean squared error, is different. This has implications for further modeling, in which less than five predictor variables can be used to model the response of fluxes. The partial dependency plots indicated that shrublands of the Northern Chihuahuan desert are predominantly above the critical zone of vapor pressure deficit at which any C4 plants would be able to withhold enough water to survive extreme conditions for long periods of time (Marshall & Woodward 1985). Seasonal changes appeared in general when the vegetation is switching on/off photosynthesis during the growing season (mid-May through mid-September). Similar to other shrublands in western US described by Yufei *et al.* (2010), there is a bimodal maximum uptake distributed at the beginning of the growing season (early-May) and at the peak of the monsoon season (mid -August). Our records indicated the drought in 2011 represented 70 days delay of active growth during the period of study, this difference accounted for more than half of the carbon uptake recorded during 2012. Despite 2010 received the largest amount of precipitation, the system acted as a modest carbon sink of -78.80 $gCm^{-2}$ $y^{r-1}$. This suggest that there are other mechanisms beside precipitation and temperature that control net ecosystem exchange in/out the system (M. C. Duniway 2010; Yufei *et al.* 2010; Shao *et al.* 2013a). It seems that 2010-2011 winter precipitation was enough to support plant activity until early spring 2011. However, since water availability was limited due to the shift in

precipitation timing and magnitude, the system was unable to support new/adult growths of existing species as usually occurs during summer precipitation in the Northern Chihuahuan desert (Robertson *et al.* 2010). Therefore, an important decrease in carbon sequestration occurs during the usual peak growing season. In turn an increase in respiration occurs, thus the system shifts to a small sink of carbon up to -30 $gCm^{-2}$ $y^{r-1}$. Summer precipitation supported carbon sequestration bringing the total annual cumulative to -65.47 $gCm^{-2}$ $y^{r-1}$ in 2011. The following c2012 the system received a small amount of winter precipitation (~5 mm), enough to supply moisture in the system to recruit new growths that started leafing out at the beginning of the growing season as soon as temperatures increased at the end of winter 2012. Summer rainfall promoted the growth of deeper rooted shrubs and fobs. Essentially, because of fairly constant and evenly distributed rain events throughout the year, the system acted as the largest sink during the period of study (-130.85 $gCm^{-2}$ $y^{r-1}$).

**Research Objective 2 was focused on** assessing the effect of extreme climatic events on ecosystem fluxes of carbon in shrubland ecosystem, and assessing the relative importance of these events to annual sink-source dynamics.

The study identified and quantified extreme events in the 4-year study period relative to long-term climatic records. It also, determined the importance of the identified extreme events relative to cumulative annual fluxes. Lastly, it estimated the difference of 4yr cumulative NEE and evaluated the controls of ecosystem fluxes under normal vs. non-normal conditions.

*Climatology*

The analysis of the climatology and the standardized precipitation-evapotranspiration index of the last 30-years indicated that similar to other regions of western North America, the

JER is undergoing a trend towards drier and warmer climate (Seager *et al.* 2007). The mean annual temperature in the last 30 years was 3°C above the long-term annual temperature and precipitation was 73mm below the long term maximum precipitation estimated by Wainwright (2006). Specifically for the period of study from 2010 to 2014, the JER experienced the lowest mean annual precipitation of the last 30-years in 2011 (98.9mm), but still above the long-term record of 70mm in 1974.

*Cold anomalies*

Cold anomalies had precedent in western North America in 1983, 1989, 2003, 2006, 2008, and 2010 (Federal Energy Regulatory Commission 2011). However, the cold anomaly event of February 2011 was the coldest of the region on record. The event was caused by an intense arctic air mass that was moved into southern New Mexico and far West Texas by a strong upper level high pressure ridge across western Canada and the Arctic Ocean (NOAA 2011). Despite the magnitude of the event, the analysis of ecosystem fluxes did not show significant reduction in the carbon sequestration capacity. These results agree well physiological studies that suggest *Larrea tridentata* can withstand sustained freezing temperatures and maintain relatively high rates of photosynthesis rates are maintained under temperatures of -24C (Medeiros *et al.* 2012). In fact, the subsequent cold anomalies increased the carbon sequestration capacity of the system. Snow increases albedo (Davidson & Wang 2004) and if it melts, can wets soil layers deeper than the surface, therefore stimulating photosynthesis and the subsequent green-up of the shrub canopy (Sanchez-Mejia 2013). However, Plants are very sensitive to changes in temperature (Martin *et al.* 2010), thus timing of cold anomalies demonstrate to be important, because when cold anomalies occur at leaf bud or leaves of their lifecycle, the system shifted to a small source of carbon.

*Warm anomalies*

Warm anomalies were infrequent and ranged from one to three consecutive days. Their occurrence led to heat stress that inhibited photosynthesis and promoted increased respiration mainly in winter. Their cumulative effect may lead to dehydration and substantial decrease in the accumulation of carbon stocks (Anderson-Texeira *et al.* 2011). Similar effects have been reported in other shrublands in the US southwest (Hüve *et al.* 2011).

*Drought*

The estimation of the hydrological drought by the SPEI indicated the unfolding of a drier state of the region since 1993. Recent studies in the US southwest show evidence that these conditions have been triggered and exacerbated by the increasing intensity of El Niño–Southern Oscillation (ENSO) of 1992-93 and 1997-98 (Seager *et al.* 2007). The latter, with greater magnitude, had remarkable impact on water supply and storage in the region, causing an unprecedented drought since the last 800 years. In the 30-year period of analysis, the turn of the century drought was depicted in the 1-month SPEI as exceptionally drought conditions between 2002 and 2003. Severe drought conditions were experienced sporadically in subsequent years (2004, 2005, 2011, and 2013). This study focused on severe drought periods that prevailed in 2011 and 2013. Severe drought had repercussion on the carbon sequestration capacity of the system, especially in 2011. Although, the study site remained a small carbon sink during the peak of the severe drought conditions depicted by the SPEI, its effects were not perceived until 1 to 2 months later, when respiration rates favored GPP, and the system became a small source carbon. Similar patterns were reported by Anderson-Texeira et al (2011) for shrublands of the Sevilleta –LTER. Conversely sensible heat flux rates held constant seasonality throughout the 4-years, with higher rates on cold events, with the exception of 2011, where warm events represent two times higher rates than cold anomalies and drought.

*SPEI-Wet*

The overall period of study did not have exceptionally wet conditions. In fact, the 30-years data revealed a substantial decrease in precipitation since 1983. The SPEI reflects values of water supply slightly higher than the demand of water for this period. Thus, in this study the denominated wet period is not a direct reflection of wet conditions caused by precipitation pulses in relationship with the carbon sequestration capacity of the system.

*Extreme events and annual cumulative fluxes*

Annual cumulative fluxes shown differences in the period of study, this are attributed to the occurrence of extreme events; as it has been demonstrated that extreme events contribute to a small but significant amount to the variability of carbon balance (Zscheischler, J., et al 2014). These results suggest the occurrence of extreme events have important implications of a multiyear cumulative net carbon uptake in the system. Extreme drought conditions had the biggest impact on reducing carbon sink capacity of the system. These results suggest that the interaction of precipitation and evaporation are critical to inhibit/promote carbon sink capacity of the system, similar to other regions of the Chihuahuan desert reported by Texeira, et al (2010).

**Research Objective 3 was focused on** evaluating the effectiveness of range of spectral indices derived from hyperspectral robotic tramline system and phenocams to model ecosystem fluxes of carbon in shrublands.

This study demonstrated that both platforms have the ability to capture photosynthetic activity for the desert shrublands but only under specific conditions. The use of phenocams to monitor plant phenology and seasonal patterns of carbon uptake appears to be a reliable method for establishing an automatic, low cost monitoring system that allows for the prediction of ecosystem GPP in the desert shrubland study site; hence as Mizunuma *et al.* (2013) described, it has become a mainstream to monitor ecosystem phenology and facilitate scaling-up of net ecosystem fluxes. In this study, 2GRBi was the most strongly correlated indices with GPP

derived from the phenocams. Studies performed in creosote shrublands by Kurc & Benton (2010), also reported the use of greenness indices derived from phenocams were sensitive to reflect carbon uptake peak during the growing season. In this latter study, 2GRBi was sensitive to inter-annual changes of carbon uptake; however, this study also found that in years with low precipitation, there appeared to be a delay between the beginning of peak of carbon uptake and 2GRBi seasonal peak. Similar findings were recently reported by Yang *et al.* (2014) ; and (Kurc & Benton 2010). This is attributed to complex processes at leaf level that are not directly reflected by using canopy greenness.

The sampling range of the robotic tram line system provides a nominal spectral range (between 350nm to 1100 nm) that allows for the assessment of photosynthetic activity for ecosystems beyond the visible portion of the electromagnetic spectrum (Sims & Gamon 2002; Goswami *et al.* 2011). Data collection using robotic tram systems require substantial effort for both deployment and data processing. Spectral indices were highly correlated with GPP. The inter-annual variability of GPP was detected by spectral indices. Specifically, spectral indices that sense activity in the red edge of the electromagnetic spectrum were recognized as top predictors of carbon uptake during 2010 when precipitation was high. Whereas, different set of indices were recognized as top predictors of GPP during the 2$^{nd}$ wettest year of the period of study (2013); the assembly of indices encompasses photosynthetic activity in the red, green and blue portions of the electromagnetic spectrum. The fact that the top predictors of carbon uptake varied between years, suggests that similar to webcam derived spectral indices, hyperspectral indices are sensitive to detect photosynthetic activity of plants under different stress, especially water deficit.

**Research Objective 4 was focused on** designing an end-to-end Cyberinfrastructure to improve i) site selection, ii) semantic description of the data acquisition and processing methods, and iii) gap filling techniques for eddy covariance datasets.

The end-to-end framework to complement various components of the standard work flow for eddy covariance systems through the exploration and developments of cases studies approach was successful as it allow the integration of different processes and methods designed and built by the flux community and also exported methods from other disciplines. This approach constitutes the first steps towards a more integrative approach from which other research groups from small labs can benefit.

The use of concept maps proved useful throughout the case studies presented above. In particular, they were useful tools for efficiently documenting, communicating, and sharing details related to the flow of information, processes, and data products at the JER site, which has the potential to facilitate knowledge transfer and ensure the continuation of the legacy dataset at this site (Salayandia *et al.* 2011). Utilizing and repurposing site selection algorithms used successfully by other disciplines proved useful for narrowing site selection by simultaneously incorporating a range of technical, logistic, and computational constraints (Jaimes *et al.* 2010a, 2010b). The design and development of VisFlux as a software tool for parsing, visualizing, and reducing eddy covariance data streamlined these processes. Image Inpainting was a useful resource for gap filling 30min meteorological data because the inherent seasonality is recognized by the algorithm as a structure in the wavelet domain (Ramirez *et al.* 2011).

**Suggestions for Future Research**

Determining differences or similarities in biophysical drivers of ecosystem fluxes under different land cover types at the Jornada Experimental Range can provide a robust data set that could enhance model parameterization. Information about tipping points and thresholds of carbon uptake, evapotranspiration rates and energy balance in different land cover types has important implications for land management.

A comprehensive analysis about the eco-physiological adaptations of shrublands, grasslands exposed to the isolated or combined effects of extreme climatic events will aid elucidating ecosystem adaptation to future shifts in climate. Also, it will be interesting to investigate the legacy of extreme events in ecosystem fluxes and the overall ecosystem dynamics (phenology, soil microbial activity, etc).

Future research should also include leaf level analysis of photosynthetic activity and pigments of shrublands exposed to different environmental conditions that cause stress to plants, this will improve estimations and parameterization of spectral indices that can yield to more accurate representations of ecosystem carbon uptake and evapotranspiration.

Although great effort had been done, and continue to evolve from the scientific community, to improve the interoperability of eddy covariance systems; there is still a ßneed to consolidate tools such as *VisFlux* to assist the interoperability of the eddy covariance method.

This tool can also be used as an educational tool for those users wishing to combine the vast theory published by the community.

# CONCLUSIONS

This study focused on furthering the understanding of land-atmosphere interaction on shrublands representative of the Chihuahuan desert and assessing the temporal variability and controls of land atmosphere of carbon dioxide, water and energy of a desert shrubland in the northern Chihuahuan Desert and identified their impact over multiple time periods.

Estimation of biophysical drivers and their impact on ecosystem fluxes were extracted from a three year period. The examination of response curves of ecosystem fluxes and drivers was critical to construct the basis of a deterministic model. A deterministic model was constructed with certain level of accuracy as a tool to conceptualize, assess, and evaluate different scenarios and hypothesis that can later on be implemented on a more robust model. Real scenarios associated to the occurrence of extreme climatic events were investigated with the mind set of using this information as input to be evaluated in the deterministic model. Hence, the characterization of SPEI-Drought, SPEI-Wet, Warm and Cold anomalies was done.

The identification of Extreme events using the combined methodology of anomalies detection proposed by IPCC (Mirle *et al.* 2013), and the drought index (Fuchs 2012) was able to identify subsequent occurrence of extreme climatic events in the period of study. Even though extreme events are erratic in occurrence and duration (from days to 2-months), their incidence have important implications on regulating ecosystem fluxes because they modify seasonal patterns of their biophysical controls. Drought and warm events decreased carbon uptake in comparison with cold and SPEI-wet events. The period of study comprised isolated and

combined extreme events, making it an ideal setting to test some of the laboratory experimental theories that describe Eco physiological adaptations of shrubs to extreme events such as freezing (Medeiros *et al.* 2012). Inter-annual variability showed important differences in carbon uptake and latent heat flux, especially during years when severe drought was documented. If near-future climate predictions for Western North America are carried through and we are experience the transition towards a drier and warmer climate(Seager 2007). The success of shrubs to withhold under these conditions is remarkable. The success of shrubs under these conditions will increase desertification rates; because richness and diversity of C3 plants, such as grasses and forbs, are less adapted and will be displaced by the more resilient and adapted C4 shrubs.

Results indicate that spectral and greenness indices derived from hyperspectral and webcams have the capacity to model carbon uptake, latent of desert shrublands. Sensible heat can also be modeled using hyperspectral indices. Spectral indices that detect chlorophyll activity were linearly correlated to carbon uptake, especially during relative wet conditions. During dry conditions, modeling carbon uptake or latent heat from spectral or greenness indices is more challenging. A more detailed characterization of leaf level physiological processes of C4 shrublands to variability of environmental drivers needs to be further investigated.

The end-to-end framework to complement various components of the standard work flow for eddy covariance systems used by the community (Burba & Anderson 2010) through the exploration and developments of cases studies approach was successful as it allow the integration of different processes and methods designed and built by the flux community and also exported methods from other disciplines.

## Conclusions

Local climatology indicates a decreasing trend of increasing precipitation and decreasing temperature in the JER. Annual precipitation at the study site was substantially below the long term mean annual precipitation estimated for both Sonoran and Chihuahuan desert of the Santa Rita Experimental Range and Sevilleta Experimental Range, respectively.

Shrublands of the Northern Chihuahuan Desert were larger sinks of carbon than other arid and semiarid areas of the Southwest desert. The three year cumulative carbon sink was equivalent to annual cumulative estimates for Pinon Juniper woodland of New Mexico Elevation Gradient.

Net ecosystem exchange of $CO_2$ is greatly affected by hot and dry conditions which inhibit the accumulation of significant carbon stocks in desert shrublands. The ratio of respiration: gross primary production increases with temperature and decreases with increasing soil moisture and cooler soil temperatures in deeper soil profiles.

The quadratic model was able to validate the predictive capacity of the variables of importance of ecosystem fluxes. This model is a great tool to explore possible changes in ecosystem fluxes response to specific changes of their drivers. More robust models are suggested to predict net ecosystem exchange. Some limitations of the study, the predictive potential of the partial dependency plots assumes the system will remain in steady state, therefore more robust modeling technique are suggested to decrease uncertainty if predictive values when change is input into the ecosystem

Even though extreme events are erratic in occurrence and duration (from days to 2-months), their incidence have important implications on regulating ecosystem fluxes because they modify seasonal patterns of their biophysical controls Hence, Regardless of the duration length of the event, they have important effects on the annual cumulative of ecosystem fluxes.

Inter-annual variability showed important differences in carbon uptake especially during years when severe drought was documented. The severe drought of 2011 decreased the sink capacity of the system and was also reflected on the carbon sequestration of 2012; the system recovers on 2013. Conversely, sensible heat flux presented small variations in magnitude per year.

If the current trends toward drier and warmer climate continue, it is likely shrubs withhold under these conditions. The success of shrubs under these conditions will increase desertification rates; because C3 plants are less adapted and will be displaced by the more resilient and adapted shrubs.

This study provided a comprehensive exploratory analysis of the feasibility of modeling GPP using a range of spectral indices derived from two spectral platforms. Results indicate that spectral indices derived from hyperspectral remote sensing and phenocams have the capacity to model GPP in desert shrublands. Specifically Volgeman and SR03 were better correlate with GPP, specially during wet conditions. Estimating GPP from either spectral indices was less successful. A more detailed characterization of leaf level physiological processes of C4 shrublands to variability of environmental drivers needs to be further investigated.

In this study, prototype cyberinfrastructure (tools and methods) have been developed for the eddy covariance method employed at UTEP's study site on the Jornada Experimental Range. Through the use of case studies this chapter documents an end-to end concept map that improves documentation of data provenance, identifies needs for interoperability, and shares knowledge for the intricacies of the eddy covariance method used at the site; a quantitative method that optimizes site selection of an eddy covariance tower; an interoperable work-flow driven software that enhances processing and visualization of eddy covariance data and derives data products typically expected by the community; a tool for gap filling micrometeorological data; and an evaluation of the accuracy of eddy covariance system used at the JER study site.

# 7. References


Alfieri, J.G., Niyogi, D., LeMone, M.A., Chen, F. & Fall, S. (2007). A simple reclassification method for correcting uncertainty in land Use/Land cover data sets used with land surface models. Pure Appl. Geophys., 164, 1789–1809.

Anderson, J. (2013). LTER Weather Station daily summary climate data [WWW Document]. Jorn. LTER Weather Stn. Clim. Data. URL http://jornada.nmsu.edu/content/lter-weather-station-daily-summary-climate-data.

Anderson-Teixeira, K.J., Delong, J.P., Fox, A.M., Brese, D. a. & Litvak, M.E. (2011). Differential responses of production and respiration to temperature and moisture drive the carbon balance across a climatic gradient in New Mexico. Glob. Chang. Biol., 17, 410–424.

Ansley, R.J. & Castellano, M.J. (2007). Prickly pear cactus responses to summer and winter fires. Rangel. Ecol. Manag., 60, 244–252.

Archer, K.J. & Kimes, R. V. (2008). Empirical characterization of random forest variable importance measures. Comput. Stat. Data Anal.

Archer, S., Schimel, D.S. & Holland, E.A. (1995). Mechanisms of shrubland expansion- land use, climate or $CO_2$. Clim. Change, 29, 91–99.

Arguez, A. & Vose, R.S. (2011). The Definition of the Standard WMO Climate Normal: The Key to Deriving Alternative Climate Normals. Bull. Am. Meteorol. Soc., 92, 699–704.

Asner, G. P. (2001). Analysis of EO-1 Hyperion Imagery for Desertification Research Applications in Argentin. EO1.GSFC. Goddard Space Flight Center.

Asner, G.P. (1998). Biophysical and biochemical sources of variability in canopy reflectance. Remote Sens. Environ., 64, 234–253.

Baldocchi, D., Falge, E. & Wilson, K. (2001). A spectral analysis of biosphere – atmosphere trace gas flux densities and meteorological variables across hour to multi-year time scales. Agric. For. Meteorol., 107, 1–27.

Baldocchi, D., Hincks, B.B. & Meyers, T.P. (2008). Measuring Biosphere-Atmosphere exchanges of biologically related gases with micrometeorological methods. Ecol. Soc. Am., 69, 9.

Balzarolo, M., Anderson, K., Nichol, C., Rossini, M., Vescovo, L., Arriga, N., et al. (2011). Ground-Based Optical Measurements at European Flux Sites: A Review of Methods, Instruments and Current Controversies. Sensors, 11, 7954–7981.

Beasley, T., Keller, M., Damiani, B. & Cilke, D. (2010). NEON Level 1 - 3 Data Products. Cat. Dir. Eng.

Begueria, S. & Serrano, V. (2013). R Package: Calculation of Standardised Precipitation - Evapotranspiration index.

Beltran-Przekurat, A., Pielke, R., Peters, D., Snyder, K. & Rango, A. (2008). Modeling the effects of historical vegetation change on near-surface atmosphere in the northern Chihuahuan Desert. J. Arid Environ., 72, 13.

Lawrence Berkeley National Lab (LBNL). (2014). : Research Network of the Americas [WWW Document]. URL http://.lbl.gov/.

Betts, A.K. & Dias, M. (2010). Progress in Understanding Land-Surface-Atmosphere Coupling from LBA Research. J. Adv. Model. Earth Syst., 2.

Binder, A.B., Roberts, D.L. & Center, A.S. (1970). Criteria for lunar site selection. Chicago, Ill. : Astro Sciences Center, IIT Research Institute.

Bowling, D.R., Grote, E.E. & Belnap, J. (2011). Rain pulse response of soil CO 2 exchange by biological soil crusts and grasslands of the semiarid Colorado Plateau, United States. J. Geophys. Res., 116, G03028.

Breiman, L. & Cutler, A. (2013). R Package " randomForest ."

Burba, G. & Anderson, D. (2010). Eddy Covariance flux measurements. Linconl, Nebraska.

Burnham, K.P. & Anderson, D.R. (2002). Model selection and multimodel inference: a practical information-theoretic approach. Ecol. Modell. Springer.

Campbell, P., Middleton, E., Raymond, K., Lagomasino, D. & Huemmrich, K.F. (2011). EO-1 Hyperion capturing seasonal dynamics in vegetation phenology and spectral properties associated with CO2 uptake. Sci. Meet. 3rd NACP all - Investig. Metting.

Campbell, Scientific, (2004). Introduction to the Eddy Covariance Method.

Campbell, Scientific, (2004). Instruction Manual: TE525 Tipping Bucket Rain Gauge.

Campbell, Scientific, (2005). Instruction manual: CSAT Three Dimensional Sonic Anemometer.

Campbell, Scientific, (2006). Open Path Eddy Covariance System. Logan, Utah, US. 90p.

Castellvi, F., Snyder, R.L. & Baldocchi, D.D. (2008). Surface energy-balance closure over rangeland grass using the eddy covariance method and surface renewal analysis. Agric. For. Metereology, 148, 13.

Cavanaugh, M.L., Kurc, S.A. & Scott, R.L. (2011). Evapotranspiration partitioning in semiarid shrubland ecosystems: a two-site evaluation of soil moisture control on transpiration. Ecohydrology, 4, 671–681.

Charney, J.G. (1975). Dynamics of deserts and drought in the Sahel. Q. J. R. Meteorol. Soc., 101, 193–202.

Cheng, Y.-B., Middlenton, E.M., Hilker, T., Coops, N.C., Black, A. & Krishnan, P. (2009). Dynamics of spectral bio-indicators and their correlation with light use efficiency using directional observations at a Douglas-fir forest. Meas. Sci. Technol., 20.

Cipriotti, P.A., Flombaum, P., Sala, O.E. & Aguiar, M.R. (2008). Does drought control emergence and survival of grass seedlings in semi-arid rangelands? An example with a Patagonian species. J. Arid Environ., 72, 162–174.

Clement, R. (2010). Footprint Tool. School of GeoSciences, The University of Edinburgh Website: http://www.geos.ed.ac.uk/abs/research/micromet/EdiTools/

Cutler, D.R., Edwards, T.C., Beard, K.H., Cutler, A., Hess, K.T., Gibson, J., et al. (2007). Random forests for classification in ecology. Ecology, 88, 2783–2792.

D'Odorico, P., Bhattachan, A., Davis, K.F., Ravi, S. & Runyan, C.W. (2013). Global desertification: Drivers and feedbacks. Adv. Water Resour., 51, 326–344.

D'Odorico, P., Fuentes, J.D., Pockman, W.T., Collins, S.L., He, Y., Medeiros, J.S., et al. (2010). Positive feedback between microclimate and shrub encroachment in the northern Chihuahuan desert. Ecosphere, 1.

Dalgaard, P. (2008). Introductory Statistics with R. Statistics and Computing. Springer Science and Business Media. 357p.

Davidson, A. & Wang, S.S. (2004). The effects of sampling resolution on the surface albedos of dominant land cover types in the North American boreal region. Remote Sens. Environ., 93, 211–224.

Davidson, M., Berger, M., Moreno, J., Stoll, M. & Miller, J. (2003). Mapping Photosynthesis from Space -a new vegetation-fluorescence technique. ESA, 34–37.
42. Diehl, H. & Lutz, A. (2010). Observed and Projected Climate and Hydrologic Trends in Eastern Nevada and Western Utah. University of Idaho.

Dominguez, F., Canon, J. & Valdes, J. (2010). IPCC-AR4 climate simulations for the Southwestern US: the importance of future ENSO projections. Clim. Change, 99, 499–514.

Falge, E., Baldocchi, D., Olson, R., Anthoni, P., Aubinet, M., Bernhofer, C., et al. (2001). Gap filling strategies for long term energy flux data sets, 107, 71–77.

Farmer, N. (1990). The encroaching desert. Considering Conservation. Dryad, London. 64p.

Federal Energy Regulatory Commission of North America. (2011). Outages and Curtailments During the Southwest Cold Weather Event: causes and recommendations. 30p.

Feng, S. & Fu, Q. (2013). Expansion of global drylands under a warming climate. Atmos. Chem. Phys., 13, 10081–10094.

FLUXNET. (___). Global Network of Eddy Covariance Towers [WWW Document]. URL http://daac.ornl.gov/FLUXNET/fluxnet.shtml.

Foken, T. (2004). A combination of quality assessment tools for eddy covariance measurements with footprint modeling for the characterization of complex sites. Agric. For. Meteorol., 127, 14.

Fountoulis, I., Mariolakos, D., Spyridos, E. & Andreadakis, E. (2003a). Geological criteria and methodology for landfill sites selection. Environm.Sci.Technol.

Fuchs, B. (2012). Using the Standardized Precipitation Index ( SPI ) and the Standardized Precipitation Evapotranspiration Index ( SPEI ).

Fuentes, D.A. & Zhiyan M., (2006). Mapping carbon and water vapor fluxes in a chaparral ecosystem using vegetation indices derived from AVIRIS. Remote Sens. Environ., 103, 12.

Gamon, J., Coburn, C., Flanagan, L., Huemmrich, K.F., Kiddle, G., Sanchez-Azzofeita, G.., et al. (2011). SpecNet revisited: bridging flux and remote sensing communities. Can. J. Remote Sens., 36.

Gamon, J.A., Field, B., Goulden, L., Griffin, K., Hartley, A., Geeske, J., et al. (1995). Relationships between NDVI canopy structure and photosynthesis. Ecol. Appl., 5, 28–41.

Gamon, J.A., Penuelas, J. & Field, B. (1992). A narrow-waveband spectral index that tracks diurnal changes in photosynthetic efficiency.pdf. Remote Sens. Environ., 41, 35–44.

Ge, J. & Zou, C. (2013). Impacts of woody plant encroachment on regional climate in the southern Great Plains of the United States. J. Geophys. Res. Atmos., n/a–n/a.

Geist, H. (2005). The causes and progression of desertification. Ashgate publishing.

Gitelson, A. & Merzlyak, M. (1994). Spectral reflectance changes associated with autum senescence of Aesculus hippocastanum L. and Acer platanoides L. Leaves Spectral features and relation to chorophyll estimation. J. Plant Physiol., 143, 286–292.

Gitelson, A. & Merzlyak, M. (1997). Remote estimation of chlorophyll content in higher plant leaves. Int. J. Remote Sens., 18, 2691–2697.

Gitelson, A.A., Zur, Y., Chivkunova, O.B. & Merzlyak, M.N. (2002). Assessing Carotenoid Content in Plant Leaves with Reflectance, 75, 272–281.

Gonzalez, L. (2011). Development of a low cost network of phenocams for monitoring plant phenology in a Chihuahuan Desert shrubland. Thesis. The University of Texas at El Paso. 130p.

Goswami, S., Gamon, J.A. & Tweedie, C. (2011). Surface hydrology of an arctic ecosystem: Multiscale analysis of a flooding and draining experiment using spectral reference. J. Geophys. Res., 116, 14.

Gutschick, V.P. & Snyder, K.A. (2006). Water and Energy Balances within the Jornada Basin. In: Struct. Funct. Chihuahuan desert Ecosyst. (eds. Kris, H., Huenneke, L.F. & William, H.S.). pp. 176–188.

Hamerlynck, E.P. & Huxman, T.E. (2009). Ecophysiology of two Sonoran Desert evergreen shrubs during extreme drought. J. Arid Environ., 73, 582–585.

Hastie, T., Tibshirani, R. & Friedman, J. (2011). The Elements of statistical learning. Springer Series in Statistics.

Hastings, S., Oechel, W. & Muhlia, A. (2005). Diurnal, seasonal and annual variation in the net ecosystem CO2 exchange of a desert shrub community (Sarcocaulescent) in Baja California, Mexico. Glob. Chang. Biol.

Havstad, K., Huenneke, L. & Schlesinger, W. (2006). Structure and function of a chihuahuan desert ecosystem: The Jornada Basin Long-Term Ecological Research Site. Long-Term Ecol. Res. Network. Oxford. 447p.

Hilton, T.W., Fox, A.M., Krofcheck, D. & Litvak, M.E. (2013). Modeling the carbon cycle in semi-arid biomes. Poster presentation. In: Natl. Carbon Program-NACP All Investig. Meeting. Albuquerque, NM., February 4-7 2013.

Huemmrich, K.F., Black, T.A., Jarvis, P.G., McCaughey, J.H., Hall, F.G. & Boreas, S. (1999). High temporal resolution NDVI phenology from micrometeorological radiation sensors. Boreas, 104.

Hüve, K., Bichele, I., Rasulov, B. & Niinemets, U. (2011). When it is too hot for photosynthesis: heat-induced instability of photosynthesis in relation to respiratory burst, cell permeability changes and $H_2O_2$ formation. Plant. Cell Environ., 34, 113–26.

Huxman, T.E., Cable, J.M., Ignace, D.D., Eilts, J.A., English, N.B., Weltzin, J., et al. (2004). Response of net ecosystem gas exchange to a simulated precipitation pulse in a semi-arid grassland: the role of native versus non-native grasses and soil texture. Oecologia, 141, 295–305.

IHMC. (2014). CmapTools Knowledge modeling kit [WWW Document]. URL http://cmap.ihmc.us/.

Jaimes, A., Tweedie, C., Mago, T., Kreinovich, V. & Ceberio, M. (2010b). Multi-Objective Optimization under Positivity Constraints , with a Meteorological Example. In: IEEE World Congr. Comput. Intell. p. 12.

Jet Propulsion Lab, (JPL). (1978). PO.DAAC Ocean ESIP Tool (POET) [WWW Document]. Calif. Inst. Technol. URL podaac.jpl.nasa.gov.

Joos, F., Prentice, I.C., Sitch, S., Meyer, R., Hooss, G., Plattner, G.K., et al. (2001). Global warming feedbacks on terrestrial carbon uptake under the Intergovernmental Panel on Climate Change (IPCC) emission scenarios. Global Biogeochem. Cycles, 15, 891–907.

Kaiman, J.C. & Finnigan, J.J. (1994). Atmospheric Boundary Layer Flows. Oxford University Press, Oxford. 289p.

Karels, T.J., Bryant, A.A. & Hik, D.S. (2004). {C}omparison of discriminant function and classification tree analyses for age classification of marmots. Oikos, 105, 575–587.

Kim, J., Guo, Q., Baldocchi, D.D., Leclerc, M.Y., Xu, L. & Leclercl, M.Y. (2006). Upscaling fluxes from tower to landscape: Overlaying flux footprints pn high-resolution (IKONOS) images of vegetation cover. Agric. For. Metereology, 136, 14.

Kjun N., Barr A., McCaughey C, et al. (1997). Air temperature (T. In: Footpr. Appl. to long term CO2 flux Obs. pp. 2–5.

Krishnan, P., Meyers, T.P., Scott, R.L., Kennedy, L. & Heuer, M. (2012). Energy exchange and evapotranspiration over two temperate semi-arid grasslands in North America. Agric. For. Meteorol., 153, 31–44.

Kurc, S. (2008). Extreme makeovers: Crossing critical thresholds into desertification. Aridlands, 8.

Kurc, S.A. & Benton, L.M. (2010). Digital image-derived greenness links deep soil moisture to carbon uptake in a creosotebush-dominated shrubland. J. Arid Environ., 74, 585–594.

Kurc, S.A. & Small, E.E. (n.d.). Simple ecohydrological models: comparison to observations of dryland water and carbon fluxes.

Laney, C.M., Tweedie, C.E., Villanueva-Rosales, N., Gill, T., Karl, J., Roach, S., (2013). Toward new data and information management solutions for data intensive ecological research. Dissertation. The University of Texas at El Paso.

Lasslop, G., Reichstein, M., Papale, D., Richardson, A.D., Arneth, A., Barr, A., et al. (2010). Separation of net ecosystem exchange into assimilation and respiration using a light response curve approach: critical issues and global evaluation. Glob. Chang. Biol., 16, 187–208.

Lee, X., Massman, W. & Law, B. (2004). Handbook of micrometereology. Kuwler academic publishers.

Liaw, A. & Wiener, M. (2002). Classification and Regression by randomForest. R news, 2, 18–22.

LICOR. (2011). EddyPro Software.[WWW.Document]: http://www.licor.com/env/products/eddy_covariance/software.html

Lincoln, D.S. (2008). Towards a cyberinfrastructure for the biological sciences: progress, visions and challenge, 9, 678.

Litvak, M., Hilton, T., Krofcheck, D., Neuenschwander, A. & Fox, A. (2013). Quantifying the vulnerability of carbon stocks and fluxes in six semi-arid biomes in the Southwestern US to both temperature and precipitation extremes. In: Natl. Carbon Program-NACP All Investig. Meet.

Loarie, S.R., Lobell, D.B., Asner, G.P. & Field, C.B. (2011). Land-Cover and Surface Water Change Drive Large Albedo Increases in South America. Earth Interact., 15.

Duniway, M., (2010). Spatial and temporal patterns of water availability in a grass-shrub ecotone and implications for grasslands recovery in arid environments, 3, 55.

Maderos, J.. & Pockman, W.T. (2011). Drought increases freezing tolerance of both leaves and xylem of Larrea tridentata. Oecologia, 73–84.

Mark, C., Lihong, S., Albert, R., Martonchik, J. V, Debra, P. & Andrea, L. (2008). Remote sensing oof woody dhrub cover in desert grassland using MIRS with a geometric-optical canopy reflectance model. Remote Sens. Environ., 112, 15.

Marshall, B. & Woodward, F.I. (1985). Instrumentation for environmental physiology. Soc. Exp. Biol. Cambridge University Press, Cambridge.

Martin, M., Gavazon, K., Korner C, HattenSchiwiler, S. & Rixen, C. (2010). Reduced early growing season freezing resistance in alpine treeline plants under elevated atmospheric CO 2. Glob. Chang. Biol., 16, 1057–1070.

Max Plank Institute, B. (2012). Eddy covariance gap-filling and flux partitioning tool [WWW Document]. Max Plank Inst. Biochem. URL http://www.bgc-jena.mpg.de/~MDIwork/eddyproc/.

Medeiros, J.S., Marshall, D., Maherail, H. & Pockman, W.T. (2012). Variation in seedling freezing response is associated with climate in Larrea. Oecologia, 169, 73–84.

Mendez-Barroso, L.A. & Vivoni, E.R. (2010). Observed shifts in land surface conditions during the North American Monsoon: Implications for a vegetation-rainfall feedback mechanism. J. Arid Environ., 74, 549–555.

Middlenton, E. (2010). Spectral Bio-Indicators of Ecosystem Photosynthetic Efficiency II: Synthesis and Integration.

Mirle, K., Allen, M.R., Blindoff, N.., Stott, P.., AchutaRao, K.., Allen, M.., et al. (2013). Detection and Attribution of Climate Change: from Global to Regional. In: IPCC (eds. Bartholy, J., Vautard, R. & Yasunari, T.). Cambridge University Press, Cambridge.

Mizunuma, T., Wilkinson, M., L. Eaton, E., Mencuccini, M., I. L. Morison, J. & Grace, J. (2013). The relationship between carbon dioxide uptake and canopy colour from two camera systems in a deciduous forest in southern England. Funct. Ecol., 27, 196–207.

Moffat, A.., Papale, D., Reichstein, M., Hollinger, D., Richardson, A., Barr, A., et al. (2007). Comprehensive comparison of gap-filling techniques for eddy covariance net carbon fluxes. Agric. For. Meteorol., 147, 209.

Mokhtari, M.H., Adnan, R. & Busu, I. (2013). A new approach for developing comprehensive agricultural drought index using satellite-derived biophysical parameters and factor analysis method. Nat. Hazards, 65, 1249–1274.

Van der Molen, M.K., Dolman, a. J., Ciais, P., Eglin, T., Gobron, N., Law, B.E., et al. (2011). Drought and ecosystem carbon cycling. Agric. For. Meteorol., 151, 765–773.

Moncrieff, J.B., Malhi, Y. & Leuning, R. (1996). The propagation of errors in long-term measurements of land-atmosphere fluxes of carbon and water. Glob. Chang. Biol., 2, 10.

Munson, S.M., Muldavin, E.H., Belnap, J., Peters, D.P.C., Anderson, J.P., Reiser, M.H., et al. (2013). Regional signatures of plant response to drought and elevated temperature across a desert ecosystem. Ecology, 94, 2030–41.

National Drought Mitigation Center (2011). The Drought Monitor.[WWW Document]: http://drought.unl.edu/

NCDC-NOAA, (2008). World's Largest Archive of Climate Data. [WWW Document]: http://www.ncdc.noaa.gov/

Nicholson, S. (2011). Dryland Climatology. Cambridge University Press, Cambridge. 528p.

Nicholson, S.E., Tucker, C.J. & Ba, M.B. (1998). Desertification, drought, and surface vegetation: An example from the West African Sahel. Bull. Am. Meteorol. Soc., 79, 815–829.

NOAA. (2011). National Climatic Data Center [WWW Document]. U.S. Dep. Commer. URL www.ncdc.noaa.gov.

Novak, D.J. & Canias, J.A. (2006). The Theory underlying concept maps and how to construct and use them.

Okin, G.S., Parson, A.J., Wainwright, J., Herrick, J.E., Bestelmeyer, B.T., Peters, D.C. (2009). Do Changes in connectivity explain desertification. Bioscience, 59, 13.

Penuelas, J., Filella, I. & Gamon, J. (1995). Assessment of photosynthetic radiation use efficiency with spectral reflectance. New Phytol., 291–296.

Penuelas, J., Rutishauser, T. & Filella, I. (2009). Phenology Feedbacks on Climate Change. Science (80-. )., 324, 887–888.

Peters, D. & Laney, C. (2009). ECOTRENDS in Long Term Ecological Research.

Peters, D., Sala, O., Allen, C., Covich, A. & Brunson, M. (2007). Cascading events in linked ecological and socioeconomics systems. Ecol. Soc. Am., 4.

Peters, D., William, H.S., Herrick, J.E., Huenneke, L. & Havstad, K. (2006). Future direction in Jornada research: Applying an interactive landscape model to solve problems. In: Struct. Funct. a Chihuahuan Desert Ecosyst. (eds. Havstad, K., Huenneke, L. & Schlesinger, W.). Oxford University Press, p. 447.

Peters, D.P., Archer, S.R., Bestelmeyer, B.T., Brooks, M.L., Joel, B., Comerie, A., et al. (2011). Vulberability of ecosystem services to cumulative threats that result iin desertification. US Department of Agricultural Research Service, Jornada Experimental Range. 50p

Peters, D.P. Yao, J., Browning, D. & Rango, A. (2013). Mechanisms of grass response in grasslands and shrublands during dry or wet periods. Oecologia. 174(4):1323-34.

Ponce Campos, G.E., Moran, M.S., Huete, A., Zhang, Y., Bresloff, C., Huxman, T.E., et al. (2013). Ecosystem resilience despite large-scale altered hydroclimatic conditions. Nature, 494, 349–52.

Ramirez, C., Jaimes, A., Argaez, M. & Tweedie, C. (2012). The Role of Image Inpainting in Micrometeorological Analysis. In: IEEE Int. Conf. Image Process. IEEE image processing, p. 4.

Reichstein, M., Stoy, P., Desai, A., Lasslop, G. & Richardson, A. (2012). Partitioning of Net Fluxes. In: Eddy covariance A Pract. gruide to Meas. data Anal. (eds. Aubinet, M., Vesala, T. & Papale, D.). Springer New York, New York, NY, pp. 263–283.

Reichstein, M., Stoy, P., Desai, A., Lasslop, G. & Richardson, A. (2012b). No Partitioning Net Fluxes. In: Eddy covariance A Pract. guide to Meas. data Anal. p. 263.

Reynolds, J.F., Stafford Smith, D.M., Lambin, E.F., Turner, B.L., Mortimore, M., Batterbury, S.P.J., et al. (2007). Global desertification: Building a science for dryland development. Science 316, 847–851.

Rich, P.M., Breshears, D.D. & White, A.B. (2008). Phenology of mixed woody-herbaceous ecosystems following extreme events: Net and differential responses. Ecology, 89, 342–352.

Richardson, A.D., Braswell, B.H., Hollinger, D.Y., Jenkins, J.P. & Ollinger, S. V. (2009). Near-surface remote sensing of spatial and temporal variation in canopy phenology. Ecol. Appl., 19, 1417–28.

Richardson, A.D., Jenkins, J.P., Braswell, B.H., Hollinger, D.Y., Ollinger, S. V & Smith, M.L. (2007). Use of digital webcam images to track spring green-up in a deciduous broadleaf forest. Oecologia, 152, 323–334.

Richardson, A.D., Keenan, T.F., Migliavacca, M., Ryu, Y., Sonnentag, O. & Toomey, M. (2013). Climate change, phenology, and phenological control of vegetation feedbacks to the climate system. Agric. For. Meteorol., 169, 156–173.

Robertson, T.R., Zak, J.C. & Tissue, D.T. (2010). Precipitation magnitude and timing differentially affect species richness and plant density in the sotol grassland of the Chihuahuan desert. Oecologia, 162, 12.

Salayandia, L. (2011). A Framework to Create Ontologies for Scientific Data Management. Dissertation. The University of Texas at El Paso.

Sanchez-Mejia, Z.M. (2013). Monsoon dependent ecosystems: Implications of the vertical distributions of soil moisture on land surface-atmosphere interactions. 186p.

Schaefer, K., Schwalm, C.R., Williams, C., Arain, M.A., Barr, A., Chen, J.M., et al. (2012). A model-data comparison of gross primary productivity: Results from the North American Carbon Program site synthesis. J. Geophys. Res., 117, G03010.

Schwalm, C.R., Williams, C. a., Schaefer, K., Baldocchi, D., Black, T.A., Goldstein, A.H., et al. (2012). Reduction in carbon uptake during turn of the century drought in western North America. Nat. Geosci., 5, 551–556.

Schwinning, S. & Sala, O.E. (2004). Hierarchy of responses to resource pulses in and and semi-arid ecosystems. Oecologia, 141, 211–220.

Scott, R.L., Edwards, E.A., Shuttleworth, W.J., Huxman, T.E., Watts, C. & Goodrich, D.C. (2004). Inter-annual and seasonal variation in fluxes of water and carbon dioxide from a riparian woodland ecosystem. Agric. For. Meteorol., 122, 65–84.

Scott, R.L., Hamerlynck, E.P., Jenerette, G.D., Moran, M.S. & Barron-Gafford, G. a. (2010). Carbon dioxide exchange in a semidesert grassland through drought-induced vegetation change. J. Geophys. Res., 115, G03026.

Scott, R.L., Huxman, T.E., Cable, W.L. & Emmerich, W.E. (2006). Partitioning of evapotranspiration and its relation to carbon dioxide exchange in a Chihuahuan Desert shrubland. Hydrol. Process., 20, 3227–3243.

Seager, R. (2007). The Turn of the Century North American Drought: Global Context, Dynamics, and Past Analogs. J. Clim., 20, 5527–5552.

Seager, R., Mingfang, T., Held, I., Yochanan, K., Jian, L., Vecchi, G., et al. (2007). Model Projections of an Imminent Transition to a More Arid Climate in Southwestern North America. Science (80)., 316, 1181.

Shao, C., Chen, J. & Li, L. (2013a). Grazing alters the biophysical regulation of carbon fluxes in a desert steppe. Environ. Res. Lett., 025012.

Shao, C., Chen, J. & Li, L. (2013b). Grazing alters the biophysical regulation of carbon fluxes in a desert steppe, 025012.

Shevliakova, E., Pacala, S.W., Malyshev, S., Hurtt, G.C., Milly, P.C.D., Caspersen, J.P., et al. (2009). Carbon cycling under 300 years of land use change: Importance of the secondary vegetation sink. Global Biogeochem. Cycles, 23, 16.

Sims, D. a & Gamon, J. a. (2002). Relationships between leaf pigment content and spectral reflectance across a wide range of species, leaf structures and developmental stages. Remote Sens. Environ., 81, 337–354.

Small, E.E. (2001). The influence of soil moisture anomalies on variability of the North American monsoon system. Geophys. Res. Lett., 28, 139–142.
154. Sponseller, R.A. (2007). Precipitation pulses and soil CO2 flux in a Sonoran Desert ecosystem. Glob. Chang. Biol., 13, 426–436.

Stein, L.D. (2008). Towards a cyberinfrastructure or the biological sciences:Progress, visions and challenges. Nat. Rev., 9, 11.

Strobl, C., Boulesteix, A.-L., Zeileis, A. & Hothorn, T. (2007). Bias in random forest variable importance measures: illustrations, sources and a solution. BMC Bioinformatics, 8, 25.

Sura, P. (2012). Stochastic Models of Climate Extremes : Theory and Observations. Dissertation. The Florida State University. 75p

Szilagy, J., Rundquist, D. & Gosselin, C. (1998). NDVI relationship to monthly evaporation. Geophys. Res. Lett., 25, 1753–1756.

Thomey, M.L., Ford, P.L., Reeves, M.C., Finch, D.M., Litvak, M.E., Collins, S.L., et al. (2014). Review of Climate Change Impacts on Future Carbon Stores and Management of Warm Deserts of the United States. 26p.

Trenberth, K.E., Dai, A., Rasmussen, R.M. & Parsons, D.B. (2003). The changing character of precipitation. Bull. Am. Meteorol. Soc., 84, 1205.

Turner, D.P., Ritts, W.D., Cohen, W.B., Maeirsperger, T.K., Gower, S.T., Kirschbaum, A. a., et al. (2005). Site-level evaluation of satellite-based global terrestrial gross primary production and net primary production monitoring. Glob. Chang. Biol., 11, 666–684.

Ubinet, M., Vesala, T. & Papale, D. (2012). Eddy Covariance: A Practical Guide to Measurement and Data Analysis. Springer atmospheric sciences.

Vargas, R., Baldocchi, D.D., Querejeta, J.I., Curtis, P.S., Hasselquist, N.J., Janssens, I.A., et al. (2010). Ecosystem $CO_2$ fluxes of arbuscular and ectomycorrhizal dominated vegetation types are differentially influenced by precipitation and temperature. New Phytol., 185, 226–236.

Wainwright, J. (2006). Climate and Climatological Variations in the Jornada Basin. In: Struct. Funct. a Chihuahuan desert Ecosyst. (eds. Havstad, K., Huenneke, L. & Schlesinger, W.). Oxford, pp. 44–81.

Webb, E.K., Pearman, G.I. & Leuning, R. (1980). Correction of flux measurements for density effects due to heat and water vapour transfer. Q. J. R. Meteorol. Soc., 106, 85–100.

Wohlfahrt, G., Fenstermaker, L.F. & Arnone, J.A. (2008). Large annual net ecosystem CO2 uptake of a Mojave Desert ecosystem. Glob. Chang. Biol., 14, 1475–1487.

Woodhouse, C.A., Meko, D.M., MacDonald, G.M., Stahle, D.W. & Cooke, E.R. (2010). A 1,200-year perspective of 21st century drought in southwestern North America. Proc. Natl. Acad. Sci. U. S. A., 107, 21283–21288.

Xu, L. (2004). How soil moisture, rain pulses, and growth alter the response of ecosystem respiration to temperature. Global Biogeochem. Cycles, 18, GB4002.

Yang, X., Tang, J. & Mustard, J. (2014). Beyond leaf color: comparing camera-based phenological metrics with leaf biochemical, biophysical and spectral properties throughout the growing season of a temperate deciduous forest. Am. Geophys. Union.

Yi, C., Rustic, G., Xu, X., Wang, J., Dookie, A., Wei, S., et al. (2012). Climate extremes and grassland potential productivity. Environ. Res. Lett., 7, 035703.

Yuan, W., Liu, S., Zhou, G., Zhou, G., Tieszen, L.L., Baldocchi, D., et al. (2007). Deriving a light use efficiency model from eddy covariance flux data for predicting daily gross primary production across biomes. Agric. For. Meteorol., 143, 189–207.

Yufei, H., Paolo, D., Stephan, D.W., Fuentes, J.D. & Litvak, M. (2010). On the impact of shrub encroachment on microclimate conditions in the northern Chihuahuan desert. J. Geophys. Res., 115, 10.

Kipp and Zonen. (2004). Instruction Manual: Par Lite Photosynthetic Active Radiometer.

# Appendix

## i. INSTRUMENTATION SPECIFICATION AND DATA TABLES

## List of Instruments

| Quantity | Sensor | Description |
|---|---|---|
| 1 | CSAT3 | three dimensional sonic anemometer |
| 1 | LI-7500 | open path infrared gas analyzer (CO2 and H2O) |
| 5 | FW05 | type E fine wire (0.0005 inch diameter) thermocouple |
| 1 | HMP45C | temperature and relative humidity probe |
| 1 | CS106 | barometer |
| 2 | LWS | leaf wetness sensor (2 sensors) |
| 1 | CNR 1 | net radiation sensor |
| 1 | PAR LITE | Photosynthetically active radiation sensor |
| 4 | HFP01 | soil heat flux plate (4 sensors) |
| 1 | 3001 | wind speed and direction |
| 8 | ECTM | Water content and Temperature |
| 1 | TE525 | Rain gauge |

## List of collected tables

| **Name** | **Description** | **Frequency** | **Source** |
|---|---|---|---|
| TS.dat | Timeseries of 10Hz data | 10 Hz | CR3000 |
| Flux.dat | Online fluxes calculated within the datalogger | 30 min | CR3000 |
| ECTM.dat | Soil data | 1min | CR1000 |
| .csv | Offline fluxes calculated from TS.dat table | 30min | EddyPro |

## TS.dat – Time series of 10Hz data

| *Definition* | *Field* | *Units* |
|---|---|---|
| | TIMESTAMP | TS |
| | RECORD | RN |
| Horizontal wind (x-axis) [m / s] | Ux | m/s |
| Horizontal wind (y-axis) [m / s] | Uy | m/s |
| Vertical wind [m / s] | Uz | m/s |
| Sonic temperature [C] | Ts | C |
| LI-7500 carbon dioxide mass density [mg / m^3] | CO2 | mg/m^3 |
| LI-7500 water vapor mass density [g / m^3] | H2O | g/m^3 |
| FW05 temperature [C] | fw | C |
| LI-7500 system pressure [kPa] | press | kPa |
| CSAT3 diagnostic word [unitless] | diag_csat | unitless |
| Automatic gain control [unitless] | agc | unitless |
| HMP45C temperature [C] | t_hmp | C |
| HMP45C vapor pressure [kPa] | e_hmp | kPa |
| CS106 atmospheric pressure [kPa] | atm_press | kPa |

## Flux.dat – Online flux calculations

| | *Definition* | *Field* | *Units* |
|---|---|---|---|
| | | TIMESTAMP | TS |
| | | RECORD | RN |
| 1 | Sensible heat flux using sonic temperature [W / m^2] | Hs | W/m^2 |
| 2 | Sensible heat flux using finewire temperature [W / m^2] | H | W/m^2 |
| 3 | Carbon dioxide (LI-7500) flux, with Webb et al. term [mg / {m^2 s}] | Fc_wpl | mg/(m^2 s) |
| 4 | Latent heat (LI-7500) flux, with Webb et al. term [W / m^2] | LE_wpl | W/m^2 |
| 5 | Sensible heat calculated from Hs and LE_wpl [W / m^2] | Hc | W/m^2 |
| 6 | Momentum flux [kg / {m s^2}] | tau | kg/(m s^2) |
| 7 | Friction velocity [m / s] | u_star | m/s |
| 8 | Average sonic temperature [C] | Ts_mean | C |
| 9 | Standard deviation of sonic temperature [C] | stdev_Ts | C |
| 10 | Covariance of sonic temperature and horizontal wind (x-axis) [m C / s] | cov_Ts_Ux | m C/s |
| 11 | Covariance of sonic temperature and horizontal wind (y-axis) [m C / s] | cov_Ts_Uy | m C/s |
| 12 | Covariance of sonic temperature and vertical wind [m C / s] | cov_Ts_Uz | m C/s |
| 13 | Average carbon dioxide (LI-7500) density [mg / m^3] | CO2_mean | mg/m^3 |

| | | | |
|---|---|---|---|
| 14 | Standard deviation of carbon dioxide (LI-7500) density [mg / m^3] | stdev_CO2 | mg/m^3 |
| 15 | Covariance of carbon dioxide (LI-7500) density and horizontal wind (x-axis) [mg / {m^2 s}] | cov_CO2_Ux | mg/(m^2 s) |
| 16 | Covariance of carbon dioxide (LI-7500) density and horizontal wind (y-axis) [mg / {m^2 s}] | cov_CO2_Uy | mg/(m^2 s) |
| 17 | Covariance of carbon dioxide (LI-7500) density and vertical wind [mg / {m^2 s}] | cov_CO2_Uz | mg/(m^2 s) |
| 18 | Average water vapor (LI-7500) density [g / m^3] | H2O_Avg | g/m^3 |
| 19 | Standard Deviation of water vapor (LI-7500) density [g / m^3] | stdev_H2O | g/m^3 |
| 20 | Covariance of water vapor (LI-7500) density and horizontal wind (x-axis) [g / {m^2 s}] | cov_H2O_Ux | g/(m^2 s) |
| 21 | Covariance of water vapor (LI-7500) density and horizontal wind (y-axis) [g / {m^2 s}] | cov_H2O_Uy | g/(m^2 s) |
| 22 | Covariance of water vapor (LI-7500) density and vertical wind [g / {m^2 s}] | cov_H2O_Uz | g/(m^2 s) |
| 23 | Average finewire temperature [C] | fw_Avg | C |
| 24 | Standard deviation of finewire temperature [C] | stdev_fw | C |
| 25 | Covariance of finewire temperature and horizontal wind (x-axis) [m C / s] | cov_fw_Ux | m C/s |
| 26 | Covariance of finewire temperature and horizontal wind (y-axis) [m C / s] | cov_fw_Uy | m C/s |
| 27 | Covariance of finewire temperature and vertical wind [m C / s] | cov_fw_Uz | m C/s |
| 28 | Average horizontal wind (x-axis) [m / s] | Ux_Avg | m/s |
| 29 | Standard deviation of horizontal wind (x-axis) [m / s] | stdev_Ux | m/s |
| 30 | Covariance of horizontal winds (x-axis and y-axis) [(m / s)^2] | cov_Ux_Uy | (m/s)^2 |
| 31 | Covariance of horizontal wind (x-axis) and vertical wind [(m / s)^2] | cov_Ux_Uz | (m/s)^2 |
| 32 | Average horizontal wind (y-axis) [m / s] | Uy_Avg | m/s |
| 33 | Standard deviation of horizontal wind (y-axis) [m / s] | stdev_Uy | m/s |
| 34 | Covariance of horizontal wind (y-axis) and vertical wind [(m / s)^2] | cov_Uy_Uz | (m/s)^2 |
| 35 | Average vertical wind [m / s] | Uz_Avg | m/s |
| 36 | Standard deviation of vertical wind [m / s] | stdev_Uz | m/s |
| 37 | Average barometric pressure (LI-7500) [kPa] | press_Avg | kPa |
| 38 | Average barometric pressure (CS105) [kPa] | atm_press_mean | kPa |
| 39 | Average temperature from HMP45C [C] | t_hmp_mean | C |
| 40 | Average water vapor density from HMP45C [g / m^3] | H2O_hmp_mean | g/m^3 |
| 41 | Average relative humidity HMP45C [percent] | rh_hmp_mean | percent |
| 42 | Average air density [kg / m^3] | rho_a_mean | kg/m^3 |
| 43 | Resultant wind direction using compass coordinate system [degrees] | wnd_dir_compass | degrees |
| 44 | Resultant wind direction using the CSAT3's right handed coordinate system [degrees] | wnd_dir_csat3 | degrees |
| 45 | Horizontal wind speed [m / s] | wnd_spd | m/s |
| 46 | Resultant horizontal wind speed [m / s] | rslt_wnd_spd | m/s |
| 47 | Standard deviation of wind direction [degrees] | std_wnd_dir | degrees |
| 48 | Carbon dioxide (LI-7500) flux without the Webb et al. term [mg / {m^2 s}] | Fc_irga | mg/(m^2 s) |
| 49 | Latent heat (LI-7500) flux without the Webb et al. term [W / m^2] | LE_irga | W/m^2 |
| 50 | Carbon dioxide (LI-7500) Webb et al. term due to latent heat | CO2_wpl_LE | mg/(m^2 s) |

| | | | |
|---|---|---|---|
| | flux [mg / {m^2 s}] | | |
| 51 | Carbon dioxide (LI-7500) Webb et al. term due to (sonic) sensible heat flux [mg / {m^2 s}] | CO2_wpl_H | mg/(m^2 s) |
| 52 | Water vapor (LI-7500) Webb et al. term due to latent heat flux [W / m^2] | H2O_wpl_LE | W/m^2 |
| 53 | Water vapor (LI-7500) Webb et al. term due to (sonic) sensible heat flux [W / m^2] | H2O_wpl_H | W/m^2 |
| 54 | Number of samples in the statistics (fluxes, variances, means, etc.) [samples] | n_Tot | samples |
| 55 | Number of times any CSAT3 warning flag was set high [samples] | csat_warnings | samples |
| 56 | Number of times any LI-7500 warning flag was set high [samples] | irga_warnings | samples |
| 57 | Number of delta temperature warnings from CSAT3 [samples] | del_T_f_Tot | samples |
| 58 | Number of poor signal lock warnings from CSAT3 [samples] | sig_lck_f_Tot | samples |
| 59 | Number of amplitude high warnings from CSAT3 [samples] | amp_h_f_Tot | samples |
| 60 | Number of amplitude low warnings from CSAT3 [samples] | amp_l_f_Tot | samples |
| 61 | Number of chopper warnings from LI-7500 [samples] | chopper_f_Tot | samples |
| 62 | Number of chopper detector from LI-7500 [samples] | detector_f_Tot | samples |
| 63 | Number of chopper pll from LI-7500 [samples] | pll_f_Tot | samples |
| 64 | Number of chopper synchronization warnings from LI-7500 [samples] | sync_f_Tot | samples |
| 65 | Average AGC from LI-7500 [unitless] | agc_Avg | unitless |
| 66 | Number times the LI-7500 AGC exceeded a user set threashold [samples] | agc_thrshld_excded_Tot | samples |
| 67 | LWS1 | LWS1 | mV |
| 68 | LWS2 | LWS2 | mV |
| 69 | Average net radiation [W / m^2] | Rn_nr_Avg | W/m^2 |
| 70 | Average albedo [unitless] | albedo_Avg | unitless |
| 71 | Average downwelling short wave radiation [W / m^2] | Rs_downwell_Avg | W/m^2 |
| 72 | Average upwelling short wave radiation [W / m^2] | Rs_upwell_Avg | W/m^2 |
| 73 | Average downwelling long wave radiation, with temperature correction [W / m^2] | Rl_downwell_Avg | W/m^2 |
| 74 | Average upwelling long wave radiation, with temperature correction [W / m^2] | Rl_upwell_Avg | W/m^2 |
| 75 | Average net radiometer body temperature [K] | T_nr_Avg | K |
| 76 | Average measured downwelling long wave radiation [W / m^2] | Rl_down_meas_Avg | W/m^2 |
| 77 | Average measured upwelling long wave radiation [W / m^2] | Rl_up_meas_Avg | W/m^2 |
| 78 | Average photosynthetically active radiation [umol/mol] | par_Avg | umol/m/s |
| 79 | Average soil heat flux plate #1 [W / m^2] | hfp01_1_Avg | W/m^2 |
| 80 | Average soil heat flux plate #2 [W / m^2] | hfp01_2_Avg | W/m^2 |
| 81 | Average soil heat flux plate #3 [W / m^2] | hfp01_3_Avg | W/m^2 |
| 82 | Average soil heat flux plate #4 [W / m^2] | hfp01_4_Avg | W/m^2 |
| 83 | Total precipitation [mm] | precip_Tot | mm |
| 84 | Average 03002 horizontal wind speed [m / s] | hor_wnd_spd_mean | m/s |
| 85 | Average 03002 resultant horizontal wind speed [m / s] | hor_wnd_spd_mean_rsl | m/s |
| 86 | Average resultant horizontal wind direction [degrees] | hor_wnd_dir_mean_rslt | Deg |
| 87 | Standard deviation of wind direction [degrees] | hor_wnd_dir_stdev | Deg |

| | | | |
|---|---|---|---|
| 88 | Average CR3000 panel temperature [C] | panel_temp_Avg | C |
| 89 | Average battery voltage [V] | batt_volt_Avg | V |

## ECTM.dat – Soil probes

| *Definition* | *Field* | *Units* |
|---|---|---|
| | TIMESTAMP | |
| | RECORD | |
| Volumetric water content | VOLUMETRIC WATER CONTENTm(1) | % |
| Volumetric water content | VOLUMETRIC WATER CONTENTm(2) | % |
| Volumetric water content | VOLUMETRIC WATER CONTENTm(3) | % |
| Volumetric water content | VOLUMETRIC WATER CONTENTm(4) | % |
| Volumetric water content | VOLUMETRIC WATER CONTENTm(5) | % |
| Volumetric water content | VOLUMETRIC WATER CONTENTm(6) | % |
| Volumetric water content | VOLUMETRIC WATER CONTENTm(7) | % |
| Volumetric water content | VOLUMETRIC WATER CONTENTm(8) | % |
| Soil Temperature | Temp(1) | °C |
| Soil Temperature | Temp(2) | °C |
| Soil Temperature | Temp(3) | °C |
| Soil Temperature | Temp(4) | °C |
| Soil Temperature | Temp(5) | °C |
| Soil Temperature | Temp(6) | °C |
| Soil Temperature | Temp(7) | °C |
| Soil Temperature | Temp(8) | °C |

## TOB1_.csv

| *Definition* | *Field* | *Units* |
|---|---|---|
| Calendar year | YEAR | YEAR |
| | GAP | GAP |
| Decimal day and local time | DTIME | DTIME |
| Julian Day | DOY | DOY |
| Local time of the day | HRMIN | HRMIN |
| Friction velocity | UST | m/s |
| Air temperature | TA | deg C |
| Wind direction | WD | deg |
| Wind speed | WS | m/s |
| Net ecosystem exchange | NEE | umol/m2/s |
| Rate of vertical transfer | FC | umol/m2/s |
| CO2 storage in the canopy air layer | SFC | umol/m2/s |
| | H | W/m2 |
| | SH | W/m2 |
| Sensible heat flux | LE | W/m2 |
| Sensible heat storage in the canopy air | SLE | W/m2 |
| | FG | W/m2 |
| Soil Temperature 1 | TS1 | deg C |
| Soil Temperature 1 | TS2 | deg C |
| Precipitation | PREC | mm |
| Relative Humidity | RH | % |
| Barometric Pressure | PRESS | kPa |
| CO2 concentration above the canopy | CO2 | umol/mol |
| Vapor Pressure deficit | VPD | kPa |
| Soil water content 1 | SWC1 | % |
| Soil water content 2 | SWC2 | % |
| Net Radiation | Rn | W/m2 |
| Incoming photosynthetically active radiation | PAR | umol/m2/s |
| Incoming global solar radiation | Rg | W/m2 |
| Incoming diffuse global solar radiation | Rgdif | W/m2 |
| | PARout | umol/m2/s |
| Outgoing global solar radiation | RgOut | W/m2 |
| Incoming longwave radiation | Rgl | W/m2 |
| Outgoing longwave radiation | RglOut | W/m2 |
| Water vapor concentration | H2O | mmol/mol |
| Total ecosystem respiration | RE | umol/m2/s |
| Gross primary production | GPP | umol/m2/s |

| | | |
|---|---|---|
| | CO2top | umol/mol |
| | CO2height | m |
| Absorbed Photosynthetically active radiation | APAR | umol/m2/s |
| | PARdif | umol/m2/s |
| | APARpct | % |
| Footprint | ZL | unitless |

## II. SWAPPING CARDS ON A CR3000 DATALOGGER

Step 1. Open enclosure 1 to find CR3000.

Step 2. Press removal button on the NL115 and wait for dimming green light.

Step 3. Open SD card compartment

Step 4. Press eject button

Step 5. Remove card

Step 6. Insert removed card on CompactFlash PC Card Adapter

Step 7 Insert new empty card

Step 8 Close SD card storage device NL115

Step 9. Verify warning display on CR3000

Step 10. Verify card message on CR3000 display

Step 11 Verify initialized data tables

Step 12 Verify following tables were initialized:

- Public
- Flux
- Ts_data
- Met_data


**Figure 44** Steps to swap card on CR 3000 data logger

# Vita

Aline Jaimes earned her Bachelor of Science in Biology from Universidad Veracruzana, campus Xalapa, Veracruz, Mexico in 2001. She received her Master of Science degree in Management and Preservation of Natural resources focus on physical and biological oceanography in 2006 from the Northwest Center of Biological Research (CIBnor) La Paz, Baja California Sur, Mexico. In 2007 she joined the doctoral program in Environmental Science and Engineering at The University of Texas at El Paso.

Dr. Jaimes has been the recipient of numerous honor and awards including the Postgraduate scholarship to pursue MSc and Ph.D. degree from the National Council of Science and Technology (CONACyT). Dr. Jaimes was recipient of the Global Lake Ecological Observatory Network Fellowship from a selective NSF-funded training program in network science. She also has been the student representative and coordinator of the Outstanding Student Program Award (OSPA) of the American Geophysical Union, focus group of Earth, Space Science and Informatics. She was also selected as the Highlighted FLUXNET young scientist in newsletter of network.

While pursuing her degree Dr. Jaimes worked as a research assistant for the Environmental Science and Engineering department in a project focused on advancing the utility of Cyberinfrastructure in Environmental Science. Dr. Jaimes's dissertation, understanding and scaling patterns and controls of land-atmosphere carbonexchange in a Northern Chihuahuan desert shrubland with novel Cyberinfrastructure, was supervised by Dr. Craig Tweedie.

Permanent address: 2001 Florence St

El Paso, TX-79902

This thesis/dissertation was typed by Aline Jaimes.